6-2008

Protein Interactions with Mixed Poly(ethylene glycol)/Polyacrylic Acid Brushes

Zhenqing Li
Clemson University, lizhenqing.fudan@gmail.com

PROTEIN INTERACTIONS WITH MIXED POLY(ETHYLENE GLYCOL)/POLYACRYLIC ACID BRUSHES

A Thesis
Presented to
the Graduate School of
Clemson University

In Partial Fulfillment
of the Requirements for the Degree
Master of Science
Materials Science and Engineering

---

by
Zhenqing Li
August 2008

Accepted by
Dr. Igor Luzinov, Committee Chair
Dr. Gary Lickfield
Dr. Douglas Hirt

ABSTRACT

Tethered polymer chains that are grafted to a solid substrate by one chain end (polymer brushes) may be distinguished from other anchored polymer layers by the relatively high grafting densities gained. Potential uses of polymer brushes for interfacial modification to regulate interactions between proteins and substrates, such as drug delivery and protein separation, are widely recognized. Therefore, it is important to investigate interactions between proteins and surfaces modified with a polymer brush.

In this study, the "grafting-to" method has been used to graft mixed poly(ethylene glycol) (PEG) and polyacrylic acid (PAA) brushes onto poly(glycidyl methacrylate) (PGMA)-modified silicon wafers/glass slides to create controllable protein adsorption/desorption surfaces. Single component PAA and mixed PEG/PAA brushes exhibit an ionic-strength-dependent height transition, indicating the brush's switching capacity.

Total Internal Reflectance Fluorescence (TIRF) was used to determine the extent of protein adsorption on the PEG, PAA and mixed PEG/PAA brush surfaces. Both high grafting density PEG and PAA brushes repel proteins. The protein adsorption at equilibrium on mixed PEG/PAA brushes surface is affected by PEG grafting density and the number of monomeric units in PAA chains bonded to the surface. The protein adsorption amounts on the mixed brushes are also adjustable when the ionic strength changes. However, the mechanism for protein adsorption and desorption in this mixed polymer brush system needs further investigation.

DEDICATION

This thesis is dedicated to my parents who raised me up and taught me a lot from my childhood, and my girlfriend Zheng Fang who always gives me her sincere support and encouragement.

ACKNOWLEDGMENTS

I would like to thank my advisor, Dr. Igor Luzinov for his careful guidance and motivation during the two years of study in Clemson University. I would also thank him for all his kind help as a preeminent advisor and helpful mentor to not only the study & research but also my living and staying. I also would like to thank Dr. Gary Lickfield for his guidance, thoughtful questions about this project. I would like to thank Dr. Douglas Hirt for his time, expertise and support.

Here, I want to thank Dr. Bogdan Zdyrko for the design and assembly of TIRF machine and the insightful discussion. I would also like to thank Ms. Olha Hoy and Mr. Olesandr Burtovyy for their thoughtful opinions, Dr. Viktor Klep for the help on the synthesis of polymer, and Dr. Ruslan Burtovyy, Dr. Karthik Ramaratnam, Mr. Suraj Sharma, Mr. Taras Andrukh for their help.

Finally, I want to appreciate the funding support from Schools of Materials Science and Engineering, Clemson University and National Science Foundation (DMR0602528) without which this work was impossible.

TABLE OF CONTENTS

Page

LIST OF TABLES

LIST OF FIGURES

List of Figures (Continued)

Figure Page

List of Figures (Continued)

Figure Page

List of Figures (Continued)

Figure Page

List of Figures (Continued)

Figure Page

List of Figures (Continued)

Figure Page

CHAPTER ONE

INTRODUCTION

Control of materials properties is one of the main objectives for materials scientists. Some properties are regulated by the bulk structure or the composition of the materials, such as mechanical properties. However, biological responses mostly are regulated by the surface chemistry of materials. Thus, control of surface properties is important for designing and synthesizing bio-functional materials. Surface modification is widely used to regulate surface properties, and there are many methods for successful alternation of surfaces, including mechanical methods, chemical coating and plasma etching. Recently, the use of polymer brushes to modify surfaces has been gaining more attention.

A polymer brush is an assembly of polymer chains, each with one end tethered to a substrate surface. The chains extend away from the substrate, giving a longer end-to-end distance as they are in the freely random coiled conformation. Successful modifications through polymer brushes, resulting in adhesive, protein-repulsive, hydrophobic and hydrophilic surfaces, have been reported[1-3].

More recently, mixed polymer brushes have been used for surface modification. One advantage of mixed brushes is that the nature of the modified surface can potentially be switched from one state to another state by altering the surrounding media. For example, the surface properties can be adjusted from hydrophilic to hydrophobic, or from positively charged to negatively charged, by grafting hydrophobic/hydrophilic or positively/negatively charged polymer chains together on a single substrate.

The objective of this study is to synthesize mixed brush modified surfaces with tunable affinity to proteins. In other words, the surface can be switched between a protein

adsorptive to a protein repulsive state by changing the ionic strength of the solution in which the brush is immersed. A literature review about the synthesis and properties of polymer brushes is presented in Chapter Two. The synthetic procedures for mixed brushes are provided in Chapter Three. The results on synthesis and characterization of single-component and mixed brushes are discussed in Chapter Four. Experimental results regarding protein adsorption to the brush surfaces are presented and discussed in Chapter Five. Finally, a summary and suggestions for future work are provided in Chapter Six and Chapter Seven, respectively.

References

(1) Harris, B. P.; Kutty, J. K.; Fritz, E. W.; Webb, C. K.; Burg, K. J. L.; Metters, A. T. *Langmuir* **2006***, 22*, 4467.

(2) Piehler, J.; Brecht, A.; Geckeler, K. E.; Gauglitz, G. *Biosensors and Bioelectronics,* **1996***, 11*, 579.

(3) Minko, S., Patil, S., Datsyuk, V., Simon, F., Eichhorn, K., Motornov, M., Usov, D., Tokarev, I., Stamm, M. *Langmuir* **2002***, 18*, 289.

CHAPTER TWO

LITERATURE REVIEW

2.1 Introduction to the polymer brushes and their properties

In general, polymer brushes are self-assembled polymer chains with one end tethered to the surface. When the distance between grafted chains is smaller than their radius of gyration, *Rg*, the chains start to overlap and the excluded volume effect stretches each individual chain out from the substrate[1,2]. Many theoretical[2-7] and experimental[1,8-14] studies reveal that the polymer chains in this structure exhibit the deformed conformation, and the degree of deformation depends on the grafting density of the anchored chains. Figure 2.1 shows the dependence between the brush height and the grafting density. At a lower grafting density, the chains tethered to the surface form a coil as in the dilute solution, resulting in the "mushroom" regime. Increasing grafting density reduces the distance between chains and the excluded volume effect forces the chains to extend away from the substrate to form the brush structure, resulting in the "brush" regime. The transition boundary for the change from the "mushroom" to the "brush" regime was suggested by Brittain and Minko[15]. They defined the *reduced tether density* (Σ) as $\Sigma=\sigma\pi R^2_g$, where Rg denotes the free polymer chain's radius of gyration and σ is the grafting density. By studying many different polymer brush systems, they demonstrated that the transition boundary is located at $\Sigma = 6$ chains.

Alexander[16] was the first to calculate brush height theoretically and found it to be

linearly dependent on the molecular weight and to the 1/3 power of the grafting density:

$$h \sim (\sigma w)^{1/3} N \tag{1.1}$$

where w is the excluded volume parameter, N is the degree of polymerization and σ is grafting density. De Gennes[17] also used scaling concepts to calculate the relationship between brush height and the grafting density as well as molecular weight. He obtained the same relationship as Equation (1.1). More recently, Milner and Witten[7] found the same linear relationship to molecular weight still preserved with a more accurate parabolic end-group profile. In general, Equation (1.1) is widely accepted to remain consistent over the entire grafting density range.

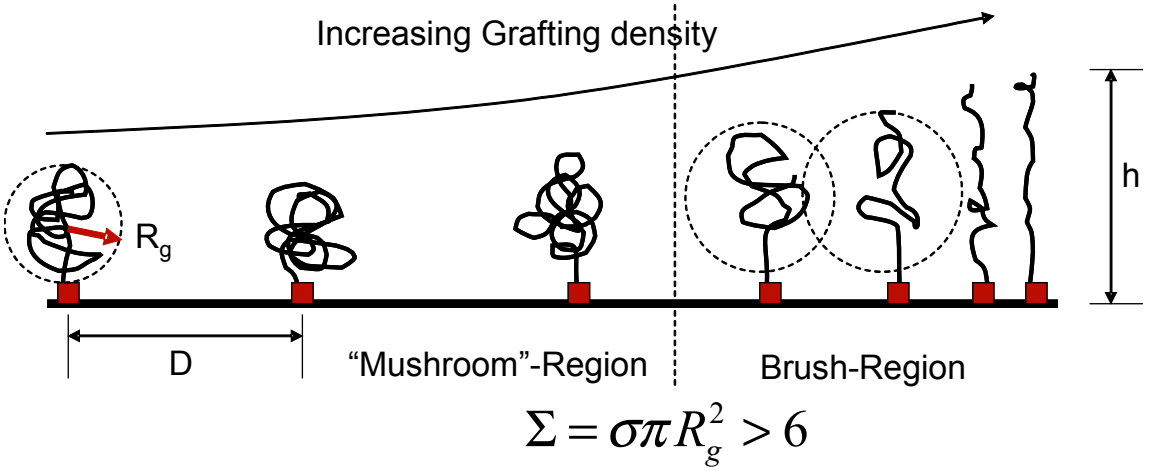

Figure 2.1: Polymer chains conformations on surface versus the grafting density.

2.2 Synthesis of the Polymer Brushes

The primary methods used to obtain polymer brushes on a flat or curved surface are physisorption, "grafting-to" and "grafting-from" methods. The schemes of these methods are shown in Figure 2.2.

Physisorption binds the polymer chains to the surface through physical forces such as van der Waals, electrostatic or hydrogen bond interactions. Normally, a block copolymer composed of two functional parts is used, with one part forming the anchor layer on the surface and the other part forming the elongated brush structure (Figure 2.2, left). For instance, Parsonage *et al.*[18] succeeded in depositing a poly(2-vinylpyridine) (P2VP) - polystyrene (PS) block copolymer on the oxidized silicon and mica substrates in toluene, which is a good solvent for PS but not for P2VP. As a result, the PS part extended from the surface while the P2VP part collapsed, attaching to substrate because of its stronger interaction with the surface. These authors discovered that when the size difference between the two blocks was small, the surface coverage by the block copolymer depended on the molecular weight of the P2VP segments. However, the surface coverage depended on the molecular weight of PS when the size difference between two blocks was large.

The disadvantage of physisorption is the weak interaction between the attached polymers and the substrate. This thermodynamic adsorption process[1] can be reversed by altering the temperature or the solvent conditions. Since the secure tethering of one end

of a polymer chain is a prerequisite for the stable polymer brush structure, a more stable connection method such as covalent bonding can be used to obtain stable brushes.

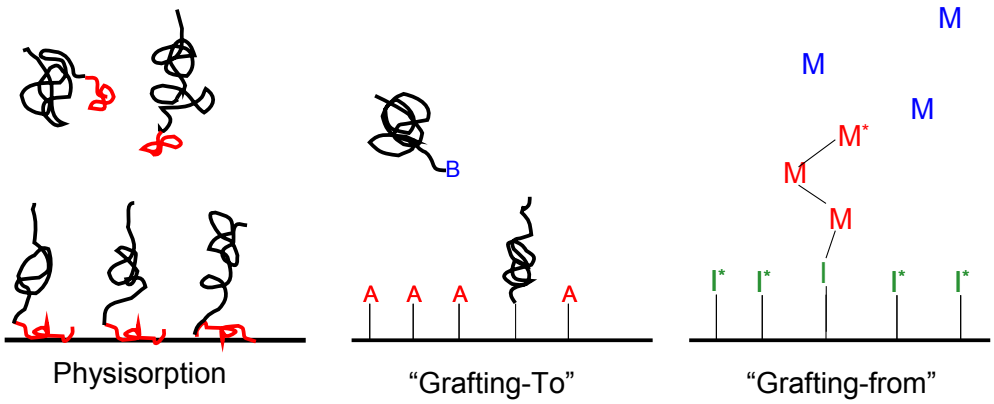

Figure 2.2: Schemes of three different methods to obtain polymer brushes.

The **"grafting-to"** method uses covalent bonding between the reactive group on the substrate (A) and terminal reactive groups in the polymer chain (B) to anchor the polymer, forming the brush structure, as shown in center scheme of Figure 2.2. This method is more reliable than physisorption because a chemical bond is formed.

Minko *et al.*[19] used PS and P2VP with end carboxyl groups to graft them sequentially onto a silicon wafer pre-coated with 3-glycidoxypropyl-trimethoxysilane. Liberelle and Giasson[20] also constructed polystyrene brushes on a mica surface via the "grafting-to" approach. They first treated the mica with plasma before grafting. Then, the trimethylchlorosilane was deposited. After that, the monochlorosilyl terminated polystyrene was added. The reaction of silanol groups on mica surface with the monochlorosilyl groups on polystyrene allowed the PS chains to tether to the surface. However, the siloxane bonds are not stable in aqueous solutions. These researchers found

that the anchored siloxane bonds between the monochlorosilyl moiety and the surface were easily hydrolyzed, detaching the PS chains. However, the hydrolysis could be reduced by increasing the length of PS chains.

Luzinov *et al.*[21] showed that a molten polymer can be used in the "grafting-to" approach. They grafted different molecular weight PS with carboxylic acid and anhydride end groups from the melt to form a uniform and stable brush structure on an epoxysilane-modified silicon substrate. They found that this grafting method was the most efficient when the molecular weight of the PS was close to its critical entanglement molecular weight, which was 31,200 g/mol.

The major advantage of the "grafting-to" method is that the molecular weight distribution of the brush is based on the molecular weight distribution of polymers used in grafting. Therefore, through using a polymer with a narrow molecular weight distribution, a brush with a narrow molecular weight distribution can be obtained. However, the "grafting-to" method cannot achieve a high grafting density because the excluded volume effect, originating from the previously grafted polymer chains, prevents continued grafting. Recently, Iyer *et al.*[22] studied poly(glycidyl methacrylate) (PGMA) as a macromolecule anchoring layer, finding it has the potential to improve grafting density via the "grafting-to" approach, while Zdyrko *et al.*[23, 24] found poly(ethylene glycol) (PEG) grafted to a PGMA-modified silicon surface can attain a higher grafting density (maximum ~1.6 chains/nm^2) than conventionally observed (less than 1 chains/nm^2).

In the **"grafting-from"** approach, the initiator (I) is immobilized on the substrate, which means the polymer chains constituting the brush are grown from the surface instead of simply being attached, as shown in the right scheme of Figure 2.2. Because the size of the initiator is relatively small, the "grafting-from" method can result in a relatively high grafting density. Wu *et al.*[4] deposited a gradient monolayer of initiator on a surface, then polymerized tert-butyl acrylate (tBA) from it. Klep *et al.*[25] used Atom Transfer Radical Polymerization (ATRP) to polymerize styrene monomer to construct a polystyrene brush. Poly(glycidyl methacrylate) was used for primary surface activation.

The disadvantage of the "grafting-from" approach utilizing traditional radical polymerization is the large polydispersity of the brush. It is known that the molecular weight distribution of the polymer synthesized from the surface is difficult to control. However, modern controlled radical polymerization, such as ATRP[26] and reversible addition-fragmentation chain transfer (RAFT)[27], could control the distribution quite well.

In this research, the "grafting-to" methodology was used to generate polymer brushes. This method was selected because it does not involve the bio-incompatible metal ions as in "grafting-from" approach utilizing ATRP, nor does it produce the unstable tethering as in physisorption. In addition, by applying the method of Iyer and Zdyrko[22-24], the relatively high grafting density of PEG brushes on PGMA could be obtained.

2.3 Charged Polymer Brushes

Polymer brushes can be divided into neutral and charged brushes. One kind of charged brushes are polyelectrolytes, which are polymers with electrolyte groups as the repeating unit. When the electrolyte dissociates, the chains can be positively or negatively charged, as shown in the left side of Figure 2.3. Based on the strength of the electrolytes, polyelectrolytes can be divided into quenched (strong electrolyte) polyelectrolyte brushes, such as poly(styrene sulfonic acid) (PSS)[13] which has fixed degree of dissociation, and annealed (weak electrolyte) polyelectrolyte brushes, such as as polyacrylic acid (PAA)[5, 9, 12] which has the degree of dissociation dependent on the pH (Figure 2.3). The presence of charges provides not only additional electrostatic interactions between chains but also the dramatic brush height transition under different solution conditions.

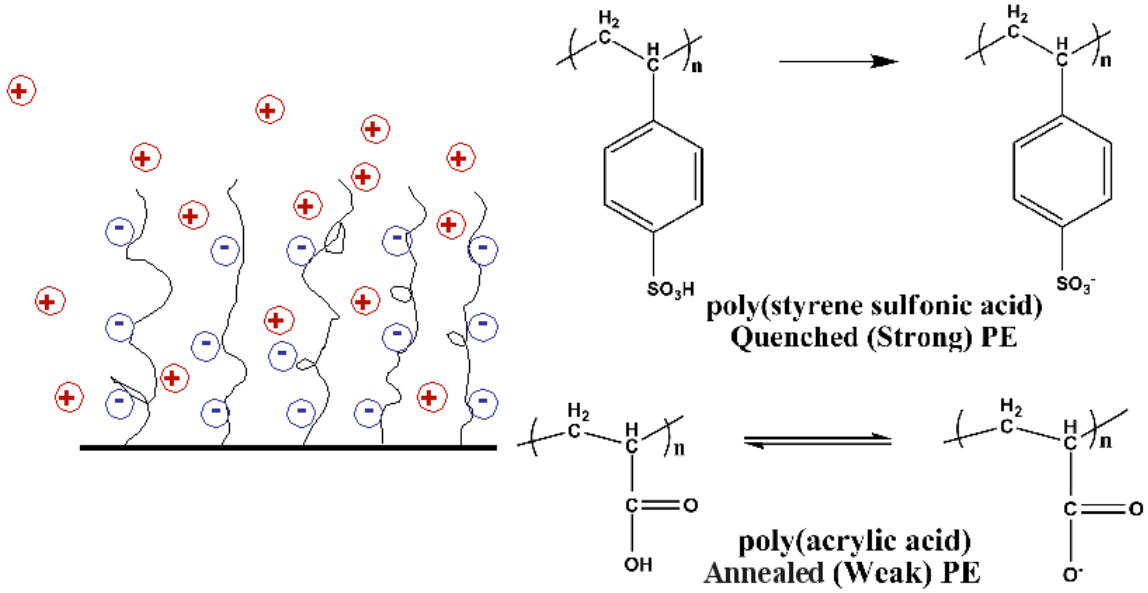

Figure 2.3: Polyelectrolytes and the two categories. Left is the representation of a polyelectrolyte brush example. Right is the structures of a strong (quenched) and a weak (annealed) polyelectrolyte.

Figure 2.4 shows the height transitions of quenched and annealed polyelectrolytes under different ionic strengths at constant pH, from the theoretical point of view. The effect of the extra ions can be divided into three regimes[5, 13, 28-30]: a neutral brush regime, a salted brush regime and an osmotic brush regime. Under the constant pH, which exceeds the pKa of the polyelectrolyte brush, the polyelectrolyte brush height becomes low when the ionic strength is high because the large amount of additional ions screen out the charges along the chains. Thus, chains are equivalently neutral, and this regime is called a neutral brush regime (Figure 2.4, NB regime). As the ionic strength is decreased, the screening effect is reduced and the chains begin to repel one another. Chains are now are in the salted brushes regime (SB regime) and are stretched more than they were in the NB

regime. Both quenched and annealed brushes show the same tendency in NB and SB regimes. However, they behave differently when the ionic strength is decreased further. For the quenched electrolytes brushes, almost all the counter-ions accumulate inside the brush. Because the degree of dissociation is fixed, the excess counter-ions extend the brush as a result of a high osmotic pressure[29] in spite of decreasing the concentration of salt ions in the solution. Thus, the brush height remains the same. However, for annealed polymer brushes, because of the variable degree of dissociation, the accumulated counter-ions inside the brush neutralize the polyelectrolyte chains, reducing the repulsion forces and, as a result, the thickness of the brushes decreases. This regime is called an osmotic brushes (OsB regime)[5].

Recently, experiments have been conducted to investigate the polyelectrolyte brush height transition under different ionic strengths. For example, Wittemann *et al.*[31] used cryogenic transmission electron microscopy (TEM) to visualize the shape of quenched polyelectrolyte brushes. Though the resolution was not high, the brush height transition from the SB regime to the OsB regime could be clearly observed from the TEM images. Later, Currie *et al.*[12] in their investigation of annealed PAA brushes at the air/water interface showed that the dependence of the annealed polyelectrolyte brush height on the solution ionic strength was a non-monotonical function. Brush height first increased, then decreased with an increasing ionic strength. Guo *et al.*[32] covered polystyrene particles with photoinitiator and then polymerized acrylic acid to form a

spherical PAA brush to investigate the dependence of the hydrodynamic radius on the ionic strength. Their results also indicated a good correlation to the nonmonotonical relationship between brush height and ionic strength. All of these experimental results support the theory for polyelectrolyte brush height transition under different ionic strength. Thus, polyelectrolyte brush should be the method of choice for creating functional and smart surfaces.

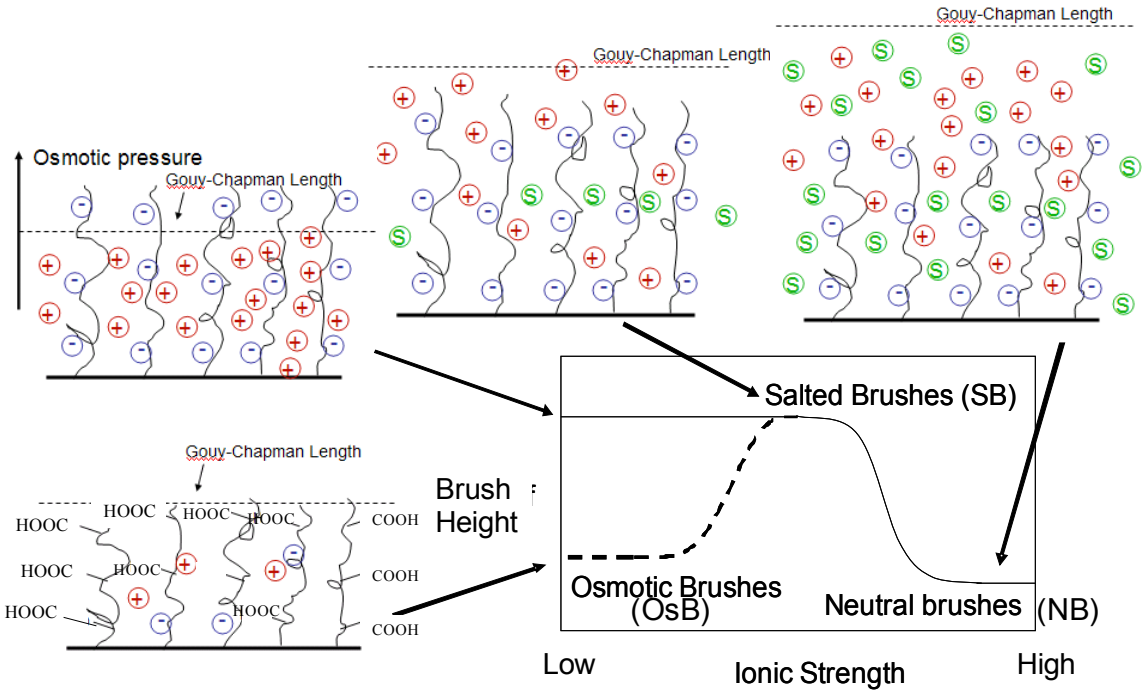

Figure 2.4: Polyelectrolyte brush height transition versus ionic strength, holding pH constant[4], S denotes the salt ions.

2.4 Mixed Polymer Brushes

To obtain combined properties in single grafted layer, a mixed polymer brush is used, where two polymer chains with different properties are grafted on a single substrate. The results show that incorporating the second species significantly affects the brush's structure.

The most important characteristic of the mixed brushes is their ability to switch their surface structures. In one of the early studies in this area, Marko[6] found that brushes made of two immiscible polymers can form two different structures: ripple and dimple (Figure 2.5), depending on the ratio between two grafted chains. Later, another stripe structure was demonstrated by Zhulina[33] based on the densely-grafted Y-shape AB copolymer with two different polymers on two arms with one arm contained A and the other arm contained the incompatible B chains.

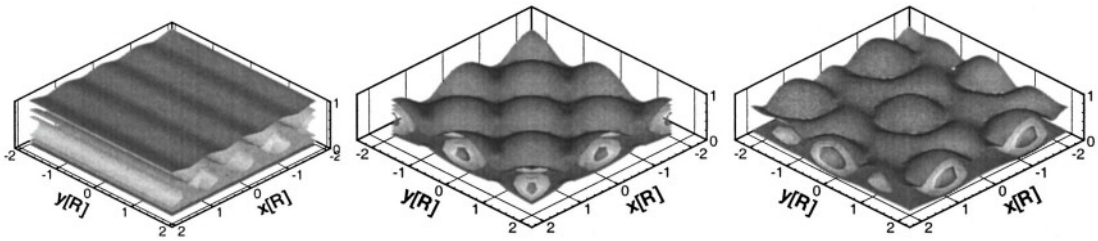

Figure 2.5: The structure transition of PS-P2VP mixed brush under different solvents: ripple (left) and two dimple structures (center and right)[34].

Minko *et al.*[19] used PS and P2VP with carboxyl end groups to graft them sequentially onto a silicon wafer pre-coated with 3-glycidoxypropyl-trimethoxysilane. They found that the mixed polymer brush, which consisted of two incompatible

polymers, demonstrated the “dimple”-“ripple” transition (Figure 2.5) after being treated with different solvents. The surface composition of the dimple structure could be changed from PS-occupied to P2VP-occupied by altering the solvent. Thus, it displayed the switchibility in the surface property from hydrophilic (P2VP) to hydrophobic (PS). Witte and Won[30] simulated mixed brushes consisting of neutral and polyelectrolyte chains. They found that the lower the degree of the polyelectrolyte's dissociation, the higher the swelling of the neutral brushes, thus increasing the area they occupied on the brush’s surface. As a contrast, increasing the degree of dissociation suppressed the neutral brushes components to the vicinity of the substrate, which reduced the surface fraction occupied by the neutral chains.

Switching in surface structure and surface composition distribution by altering the environmental conditions can be used to obtain controllable surface properties. Houbenov *et al.*[35] synthesized mixed polyelectrolyte brushes made of PAA and P2VP via the “grafting-to” approach. They demonstrated that changing pH from low to high can bring differently charged polymers up to the surface, first P2VP then PAA. Thus, surface charge can be changed from positive to negative. These experiments, along with many other examples[35-38], provide a possible route to obtain a surface with switchable properties, such as positively charged/negatively charged and hydrophobic/hydrophilic, via incorporating two or more polymers to form the brush on the surface.

To synthesize a mixed polymer brush system, both the “grafting-to” and the

"grafting-from" procedures can be used. Synthesis of mixed brushes using "grafting-to" is based on depositing end-functional group modified polymers on a pre-treated reactive surface. Besides making a PS-P2VP brushes[19], Minko *et al.*[39] also used the same "grafting-to" method to fabricate mixed poly(styrene-*co*-2, 3, 4, 5, 6 pentafluorostyrene)/poly(vinyl pyridine) brushes on PTFE foil.

To fabricate mixed brushes using the "grafting-from" method, one or two initiators are used to initiate the polymerization of two different monomers. Zhao[40] applied ATRP and then nitroxide-mediated radical polymerization (NMRP) to graft a PS/ PMMA mixed brush. Zhang *et al.*[41] succeeded in polymerizing PS and PMMA sequentially to obtain mixed brushes on clay surfaces. More recently, the combination of "grafting-to" and "grafting-from" was used. Dong *et al.*[9] first grafted PEG via PEGylated silane on a silicon wafer surface and used oxygen plasma to etch patterns on it. Then, the initiator was deposited. An acrylic acid monomer was used to grow a PAA polymer to form a PEG/PAA mixed polymer matrix.

In this research, a PEG/PAA mixed system is fabricated via the "grafting-to" approach. PEG is known as a protein repelling polymer[11, 12, 42], while PAA is a protein adsorptive polymer[10, 43-45]. The surface is intended to be tuned from a PEG-occupying surface to PAA-occupying surface, thus the protein binding property of the surface can be adjusted from protein repulsive to protein adsorptive.

2.5 Miscibility between PEG and PAA

To successfully synthesize the mixed brush and implement the tuning of protein adsorptive properties, the miscibility between PEG and PAA requires consideration. The miscibility between the two polymers is important to facilitate the grafting of the PAA through a previously grafted PEG brush to the anchoring PGMA layer. When in a protein solution, PAA and PEG should be separated into two domains so that tuning is possible to adjust the distribution of the polymer chains on the surface. PEG is known for its miscibility with PAA at any composition ratio[46]. However, detailed analysis[47,48] has shown that this may not hold true when the PAA is partially ionized.

Hydrogen bonding provides the miscibility between PEG and PAA. According to Lu and Weiss[47], when the PAA's weak carboxylic acid groups change to salt or ester form, the hydrogen bonds breaks, resulting in immiscibility. In their work, they found partially neutralized PAA (0.2-Li-PAA) demonstrated phase separation with pure PEG when the weight fraction of partially neutralized PAA was between 0.4 and 0.6. Khutoryanskiy *et al.*[48] used fluorescence and turbidimetric measurements to show that PAA/PEG (1:1) exhibited three different behaviors bounded by two critical pHs: molecular-weight-dependent pH_{c2} (3.0 ~ 3.5) and molecular-weight-independent pH_{c1} (approximately pKa of PAA, ~4.7). Above the critical pH_{c1} , PAA did not exhibit any hydrogen bonding with PEG and phase separated. Between these two critical pHs, they form a hydrophilic interpolymer complex (IPC), while below pH_{c2} they form a hydrophobic IPC. By casting

films of PEG and PAA from different pH solutions, these researchers demonstrated that the thin layer of the PEG/PAA blend exhibited phase separation above pH_{c1}. In addition, they found that the PEG/PAA pair showed a non-temperature dependent phase behavior in aqueous solution.

In general, PEG/PAA is miscible when PAA remains in its acid form and immiscible when it changes to the ionized form. In this research, the PAA in acid form was used to be grafted to the PEG-occupied PGMA layer. During protein adsorption experiments, phosphate buffer (pH~7.4) was used, which leads to the immiscibility between PAA and PEG. Thus, the switching from PEG-occupied to PAA-occupied surface is possible.

2.6 Deposition Techniques for the Polymer Thin Layers

There are two major techniques to fabricate a thin polymer layer on a substrate: dip-coating and spin-coating. In this study, dip-coating was the only method used to deposit PGMA and PAA onto the silicon substrates. During the deposition, one silicon wafer sample was immersed into and withdrawn from a target solution at a constant speed (Figure 2.6). After that, the solvent evaporated leaving the solute deposited on the surface. The layer thickness and uniformity are mainly dependent on the speed, the concentration, and the viscosity of the solution used.

In 1942, Landau and Levich[50] first used the Newtonian fluid model (ignoring

solvent evaporation) to show that the relationship between speed of withdrawal and film thickness is:

$$h = 0.944\,(Ca)^{1/6}\,\frac{\eta u_0^{1/2}}{\rho g} \qquad (1.2)$$

where h is film thickness, Ca is capillary number, η is solution viscosity, u_0 is experimental substrate withdrawal speed and ρ is solution density. Many experimental results agree well with this model[51].

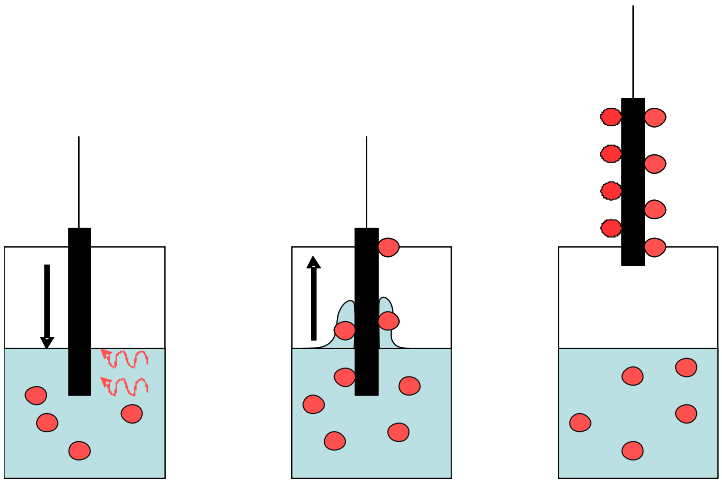

Figure. 2.6: Scheme of the dip-coating technology.

2.7 Techniques for films characterization

The main techniques used in this research were ellipsometry, AFM (Atomic Force Microscopy), contact angle measurement and TIRF (Total Internal Reflection Fluorescence). The basic principles of these techniques are discussed in this section. The

principles for TIRF will be discussed in the following separate section.

2.7.1 Ellipsometry

Ellipsometry is a sensitive way for measuring the thickness of homogeneous and isotropic layers. It is non-destructive and contactless, which makes it the main technique for thin film thickness measurement.

In ellipsometry, incident light interacts with the surface and the polarization is changed when light is reflected off the surface, which can be interpreted into surface properties, such as layer thickness, when the complex refractive index is known. The polarized light can be divided into a *p* component (wave oscillating phase parallel to the plane of incidence) and an *s* component (wave oscillating phase perpendicular to the plane of incidence)[53].

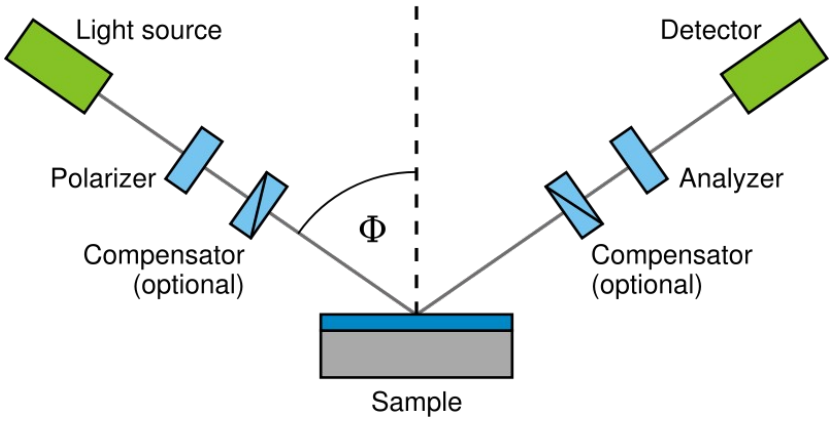

Figure. 2.7: Schematic drawing of an ellipsometer[52].

A schematic drawing of an ellipsometer is shown in Figure 2.7. The light source generates either monochromatic or broad band light. After polarization, the light normally becomes linearly polarized which incidents on the surface at a fixed angle Φ. The

elliptic polarized reflected light is collected at the other side of the sample and analyzed with the second polarizer, which is also called the analyzer. The direct parameters measured by ellipsometry are ellipsometric angle Ψ and Δ. The ellipsometric angles have such a relationship as[53]:

$$\rho = \frac{r_p}{r_s} = tan\Psi\, e^{i\Delta} \tag{1.3}$$

r_p and r_s are the amplitudes of the *p* and *s* light components, respectively. $Tan\Psi$ is the ratio of the two mutually orthogonal polarized components, while Δ is the phase-shift between the *p* component and the *s* component. Ψ and Δ are converted into layer thickness by choosing the appropriate elliptical polarization model.

2.7.2 Atomic Force Microscopy (AFM)

AFM is an efficient method to analyze surface morphology. As shown in Figure 2.8, during an AFM measurement, a tiny tip connected to the cantilever scans over the selected surface region. Due to the interaction (either attractive or repulsive) with the surface, the tip has different deflections. A laser is focused onto the tip. The deflection can be detected from the shift of the reflected laser from the tip by photodiode and converted into digital signals showing the topology of the surface.

The AFM used in this work (DI Dimension 3100) has two different scanning

modes: contact and tapping. In contact mode, the tip touches the surface directly. The variation in vertical scale can be measured by the deflection of the laser signal. In the tapping mode, the tip slightly touches the surface. It vibrates with a constant frequency and amplitude driven by cantilever. When the tip approaches the surface, the vibration is affected by the tip-surface interaction. Therefore, the amplitude measured by the laser is changed and can be interpreted as height information on the surface. Tapping mode is often used for the soft surface, such as polymer brushes, since it perturbs the surface less than the contact mode.

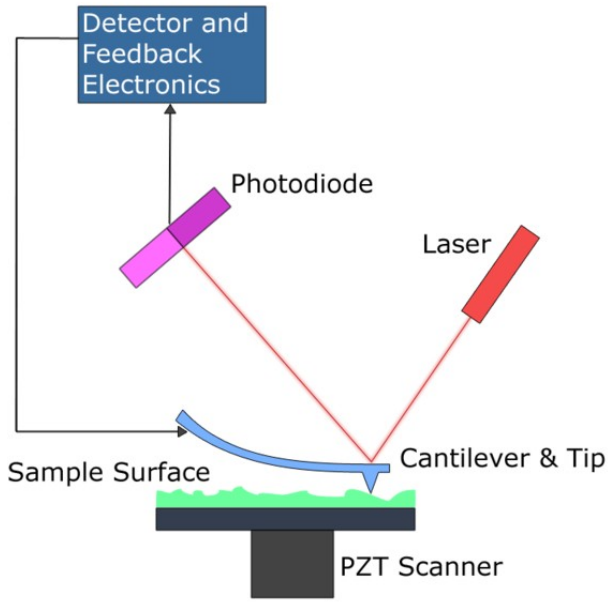

Figure 2.8: Block diagram of an AFM[54].

2.7.3 Contact Angle Measurement

When a liquid is placed on a solid substrate, it usually remains as a drop-like

shape forming a certain angle at the liquid and solid phase boundary. The contact angle is determined by the balance of liquid surface cohesive energy and the solid-liquid interfacial energy.

The wettability can be characterized base on the contact angle, as shown in Figure 2.9. Liquids which are attracted to a surface, for example, water towards a hydrophilic surface, will show a small contact angle. Liquids which do not wet the surface, for example, water on a hydrophobic surface, will have a large contact angle[67]. Figure 2.9 shows three examples of good wetting, poor wetting and complete wetting.

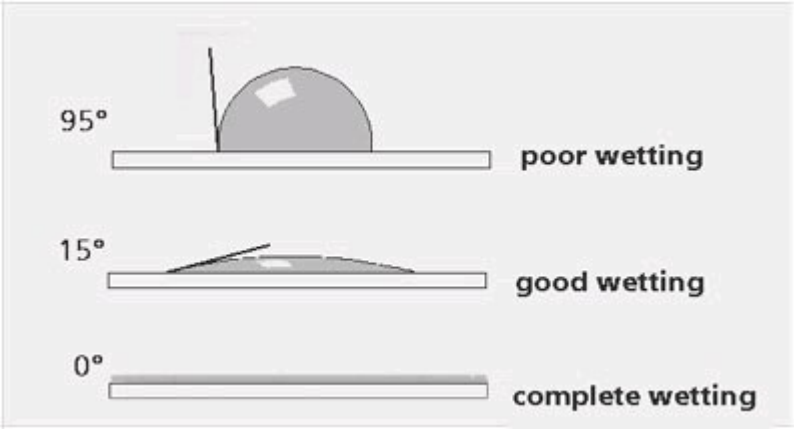

Figure 2.9: Examples of good wetting, poor wetting and complete wetting[55].

2.8 Total Internal Reflectance Fluorescence (TIRF)

When light travels from a high refractive index medium to a low refractive index medium and has an incidence angle greater than the critical angle, it is totally reflected (Figure 2.10).

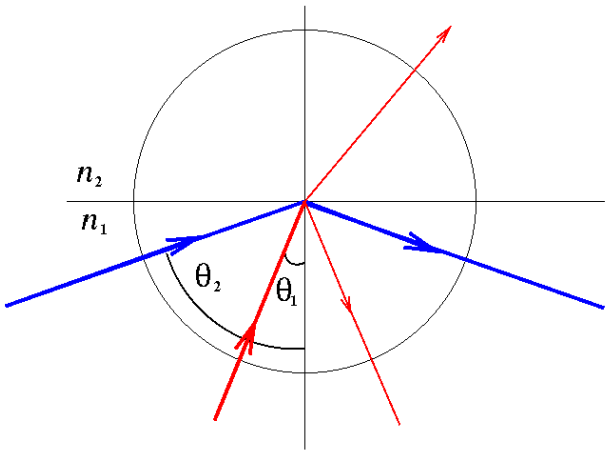

Figure 2.10: Normal reflection and refraction when the incident angle less than the critical value ($\theta_1 < \theta_c$) and the total reflection when incident angle greater than the critical value ($\theta_2 > \theta_c$). n_1 and n_2 are the refractive index of two media[56].

The critical angle is defined as $\theta_c = arcsin(n_2/n_1)$ (n_1 and n_2 are the refractive indexes for the more dense and less dense media). However, electromagnetic theory predicts that waves still penetrate into the boundary to hold the electromagnetic fields continuous. These waves are called *evanescent waves*. It is shown that the penetrating depth (d_p) for a evanescent wave is[57]:

$$d_p = \frac{\lambda_1}{2\pi}\left(n_1^2 \sin^2\theta_1 - n_2^2\right)^{-1/2} \qquad (1.4)$$

where λ_1 denotes the incident wavelength, θ_1 denotes the incidence angle and n_1 and n_2 are the refractive indexes of different media. Typically, the depth is on the order of ~100nm.

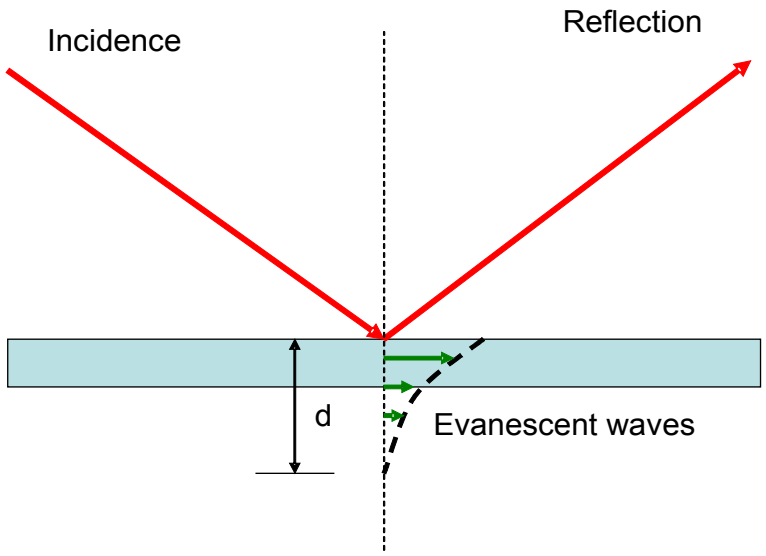

Figure. 2.11: Evanescent waves and its penetrating depth.

As shown in Figure 2.11, the evanescent wave is generated at the point where total reflection occurs. Within the penetrating depth (d), the amplitude decreases with increasing the distance from the surface. During penetration, the wave can excite the molecules in the range of d.

Since the penetration depth of the evanescent waves is on the order of 100 nm, they only excite the molecules in this narrow range, which is an efficient way to detect interfacial adsorption of optically active molecules. In this study, TIRF was used to determine the adsorption of fluorescent labeled protein on polymer brushes.

2.9 Protein – Polymer Surface Interactions

There are variety of mechanisms through which protein can interact the polymer surfaces. These protein-polymer surface interactions are classified as chemical, hydrophobic, van der Waals and electrostatic interactions. To control the protein binding on the surface, polymer brushes are often used to control the nature of the surface.

For example, Piehler *et al.*[58] found a decrease in protein adsorption when they grafted different polymer brushes, such as poly(oxyethylene) brush and polyacrylamide brush, on modified silicon wafers. Polymer brushes have also been widely used for surface modification to create biocompatible materials. Harris *et al.*[59] fabricated polymethacrylic acid brushes with RGD, a cell-adhesion peptide to facilitate cell adhesion. The surface adhesion of cells could easily be adjusted by altering the grafting density of the polymer brushes.

If the polymer surface is charged, the electrostatic interaction between the protein and the surface should be considered[60]. Dai *et al.*[43] synthesized PAA and activated the polymer with N-hydroxysuccinimide (NHS) and nitrilotriacetate (NTA)—Cu^{2+} complex sequentially. Their results indicate that the metal ion derivative of PAA significantly improved the immobilization of a protein on the surface.

However, the detailed picture of protein adsorption on a polymeric surface is still under investigation. Firstly, many different factors play roles during the interaction of such large macromolecules with a surface, such as hydrophobicity and the net charge on

the protein surface. Secondly, proteins can adopt different conformations during adsorption. When a protein approaches a polymer surface, it contacts the surface based on its initial conformation, which may not be the optimized conformation necessary for binding. Then the protein undergoes conformational changes. For example, Soderquist and Walton[66] studied the adsorption and desorption of plasma proteins (including albumin, globulin and fibrinogen) on copolypeptide and silicone surfaces. They found that the desorbed albumin had a different ellipticity, indicating that the secondary-structure of protein changed. Toscano and Santore[61] showed by AFM that fibrinogen adsorbed on a silica-based surface may have different conformations than that of the native protein.

Furthermore, when the surface already has been occupied by some protein molecules, the later contacting proteins induces another conformation change both to the molecules on the surface and to themselves. Recently, it was found that other factors may regulate the protein adsorption on the polymer surface as well, such as the surface temperature. Hollmann *et al.*[10] reported that the binding capacity of polyacrylic acid planar brushes after different heat treatments had different binding capacities. They found that adding a salt solution to PAA brushes at 40ºC increased the protein adsorption even when the brush height is decreased. In a contrast, protein adsorption to the polymer surface at 20ºC (namely room temperature) decreased when the brush height was decreased by adding salt.

Various theoretical models have been developed to quantitatively describe the

protein binding process. Basically, they can be divided into two different categories: thermo-statistical models and transport kinetic models. The thermo-statistical models describe the protein adsorption on the surface from the molecular level point of view. The benefit of this approach is that the molecular level mechanisms of adsorption are clear in these models. For instance, Szöllősi *et al.*[62] modeled three adsorption stages consisting of adsorption/desorption (stage 1), conformation changes(stage 2) and further stabilization (stage 3). The breakthrough curve obtained from this model had a similar shape to that observed in experiments. Although thermo-statistical models offer an explanation of molecular level mechanism of adsorption, they only give qualitative images of the adsorption process.

On the other hand, transport kinetic models derive the model equations using mass and charge conservation in the vicinity of the surface. Ramsden[63] studied the protein adsorption under a convective flow condition, and obtained a fairly good correlation with experiments. But, at the starting period of adsorption and desorption, the theory did not agree with the experimental results. Hlady *et al.*[64] applied pure phenomenal equations and quantitatively described the adsorption kinetics of low density lipoprotein (LDL) onto C18-silica. Tassel *et al.*[65] showed a partially reversible kinetic model of protein adsorption. They modeled the protein as a "disk" on the surface and accounted for only one conformational change for adsorbed protein. Quinn *et al.*[66] modeled a two-stage adsorption of proteins. Their results demonstrated that the interaction between proteins on

the surface decreased the adsorption rate because of steric effects. In general, transport kinetic models demonstrate quantitatively a good correlation with experimental results.

In summary, information about the surface modification with polymer brushes has been presented. Different kinds of polymer brushes have been discussed, including charged polyelectrolytes and mixed brushes. For the polyelectrolyte brush, the brush height can be adjusted by changing the ionic strength of the environment, while mixed brush can have its surface structure and composition distribution switched by changing environmental conditions. Thus, these two different types of polymer brushes provide a possible route to fabricate a modified surface with controllable properties, such as protein affinity.

References

(1) Zhao, B.; Brittain, W. J. *Progress in Polymer Science* **2000***, 25*, 677.

(2) Milner, S. T. *Science* **1991***, 251*, 905.

(3) Gong, P.; Wu, T.; Genzer, J.; Szleifer, I. *Macromolecules* **2007***, 40*, 8765.

(4) Wu, T.; Gong, P.; Szleifer, I.; Vlcek, P.; Subr, V.; Genzer, J. *Macromolecules* **2007***, 40*, 8756.

(5) Currie, E. P. K.; Sieval, A. B.; Fleer, G. J.; Stuart M. A. C.; *Langmuir* **2000***, 16*, 8324.

(6) Marko, J. F.; Witten, T. A. *Physical Review Letters.* **1991***, 66*, 1541.

(7) Milner, S.; Witten, T.; Cates, M. *Macromolecules* **1988***, 21*, 2610.

(8) Nystrom, D.; Lindqvist, J.; Ostmark, E.; Hult, A.; Malmstrom, E. *Chemical Communications* **2006***, (34)*, 3594.

(9) Dong R.; Krishnan S.; Baird B.A; Lindau M. ; Ober, C. K. *Biomacromolecules* **2007***, 8*, 3082.

(10) Hollmann, O.; Gutberlet, T.; Czeslik, C. *Langmuir* **2007***, 23*, 1347.

(11) Andruzzi, L.; Senaratne, W.; Hexemer, A.; Sheets, E. D; Ilic, B.; Kramer, E J.; Baird, B.; Ober, C.K. *Langmuir* **2004***, 21*, 2495.

(12) Dong, R.; Krishnan, S.; Baird, B. A.; Lindau, M.; Ober, C. K. *Biomacromolecules* **2007***, 8*, 3082.

(13) Ballauff, M.; Borisov, O. *Current Opinion in Colloid & Interface Science* **2006***, 11*, 316.

(14) Kawai, T.; Saito, K.; Lee, W. *Journal of Chromatography B, Analytical Technologies in the Biomedical and Life Sciences* **2003**, *790*, 131.

(15) Brittain, W. J.; Minko, S. *Journal of Polymer Science: Part A: Polymer Chemistry* **2007***, 45*, 3505.

(16) Alexander S. *J. Phys. (Paris)* **1977***, 38*, 977.

(17) de Gennes P. G. *J. Phys. (Paris)* **1976***, 37*, 1443.

(18) Parsonage, E.; Tirrell, M.; Watanabe, H.; Nuzzo, R. G. *Macromolecules* **1991***, 24*, 1987.

(19) Minko, S., Patil, S., Datsyuk, V., Simon, F., Eichhorn, K., Motornov, M., Usov, D., Tokarev, I., Stamm, M. *Langmuir* **2002***, 18*, 289.

(20) Liberelle, B.; Giasson, S. *Langmuir* **2007***, 23*, 9263.

(21) Luzinov, I.; Julthongpiput, D.; Malz, H.; Pionteck, J.; Tsukruk, V. V. *Macromolecules* **2000***, 33*, 1043.

(22) Iyer, K. S.; Luzinov, I. *Macromolecules* **2004***, 37*, 9538.

(23) Zdyrko, B.; Klep, V.; Luzinov, I. *Langmuir* **2003***, 19*, 10179.

(24) Zdyrko, B.; Varshney, S. K.; Luzinov, I. *Langmuir* **2004***, 20*, 6727.

(25) Klep, V.; Minko, S.; Luzinov, I.; *Polymeric Materials: Science & Engineering* **2003***, 89*, 248.

(26) Husseman, M.; Malmstrom, E. E.; McNamara, M.; Mate, M.; Mecerreyes, D.; Benoit, D. G.; Hedrick, J. L.; Mansky, P.; Huang, E.; Russell, T. P.; Hawker, C. J. *Macromolecules* **1999***, 32*, 1424.

(27) Baum, M.; Brittain, W. J. *Macromolecules* **2002***, 35*, 610.

(28) Ramaratnam, K.; Tsyalkovsky, V.; Klep, V.; Luzinov, I. *Chemical Communications* **2007***, 2007*, 4510.

(29) Rühe, J.; Ballauff, M.; Biesalski, M.; Dziezok, P.; Gröhn, F.; Johannsmann, D.; Houbenov, N.; Hugenberg, N.; Konradi, R.; Minko, S.; Motornov, M.; Netz, R. R.; Schmidt, M.; Seidel, C.; Stamm, M.; Stephan, T.; Usov, D.; Zhang, H. In *Polyelectrolyte Brushes;* Advances in Polymer Science; Springer: 2004; Vol. 165, 79.

(30) Witte, K. N.; Won, Y. *Macromolecules* **2006***, 39*, 7757.

(31) Wittemann, A.; Drechsler, M.; Talmon, Y.; Ballauff, M. *Journal of American Chemical Society* **2005***, 127*, 9688.

(32) Guo, X.; Weiss, A.; Ballauff, M. *Macromolecules* **1999***, 32*, 6043.

(33) Zhulina, E.; Balazs, A. C. *Macromolecules* **1996***, 29*, 2667.

(34) Minko, S.; Müller, M.; Usov, D.; Scholl, A.; Froeck, C.; Stamm, M. *Physical Review Letters* **2002***, 88*, 035502.

(35) Houbenov, N.; Minko, S.; Stamm, M. *Macromolecules* **2003***, 36*, 5897.

(36) Motornov, M.; Sheparovych, R.; Tokarev, I.; Roiter, Y.; Minko, S. *Langmuir* **2007***, 23*, 13.

(37) Ionov, L.; Sidorenko, A.; Eichhorn, K.; Stamm, M.; Minko, S.; Hinrichs, K. *Langmuir* **2005***, 21*, 8711.

(38) Draper, J.; Luzinov, I.; Minko, S.; Tokarev, I.; Stamm, M. *Langmuir* **2004***, 20*, 4064.

(39) Minko, S.; Muller, M.; Motornov, M.; Nitschke, M.; Grundke, K.; Stamm, M. *Journal of American Chemical Society* **2003***, 125*, 3896.

(40) Zhao, B. *Polymer* **2003***, 44*, 4079.

(41) Zhang, J.; Yang, Y.; Zhao, C.; Zhao, H. *Journal of Polymer Science Part A: Polymer Chemistry* **2007***, 45*, 5329.

(42) Szleifer, I. *Biophysical Journal* **1997***, 72*, 595.

(43) Dai, J.; Bao, Z.; Sun, L.; Hong, S. U.; Baker, G. L.; Bruening, M. L. *Langmuir* **2006***, 22*, 4274.

(44) Czeslik, C.; Jackler, G.; Steitz, R.; vonGrunberg, H. *Journal of Physical Chemistry B* **2004***, 108*, 13395.

(45) Wittemann, A.; Haupt, B.; Ballauff, B. *Physical Chemistry Chemical Physics* **2003***, 5*, 1671.

(46) Sperling, L. H. In *Polymeric multicomponent materials: an Introduction;* Wiley: New York, 1997.

(47) Lu X, DeSimone J. M. *Macromolecules* **1995**, *28*, 3022.

(48) Khutoryanskiy, V. V.; Dubolazov, A. V.; Nurkeeva, Z. S.; Mun, G. A. *Langmuir* **2004***, 20*, 3785.

(49) Khutoryanskiy, V. V.; Nurkeeva, Z. S.; Mun, G. A.; Dubolazov, A. V. *Journal of Applied Polymer Science* **2004***, 93*, 1946.

(50) Landau; Levich *Acta Physicochimica U. R. S. S.* **1942***, 17*, 42.

(51) Yimsiri, P.; Mackley, M. R. *Chemical Engineering Science,* **2006***, 61*, 3496.

(52) Wikipedia Ellipsometry. *http://en.wikipedia.org/wiki/Image:Ellipsometry_setup.svg* (accessed 01/21, 2008).

(53) Auciello, O.; Krauss, A. R. In *In situ real-time characterization of thin films edited by Orlando Auciello, Alan R. Krauss;* Wiley: New York, 2001; 263.

(54) "Wikipedia" Atomic Force Microscopy Block Diagram. *http://en.wikipedia.org/wiki/Image:Atomic_force_microscope_block_diagram.png* (accessed 01/19, 2008).

(55) Knuss Tensiometers Contact Angle Meter Surface Energy Surface Tension Wettability Pendant Drop Interfacial Tension Critical Micelle Concentration Bubble Pressure Tensiometer. *http://www.kruss.info/index.php?content=http%3A//www.kruss.info/techniques/contact_angle_e_2.html* (accessed 01/20, 2008).

(56) Wikipedia Total Internal Reflection. *http://en.wikipedia.org/wiki/Total_internal_reflection* (accessed 01/21, 2008).

(57) Lassen, B.; Malmsten, M. *Journal of Colloid and Interface Science,* **1996***, 179*, 470.

(58) Piehler, J.; Brecht, A.; Geckeler, K. E.; Gauglitz, G. *Biosensors and Bioelectronics,* **1996***, 11*, 579.

(59) Harris, B. P.; Kutty, J. K.; Fritz, E. W.; Webb, C. K.; Burg, K. J. L.; Metters, A. T. *Langmuir* **2006***, 22*, 4467.

(60) Dee, K. C.; Puleo, D. A.; Bizios, R. In *Protein-Surface Interactions;* Dee, K. C., Puleo, D. A. and Bizios, R., Eds.; An introduction to tissue-biomaterial interactions; Wiley-Liss: Hoboken, N.J., 2002; 37.

(61) Toscano, A.; Santore, M. M. *Langmuir* **2006***, 22*, 2588.

(62) Szöllősi, G. J.; Derényi, I.; Vörös, J. *Physica A: Statistical Mechanics and its Applications,* **2004***, 343*, 359.

(63) Ramsden, J. In *Kinetics of Protein Adsorption;* Malmsten, M., Ed.; Biopolymers at interfaces; Marcel Dekker: New York, 1998; Vol. 75, 656.

(64) Hlady, V.; Ho, C., H.; Britt, D., W. In *Quantitative Analysis of Protein Adsorption Kinetics;* Kallay, N., Ed.; Interfacial dynamics; M. Dekker: New York, 2000; Vol. 88, 741.

(65) Tassel, P. R. V.; Viot, P.; Tarjus, G *Journal of Chemical Physics* **1996***, 106*, 761.

(66) Quinn, A.; Mantz, H.; Jacobs, K; *arXiv:cond-mat/0607384,***Arxiv.org** 2007.

(67) Adamson, A. W.; Gast, A. P.; NetLibrary, I. **1997**, 784.

CHAPTER THREE

EXPERIMENTAL PROCEDURES

3.1 Introduction

In this chapter, the experimental procedures for fabricating the single-component and mixed brushes, characterization of the brushes, and protein adsorption measurements are presented. The TIRF data analysis method will be discussed in Chapter Five.

3.2 Chemical Reagents

3.2.1 Hydrogen Peroxide (H_2O_2)

Company Identification: VWR International

MSDS Name: Hydrogen Peroxide (30% solution), Reagent ACS

Catalog Numbers: VW3742-1

3.2.2 Concentrated Sulfuric Acid

Company Identification: Acros Organic

MSDS Name: Sulfuric Acid GR ACS

Catalog Numbers: 13361-0000, 13361-0010, 13361-0025

3.2.3 Toluene

Company Identification: BDH Laboratory Supplies

MSDS Name: Toluene, ACS Grade

Catalog Numbers: BDH1151-4LG

3.2.4 Methyl Ethyl Ketone

Company Identification: Spectrum Laboratory Products, Inc.

MSDS Name: Methyl Ethyl Ketone, ACS Grade

Catalog Numbers: M1265

3.2.5 Ethanol

Company Identification: EMD

MSDS Name: Ethyl Alcohol

Catalog Numbers: EMD 7272

3.2.6 Methanol

Company Identification: Aldrich

MSDS Name: Methyl Alcohol, anhydrous

Catalog Numbers: 32,241-5

3.2.7 N,N-Dimethylformamide

Company Identification: Aldrich

MSDS Name: N,N-Dimethylformamide, HPLC

Catalog Numbers: 02002MT

3.2.8 Chloroform

Company Identification: Spectrum

MSDS Name: Trichloromethane

Catalog Numbers: VO0836

3.2.9 Sodium Bicarbonate

Company Identification: Fisher

MSDS Name: Sodium Bicarbonate

Catalog Numbers: 790194

3.2.10 Sodium Carbonate

Company Identification: Fisher

MSDS Name: Sodium Carbonate

Catalog Numbers: 904799

3.2.11 Sodium Phosphate, Dibasic Anhydrous

Company Identification: J. T. Baker

MSDS Name: Sodium Phosphate, dibasic anhydrous, power

Catalog Numbers: E04H18

3.2.12 Potassium Phosphate, Monobasic

Company Identification: J. T. Baker

MSDS Name: Potassium Phosphate, monobasic, Crystal

Catalog Numbers: E09474

3.2.13 Ovalbumin

Company Identification: Sigma

MSDS Name: Albumin from Chicken Egg White, Grade V, minimum 98% agarose, gel electrophoresis

Catalog Numbers: 126K7009

3.2.14 Rhodamin B Isothiocyanate

Company Identification: AMRESCO

MSDS Name: Rhodamin B Isothiocynate

Catalog Numbers: 2387B006

3.3 Polymers Used for Surface Modification

3.3.1 Poly(glycidyl methacrylate) (PGMA)

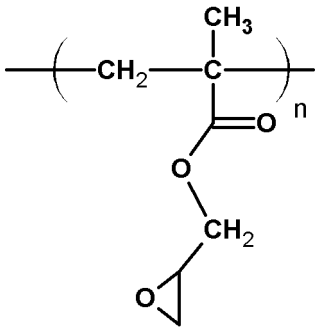

Structure 3-1: Poly(glycidyl methacrylate).

PGMA (Molecular weight 290,000g/mol, PDI=1.8) was synthesized via solution radical polymerization and purified with multiple precipitation by Dr. Viktor Klep, School of Materials Science & Engineering, Clemson University.

3.3.2 Carboxyl terminated poly(ethylene glycol)

Carboxyl terminated poly(ethylene glycol) was synthesized from a 10% solution of α-methoxy terminated poly(ethylene glycol) (M_n=5,000g/mol purchased from Aldrich) in acetone and succinic anhydride by stirring overnight at 55°C by Dr. Viktor Klep, School of Materials Science & Engineering, Clemson University.

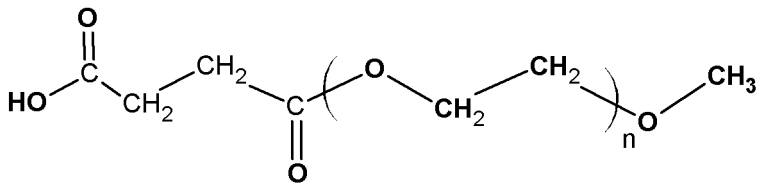

Structure 3-2: Carboxyl terminated poly(ethylene glycol).

3.3.3 Polyacrylic acid

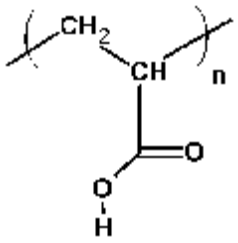

Structure 3-3: Polyacrylic acid.

Polyacrylic acid (M_n=26,500g/mol, PDI=1.12) was purchased from Polymer Source, Cat. No: P1598-AA. Polyacrylic acid (M_n~100k g/mol) was dried from a 35wt% PAA water solution obtained from Aldrich (Cat. No. : 10828MC).

3.4 Experimental Procedures for Fabrication of Polymer Thin Layer

The experimental procedures used in the present research are based on previous methods of synthesizing a single-component brush[1,2]. In this work, two different substrates were used: a silicon wafer and a glass slide. But they underwent the same procedures throughout the whole brush fabricating process. Thus, it is reasonable to suppose that the polymer brushes on the silicon wafers and glass slides have the same

structure and grafting density. After the fabrication, the brush on the silicon wafer was used for the characterization by AFM and ellipsometry. The brush on the glass slide was tested for the protein adsorption by TIRF.

Highly polished silicon wafers (<100> orientation, purchased from Semiconductor Processing Co.) were cut into the same size as the glass slides (25mm×75mm). Deionized water and ultrasonic agitation was used to rinse the wafers and slides (3×10min). Then the wafers and glass slides were cleaned using piranha solution (30% Hydrogen Peroxide : 98% Sulfuric Acid = 1:3 v/v) with 30min rinsing and ultrasonic agitation at 60ºC. After that, a Mayer Fientechnik D-3400 dip-coater was used with 4 mm/s operation speed to dip-coat the samples from 0.08% PGMA chloroform solution to form the PGMA layer. The dip-coating equipment was placed in a clean room to avoid contamination from the surroundings. Then, the samples were annealed for 60min at 110°C. After that, a 3% solution of carboxyl terminated PEG (M_n=5000 g/mol) in ethyl alcohol was deposited onto PGMA modified silicon wafers and glass slides surfaces and dried. The samples were kept in an oven at 110°C for 2hrs (short interval), 4hrs (medium interval) and overnight (approximately 15hrs, long interval) grafting time. Ungrafted PEG chains were rinsed off with methyl ethyl ketone for 30min and a total of three rinses using an ultrasonicator bath at 60°C. Wafers were stored in a nitrogen box overnight and then dip-coated from 1% PAA ethyl alcohol solution. Next, the samples were kept in an oven at a constant temperature of 55°C for 5mins (short interval), 30mins

(medium interval) and 60mins (long interval) grafting period. Ungrafted PAA chains were rinsed off with ethyl alcohol for 3min and a total of three rinses using an ultrasonicator bath at the room temperature. In this way, different PAA grafting amounts were obtained. All samples were then dried overnight at the room temperature to evaporate any residual solvent.

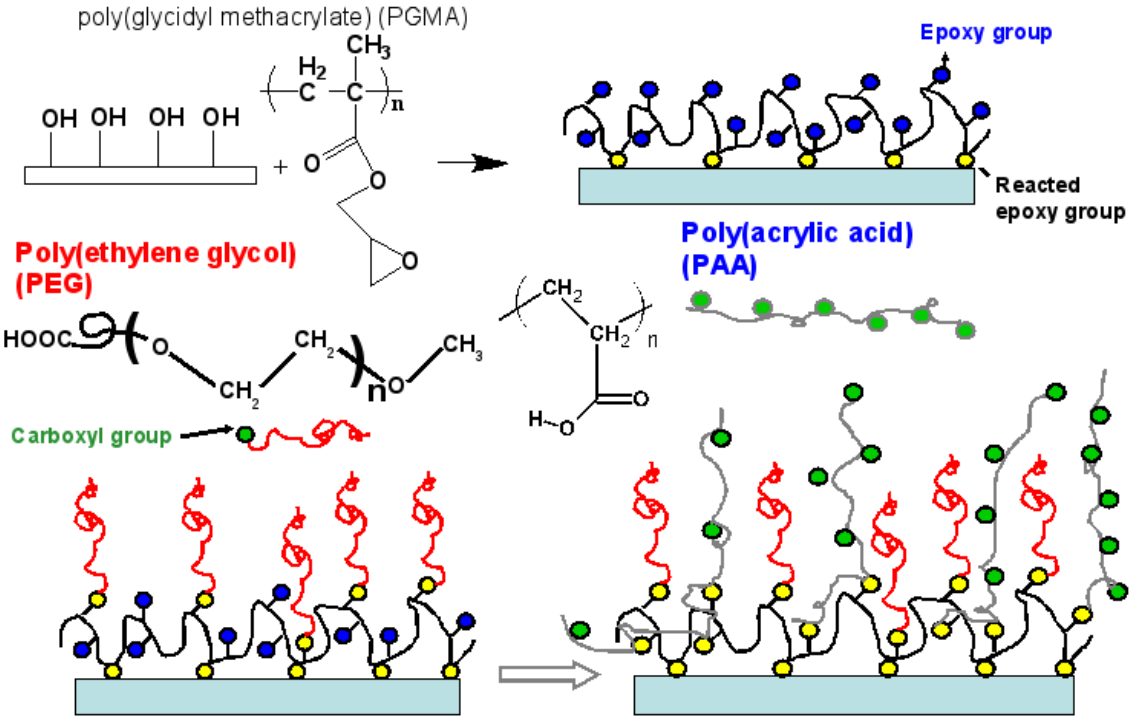

Figure 3.1: Reaction scheme of fabrication of the mixed PEG/PAA brushes.

Figure 3.1 shows the reaction scheme for fabricating the mixed PEG/PAA brushes. Firstly, epoxy groups in PGMA reacted with the hydroxy groups on the substrate. It was shown that most of the epoxy groups are preserved during this process[2,5-7]. Then, carboxy-terminated PEG was used to construct the PEG polymer brush by reacting the carboxy groups and the epoxy groups on the substrate. Finally, PAA was

used to react with the epoxy groups left on the substrate yielding mixed PEG/PAA brushes.

During the PAA layer grafting, there were two competitive reactions possible with the PGMA's epoxy groups: PAA's carboxyl groups and ethanol's hydroxyl groups (during deposition of PAA films by dip-coating). However, Wu *et al*.[3] showed that the reaction of epoxy with carboxyl groups is ten times faster than that with hydroxyl groups. When the environment is neutral or basic, the difference is even larger.

Another fact to be considered is that PAA has multiple functional groups along the chain, which can form multiple connections on the surface (loop-train-tail model[4], Figure 3.2).

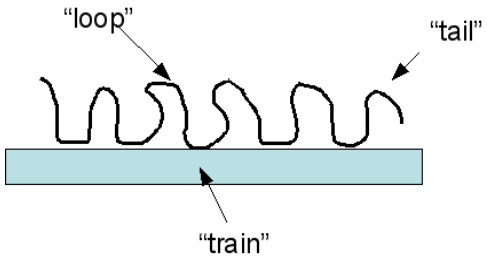

Figure 3.2: Loop-train-tail structure of adsorbed polymer chains.

3.5 Characterization Procedures for the Polymer Thin Layers

The thicknesses of the polymer brushes were measured using the COMPEL automatic ellipsometer (InOmTech, Inc.). Incident light was set to an angle of 70º. The refractive index for the polymer was set to 1.5, except for PGMA (1.525). The

compensator was applied when the film thickness was less than 11nm and removed when the thickness was more than 14nm. For thicknesses between 11nm and 14nm (including 11nm and 14nm), the average thickness was calculated with and without the compensator.

Knowing the grafting thickness, both the grafting amount and the grafting density were calculated. If the polymer density (ρ) is accepted to be the same as in bulk, the grafting amount (Γ) can be obtained by:

$$\Gamma = h\,\rho \tag{3.1}$$

where h is the brush thickness measured by ellipsometry. The grafting density (σ) is given by[1,2,5-6]:

$$\sigma = \frac{602.3\,\Gamma}{M_n} = \frac{602.3\mathrm{h}\,\rho}{M_n} \tag{3.2}$$

According to the supplier, the densities of the polymers used are 1.09g/cm^3 for PEG and 1.25g/cm^3 for PAA.

The Dimension 3100 AFM was used to study the sample's surface morphology in the dry state. Tapping mode was selected. At least 3 spots on each sample were examined to generate representative images for each substrate. Images were gathered under a scan rate of 1Hz, internal gain of 0.2 and proportional gain of 0.4. Tips from Mikro-Masch

were used as received. The tip information is shown in Table 3.1.

Full Tip Cone Angle (º)	30
Tip Height (μm)	20-25
Tip Curvature Radius (nm)	<10
Backside Coating	Aluminium
Spring Constant (N/m)	40

Table 3.1: The characteristics of the AFM tips used in this study.

Surface roughness was obtained from the AFM morphology images. The root-mean-square (RMS) value was used to characterize the roughness[26]:

$$RMS = \sqrt{\frac{\sum_{i=1}^{N} (z_i - \bar{z})^2}{N}} \tag{3.3}$$

where z denotes the height in the images and N denotes for the number of points measured.

Another surface parameter obtained from the AFM image is the power spectrum density (PSD). PSD is a parameter which shows the density of each frequency component in one image profile. It was used to find the surface periodical domain size in the structure.

A Kruss Drop Shape Analysis (DSA) system, including the Kruss G10 contact angle instrument and data analyzing (software version 1.51.0.26), was used to obtain the water contact angle. Five HPLC water drops with constant volume were placed on the sample surface. After 30 seconds the drop shape images were obtained and the "Sessile

Drop Tangent Fitting" method was used to fit the drop shape and calculate the contact angle.

3.6 Protein Labeling and the Measurement of Adsorption onto Polymer Surfaces

In this research, chicken egg white ovalbumin from Aldrich was used, which contains 345 residues and the molecular weight was approximately 45K D[9]. From the Protein Data Bank (PDB) database, ovalbumin is a small, two-leaf-like protein. Its structure is shown in Figure 3.3. The 4mg/ml protein solution was prepared in phosphate buffer (0.002mol/L KH_2PO_4 and 0.008mol/L Na_2HPO_4). Rhodamine B (RhB, Figure 3.4) was used to label the protein. One hundred milliliters protein phosphate solution were mixed with 0.25ml 8mg/ml RhB Isothiocyanate in DMSO. The labeling reaction was conducted overnight at room temperature. Then, the mixture was injected through a chromatographic column filled with Sephadex-GX50, which is a cross-linked silicon beads with a special pore size greater than the RhB but smaller than the protein. Separated labeled protein was collected. A Shimadzu UV-3101PC UV-Vis-NIR Scanning Spectrophotometer was used for measuring the protein concentration and labeling density. Detection wavelength range was selected from 250nm to 700nm with medium scan speed. The calibration curve to calculate the protein concentration and the labeling density was provided by Dr. Bogdan Zdyrko.

Figure 3.3: The structure of ovalbumin from PDB (Protein Data Bank)[10].

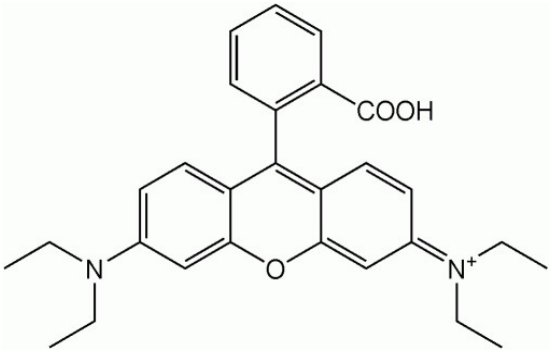

Figure 3.4: Chemical structure of Rhodamine B.

TIRF was used to quantify the amount of protein adsorption on polymer brushes. A block diagram of the TIRF apparatus, built in our lab by Dr. Bogdan Zdyrko, is shown in Figure 3.5. Monochromatic 532nm laser signal was generated by DPGL Series Modulated Green Laser Modulus (Part No.: DPGL-01S-TTL). FisherFinest Premier

microscope slides (Cat. No. 12-544-1), which have nearly the same refractive index as the prism, were used. The slides were modified with polymer brushes. The fluorescence detector (Si Photodiode, diameter is 11.0 mm, from Edmund Optics) was placed perpendicular to the prism to collect fluorescence signals from the labeled proteins. Slides with brushes were placed in the flowing cell. Protein solution (~40ppm, labeling density 0.8) were injected into the flowing cell at the rate of 0.8g/min. The fluorescence emitted was collected by the detector. The data were analyzed using LabView software to capture the time-dependent adsorption breakthrough curves.

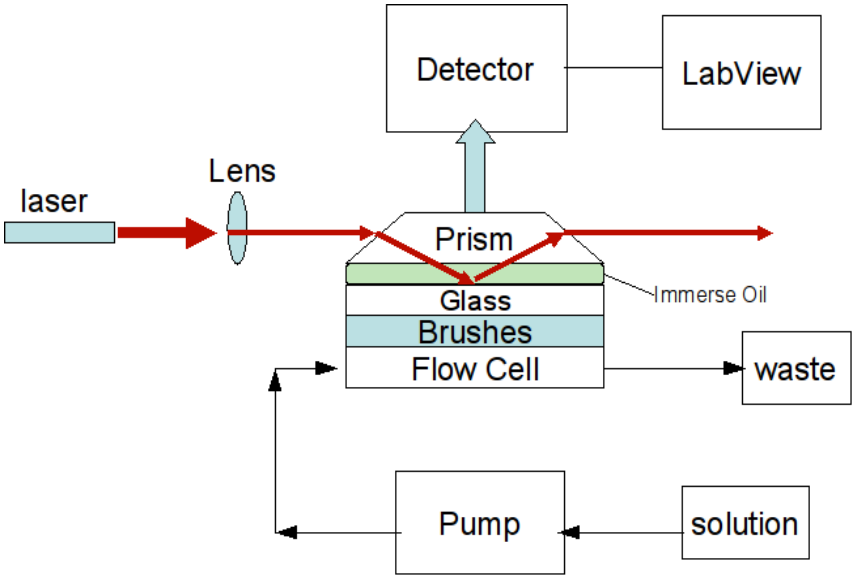

Figure 3.5: The block diagram of TIRF.

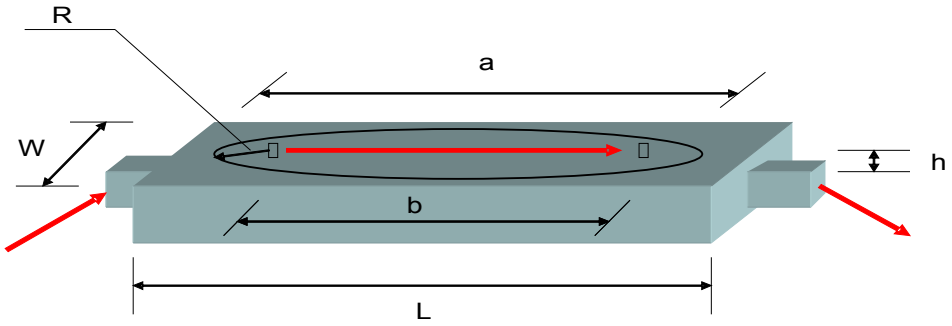

Figure 3.6: Dimension of the TIRF's flow cell. Arrows indicate the direction of liquid flow in this cell.

Figure 3.6 shows the the dimensions of the flow cell. Details are provided in Table 3.2.

L (Length)	85
W (Width)	45
a (Cell Long Axis)	65
b (Flow Part Length)	50
h (Thickness)	2
R (Radius)	20

Table 3.2: The flow cell's dimension. Units are nanometers.

References

(1) Draper, J.; Luzinov, I.; Minko, S.; Tokarev, I.; Stamm, M. *Langmuir* **2004**, *20*, 4064.

(2) Iyer, K. S.; Luzinov, I. *Macromolecules* **2004**, *37*, 9538.

(3) Wu, S.; Soucek, M. D. *Polymer*, **1998**, *39*, 5747.

(4) Jones, R. A. L.; Richards, R. W. In *Polymers at surfaces and interfaces;* Cambridge University Press: Cambridge ; New York, 1999; 377.

(5) Zdyrko, B.; Klep, V.; Luzinov, I. *Langmuir* **2003**, *19*, 10179.

(6) Zdyrko, B.; Varshney, S. K.; Luzinov, I. *Langmuir* **2004**, *20*, 6727.

(7) Bogdan, Z. PhD Thesis, *Thin Polymer Films for Biomedical Applications: Synthesis and Characterization*, School of Materials Science & Engineering, Clemson University, Clemson, SC, 29634, 2005.

(8) "Veeco Co." In *Dimension(TM) 3100 Manual;* 2000; Vol. 4.43B, 485.

(9) Nisbet,D., A.; Saundry R., H.; Moir, A.; Forthergill, A.; Fothergill, J., E; *European Journal of Biochemistry* **1981***, 115*, 335

(10) Protein Data Bank, DOI: 10.2210/pdb1ova/pdb

CHAPTER FOUR

GRAFTING OF SINGLE & MIXED PEG AND PAA BRUSHES

4.1 Introduction

Mixed polymer brushes are widely used as novel stimulus-responsive materials[1-4], because of their ability to switch surface properties under different conditions in response to changes in their environment. The surface properties of mixed polymer brush systems can be altered by changing the dominant component at the interface by applying an appropriate solution[9-11]. Mixed brushes, demonstrating transitions from hydrophobic to hydrophilic[5], from negatively charged to positively charged[4], and from adhesive to less-adhesive[6] surface states have been synthesized. A controllable protein adsorption material can be made through fabrication of binary polymer brushes, and protein affinity can be altered at the interface by modifications of a liquid medium.

In this work, to fabricate a mixed brush system with controllable protein adsorption, a "grafting-to" method was used. Poly(glycidyl methacrylate) was used as the primary anchoring layer to provide epoxy groups on the substrate for the grafting. End carboxyl terminated poly(ethylene glycol) (PEG, a protein repelling polymer), followed by polyacrylic acid (PAA, a protein adsorptive polymer) were deposited on the substrate to form the mixed brush via the reaction between carboxyl and epoxy groups. PEG, as a non-ionic polymer, is able to form a stable brush with a constant layer height under the variation of pH or ionic strength in aqueous solutions. Densely grafted PEG chains can also prevent proteins from adsorbing[7, 8]. In contrast, PAA has an affinity to bind proteins[9-14] because of its carboxyl groups and also the hydrophobic portions of its chain. In addition, it demonstrates a brush height transition in response to different ionic strengths[11, 15-19]. PAA in its acid form is also known to be miscible with PEG[30]. The

miscibility is important, because in the mixed brush synthesis, PAA needs to penetrate through grafted PEG chains in order to react with the PGMA surface. By grafting polymers with different protein affinities, it is hypothesized that this kind of mixed brush can have either a PAA-dominant or a PEG-dominant surface, allowing a switch between "turn-on" and "turn-off" status for protein adsorption. Namely, as represented in Figure 4.1, when PAA is suppressed, PEG dominates the surface and repels protein. This is the protein adsorption "off" state. When the environmental condition has been changed to favor the extension of PAA chains, PAA then occupies the surface and adsorbs protein. This is the protein adsorption "on" state.

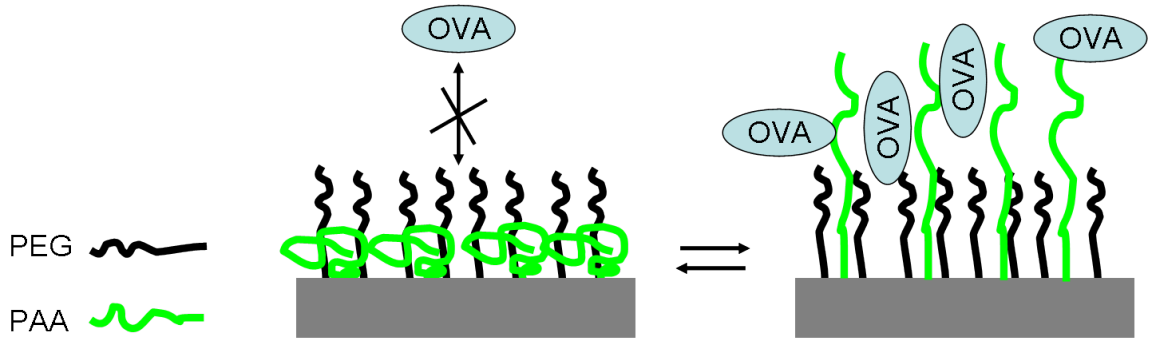

Figure 4.1: The responses of the mixed brushes under different conditions, OVA denotes to the ovalbumin. Left image shows the protein adsorption "off" status and the right shows the protein adsorption "on" status.

In this study, the first objective was to synthesize mixed brushes to optimize the structure to be effectively tuned. Longer PAA chains and shorter PEG chains are crucial for positioning PAA above and below the PEG layer. Thus, PEG with a lower number-average molecular weight (Mn) (5,000g/mol) and PAA with a higher Mn (26,500g/mol) were selected. The calculated contour length for 5k PEG is 33.4nm, while for the 26k PAA is 88.3nm. According to Merrill *et. al.*[31], the lower molecular weight PEG brushes with moderate grafting density should still repel proteins and prevent adsorption,.

During the brush synthesis, PEG was grafted first to the PGMA layer and then PAA was grafted. This grafting order was selected because PAA has much more affinity for a PGMA surface than does PEG. It was found that if the reverse order was used, i.e. the polymer with more affinity being grafted first, the grafted amount of the second polymer was significantly reduced[5].

The second objective was to establish the determining factors for protein adsorption onto this type of mixed polymer brushes. It was hypothesized that PEG and PAA grafting densities would be the crucial factors for the brush performance. Namely, when holding the PEG amount constant, the amount of protein adsorbed onto the substrate would increase if more PAA chains are grafted. When holding the PAA grafted amount constant, the protein adsorption would decrease if the amount of PEG grafted is increased. To investigate this hypothesis, a series of samples with different PEG and PAA grafting densities was prepared.

Initially, PEG brushes were prepared in three different grafting density ranges (high: greater than 1 chains/nm^2; medium: 0.5-1 chains/nm^2; and low: less than 0.5 chains/nm^2). Then, PAA brushes, at three different grafting densities depending on the previous PEG grafting density, were grafted through these PEG brushes. The nine samples with combinations of PEG and PAA grafting densities provided a mixed brush "library" with different PEG/PAA brush densities. In this chapter, the surface morphology and wettability of these mixed brush surfaces were investigated. The brush height transitions of single-component PAA brush and mixed PAA/PEG brush were also studied.

4.2 Characterizations of Single-Component PEG Brushes

The first experiment was to evaluate the PEG grafting capacity of the PGMA layers as a function of the grafting time. For this purpose, PGMA layers with different thicknesses were prepared by dip-coating silicon wafers from PGMA chloroform solutions of different concentrations. Then, PEG macromolecules were grafted onto PGMA-modified silicon wafer at 110°C for three different time periods: overnight (~15hrs), 4hrs and 2hrs. The grafted layer thickness was obtained by ellipsometry and the grafting density was calculated by Equation (3.2) and plotted against the PGMA layer thickness in Figure 4.2.

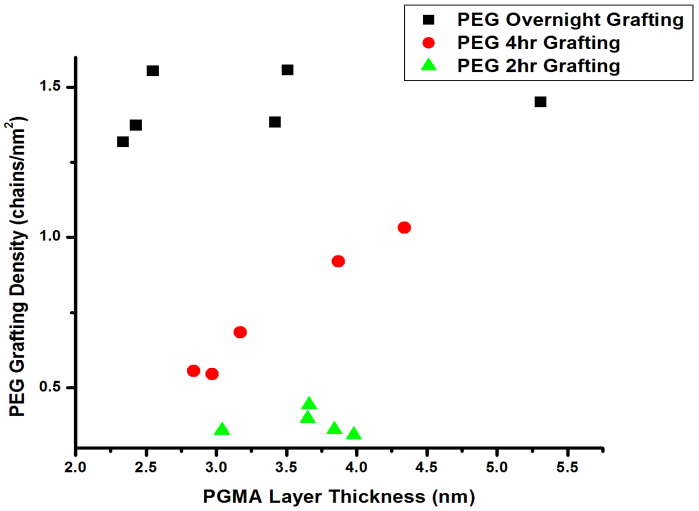

Figure 4.2: PEG grafting density versus the PGMA layer thickness with three grafting times (Overnight grafting is approximately 15 hours.).

Neither the overnight nor the short time 2 hrs grafting shows a clear dependence on PGMA layer thickness. However, the PEG grafting density at 4hrs grafting time shows an obvious dependence on the PGMA layer thickness. It is suggested that there are at least two energy barriers in the grafting process: the effective polymer reptation to the more concentrated surface region and the activation energy for the carboxyl-epoxy

reaction. Not all chain reptation brings the reactive end-groups to the vicinity of the surface. For the shortest times, diffusion of the end carboxyl group is the rate determining step for the process. For longer grafting times, the surface availability needs to be considered because the surface is already occupied with grafted chains. Thus, when the grafting time is sufficiently long, the epoxy layer is reacted to its maximum capacity, and the PEG grafting density is independent on the PGMA layer thickness. Also it should be noted that grafting densities of some overnight grafting samples were approximately 1.5 chains/nm^2 or more, which shows that the PGMA layer has a very large capacity as the primary anchoring layer. In contrast, for 4hr grafting times, the grafting density is dependent on the time which is necessary for the penetration of the PEG chains into PGMA layer. Thus, a clear dependence is seen on the PGMA layer thickness. In general, the PGMA layer has the potential to be an effective anchoring layer for grafting PEG brushes.

In this work, PGMA layers with thicknesses between 3-3.5nm were used. Fourteen samples of PEG brushes were obtained by depositing PEG onto PGMA layers with the three different annealing times (overnight, 4hrs and 2hrs). The brush heights were measured by the ellipsometry and the grafting densities were calculated from these thicknesses and are shown in the Appendix A3. The average grafting densities for each grafting time are shown in Table 4.1, and are also plotted in Figure 4.3. From Figure 4.3, it is evident that three different grafting density levels can be obtained by altering the PEG grafting time.

Surface morphologies of the grafted PEG layers by AFM tapping mode are shown in Figure 4.4 (low resolution) and Figure 4.5 (high resolution). Crystal structures can be clearly seen for high grafting density PEG samples (Figure 4.5 (1a)). The densely grafted

PEG brush is totally covered with crystals, which indicates a high grafting density. With decreasing grafting density, crystals form in isolated crystal domains[23] instead of a continuous layer on the surface images (Figure 4.5 (2a) and (3a)).

Annealing time (hr)	Average PEG grafting density and the standard deviation (chains/nm^2)
~15	1.3±0.10
4	0.8±0.09
2	0.4±0.04

Table 4.1: PEG grafting densities obtained by three different annealing times on PGMA-modified silicon wafers.

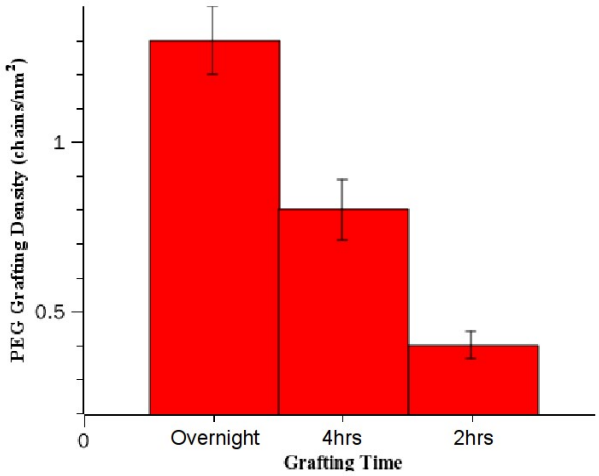

Figure 4.3: PEG grafting densities obtained by different grafting times (overnight grafting is approximately 15 hours).

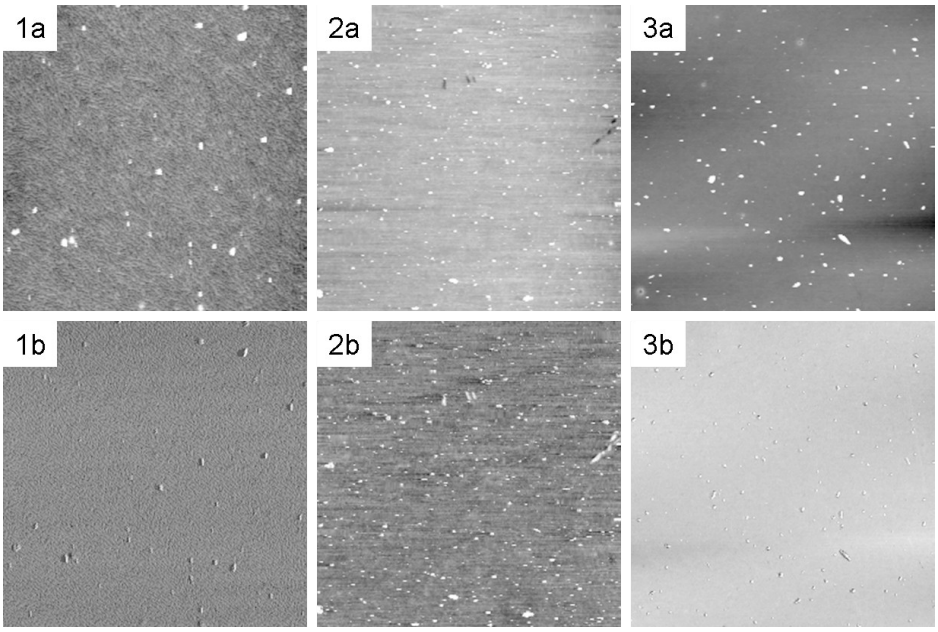

Figure 4.4: AFM images of PEG brushes, grafting density 1.38chains/nm^2 (1), 0.68chains/nm^2 (2) and 0.44chains/nm^2 (3). Row a) and row b) are height and phase images, respectively. Scan size is 10μm×10μm, vertical scale is 20nm in height and 30° in phase images.

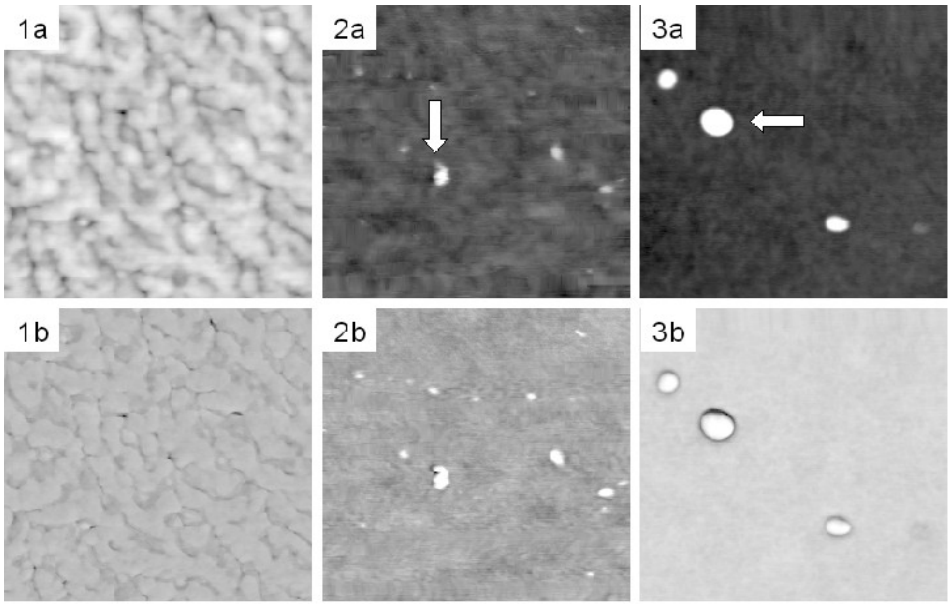

Figure 4.5: AFM images of PEG brushes,grafting density 1.38chains/nm^2 (1), 0.68chains/nm^2 (2) and 0.44chains/nm^2 (3). Row a) and row b) are height and phase images, respectively. Scan size is 1μm×1μm, vertical scale shown in picture in height is 15nm and 30° in phase images. Arrows in 2a) and 3a) indicate the individual PEG crystals.

4.3 Characterizations of PAA Brushes

Single-component PAA brushes were synthesized on PGMA surfaces to check the PGMA's capacity for grafting PAA chains. Based on the results discussed for single-component PEG brushes in section 4.2, the PGMA layer thickness was chosen to be between 3 to 3.5nm for the PAA grafting. PAA was deposited by dip-coating PGMA-modified silicon wafers into a 1% PAA solution in ethyl alcohol. The dip-coated samples were annealed for three different time periods (5mins, 30mins and 60mins) at 55°C. The brush thicknesses were measured by the ellipsometry, from which the PAA grafted amounts on the surface were calculated via Equation (3.1). The brush heights and grafted amounts are reported in the Appendix A3. The PAA grafted amounts are plotted against the grafting times in Figure 4.6. Thirty minutes and sixty minutes grafting of PAA to a PGMA surface gave 6.1mg/m^2 and 7.8mg/m^2, respectively. The grafted amount of PAA increased slowly when the grafting was done overnight (approximately 15 hours). This is because reacted PAA occupied most of the surface and prevented additional PAA chain segments from migrating to the boundary after sufficient grafting time. Therefore, the hindrance of further grafting was so high that it retarded the reaction rate.

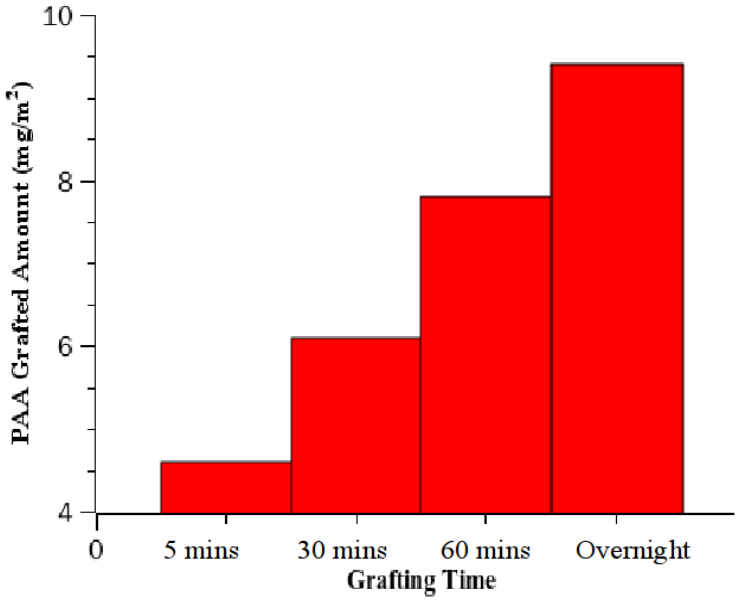

Figure 4.6: PAA grafting amount on PGMA-modified surface versus different annealing times. Overnight is approximately 15hrs (900mins).

The surface morphologies of these single-component PAA brushes were studied via tapping mode AFM. Two samples which had the grafting amounts of 4.6mg/m^2 (related to 5mins grafting) and 7.8mg/m^2 (related to 60mins grafting) were studied. The AFM images are shown in Figure 4.7 (1) and (2), respectively. Both samples have "meteor crater" structures. This structure became rougher when more PAA was grafted. This could also be seen from the Power Spectrum Density (PSD) analysis. PSD analysis of height images (Figure 4.7 (1a) and (2a)) is illustrated in Figure 4.8. The mean periodic grain size is larger for densely grafted (0.11 μm) than for sparsely grafted PAA layers (0.04μm). The possible reason is that PAA forms a cluster structure because of the multiple connections to the surface. As shown in Figure 4.9, when grafting density is low, each cluster is formed by a few PAA chain segments, which leads to small domains on the surface. When grafting density is higher, PAA chains start to form dense connections

and thus not only increase the brush height but also inflate the cluster size, which display a major periodic grain size drift in PSD. In addition, the PAA brush structures obtained are similar to that reported by Gupta *et al.*[28], who grafted PAA to PET fiber (Figure 4.7 (3)).

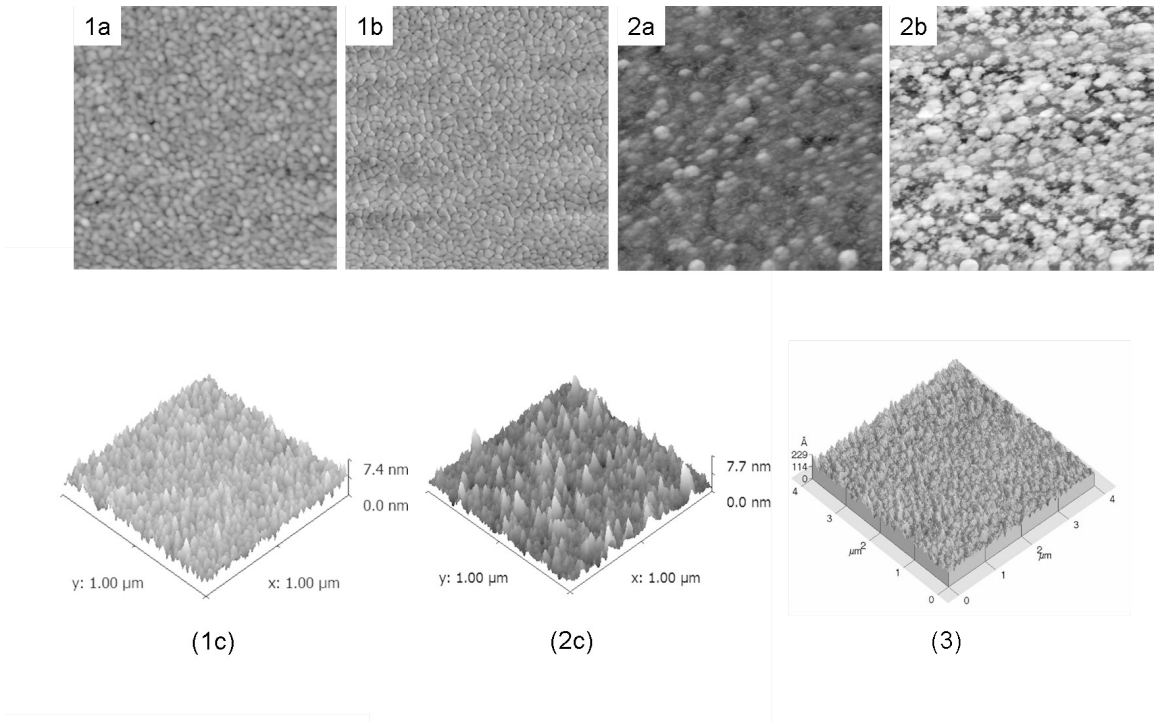

Figure 4.7: AFM morphology of one-component PAA brushes grafted on PGMA layer, with grafting amount 4.6 mg/m^2(1) and 7.8 mg/m^2(2). (a) is height image, (b) is corresponding phase image. Dimension is 1µm×1µm, vertical scale and phase scale is 10nm and 10°. Phase scale for (2b) is 60°. (3) is taken from Ref28.

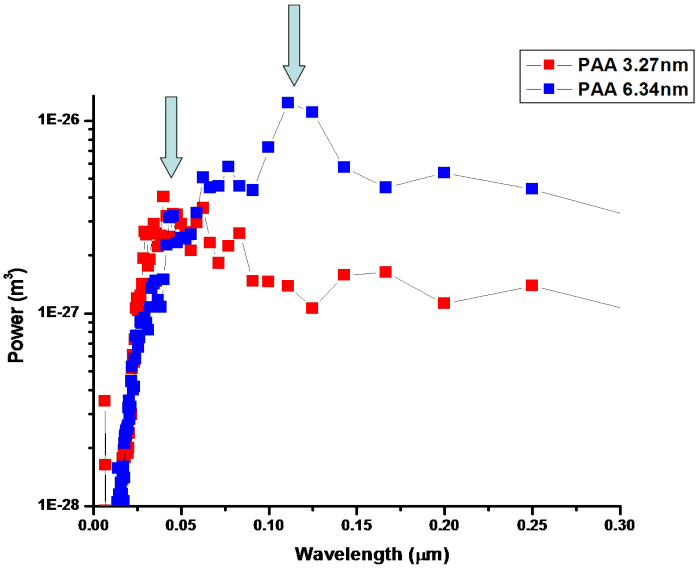

Figure 4.8: Power spectrum density (PSD) analysis of PAA brush height images Figure 4.7 1(a) and 2(a). Arrow indicate two main peaks of 40nm (Left) and 111nm (Right).

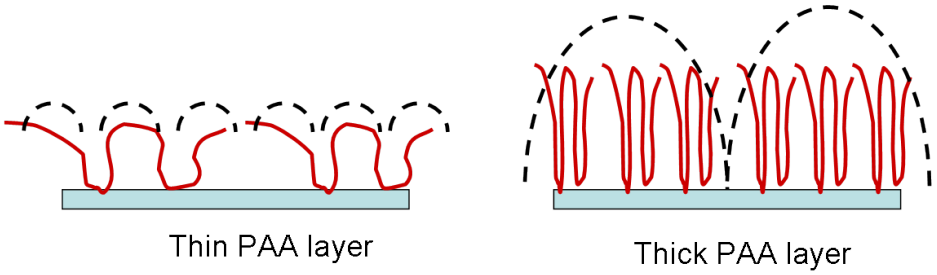

Figure 4.9: Schemes of sparsely grafted and densely grafted PAA layers structures.

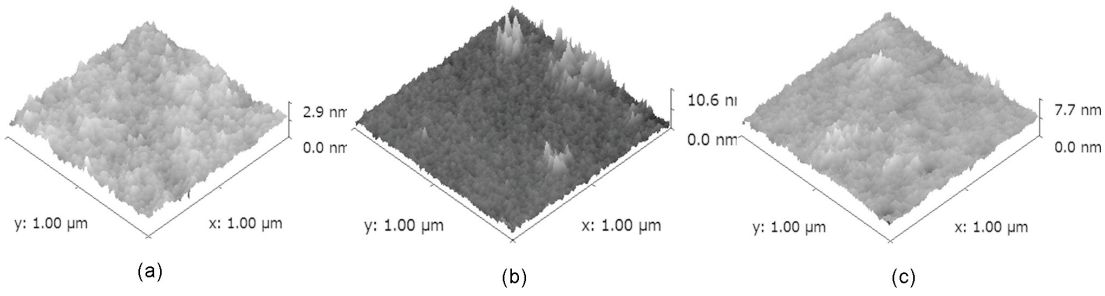

Figure 4.10: AFM morphology of dry state (a), under water (b) and under buffer with 1mol/L NaCl (c) of one component PAA brush. RMS is 0.2nm (a), 0.6nm (b) and 0.7nm (c), respectively. PAA grafting density is 0.2 chains/nm^2.

To investigate the morphology of the single-component PAA brushes in aqueous solution, another sample (PAA grafting amount 7.3 mg/m^2, grafting density 0.2 chains/nm^2, both are calculated from the brush height: 5.8nm) was scanned under water and in phosphate buffer using AFM contact mode (Figure 4.10). Under water (Figure 4.10b) and buffer (Figure 4.10c), periodic "meteor crater" structures observed were similar to that observed for the dry state.

To investigate the brush height transition under various aqueous conditions, the brush height was measured by contact mode AFM. Before the scanning, scratches were made in the same sample using one AFM tip. The sample was then scanned by contact mode AFM in ambient air, under water, under phosphate buffer and under salted phosphate buffer with 1mol/L NaCl (Figure 4.11). The brush height was obtained by subtracting the substrate height from the total height column-averaged from the AFM images. The results are plotted in Figure 4.12. Significant brush extension was observed when the sample was immersed in the buffer solution. Increasing the ionic strength in the buffer solution greatly reduced the PAA extension, from 44nm to 14nm. These results show that the polyelectrolyte brush height is influenced by ionic strength. This agrees well with the literature[19]. It also demonstrates the tuning capability of PAA chains using ionic strength.

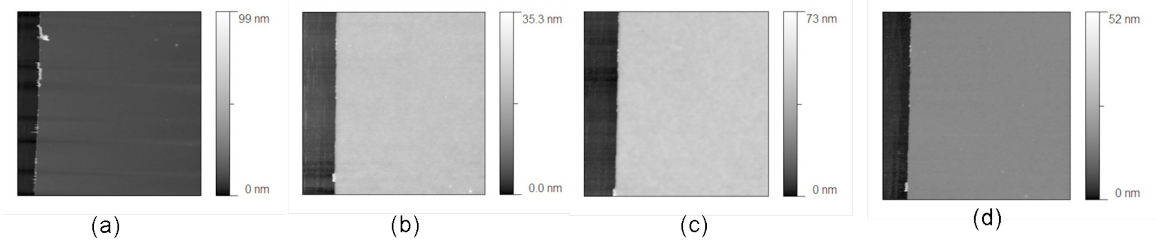

Figure 4.11: AFM height images of the single-component PAA brush with scratches on the left under dry(a), under water (b), phosphate buffer(c) and salted buffer with 1mol/L NaCl (d) by contact mode. Scanning size is 1μm×1μm.

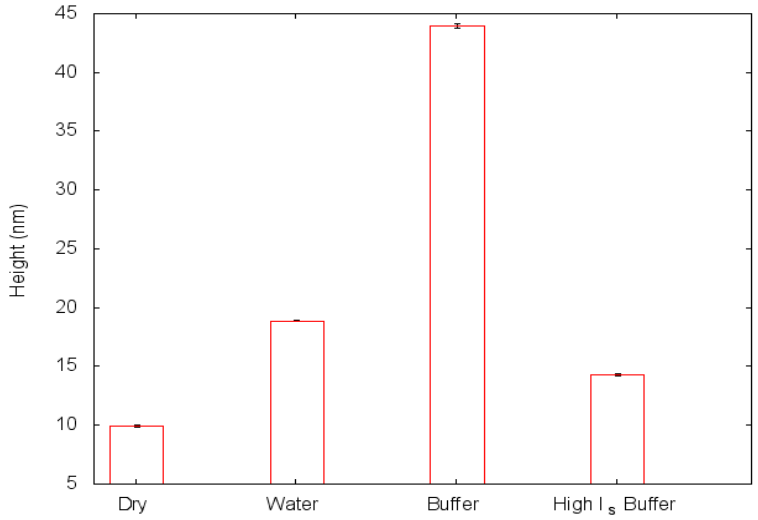

Figure 4.12: Column-averaged PAA brush height under different ionic strength. (Is denotes ionic strength.)

4.4 Grafting and Characterization of PAA/PEG Mixed Brushes

To investigate an effect of PEG grafting density on the PAA grafting density, PEG brushes reported in section 4.2 were dip-coated in a 1% PAA solution in ethyl alcohol and annealed for 5mins, 30mins and 60mins at 55°C to synthesize the mixed PAA/PEG brushes. The additional PAA brush heights were measured by the ellipsometry. The grafted amounts of PAA were calculated using Equation (3.1) and are shown in Table 4.2. The grafted PAA amounts obtained through the PEG brush are also plotted against the PEG grafting density in Figure 4.13. First, it is shown that grafting of PAA chains was possible through a dense PEG layer because PAA can form intermolecular complexes with PEG[30]. Sixty and thirty minutes grafting time resulted in a higher grafting amount of PAA than did five minutes when PEG grafting density was less than 1.1 chains/nm^2. It should be noted that when the grafting density of PEG is relatively high (above 1.3 chains/nm^2), the amount of grafted PAA is higher than that

corresponding to the lower PEG grafting density (less than 1.1 chains/nm^2) and is independent of the grafting time. This phenomenon can be associated with "layer-assisted tethering"[5], first reported in Penn *et al.*'s experiment of tethering amino-terminated PS to GPS (3-glycidoxypropylsilane)-modified glass beads[29]. When the surface is pre-covered with densely grafted PEG chains, there are less available sites and the steric repulsion on the surface is higher than that for sparsely grafted PEG brushes. Thus, only part of a PAA chain could migrate to the surface and further react with epoxy groups. These factors give PAA chains a higher extension from the surface than would occur on a surface with less PEG. In contrast, when a silicon wafer surface is covered with fewer grafted PEG chains, the steric repulsion of the PAA chains is less. The available epoxy sites on the surface are more abundant as well. These two factors caused PAA chains to have more connections to the surface, which reduced the amount of PAA grafted. This is presented schematically in Figure 4.14.

#			h_{PEG} (nm)	σ_{PEG} (chains/nm^2)	h_{PAA} (nm)	σ_{PAA} (chains/nm^2)	Average Contact Angle (deg)
9	PEG Max	PAA Max	8.1	1.1	6.5	0.2	<10
10		PAA Max	8.3	1.1	4.8	0.1	<10
12		PAA Max	11.0	1.4	9.1	0.3	<10
11		PAA Med	11.9	1.6	11.2	0.3	<10
13		PAA Min	10.5	1.4	11.4	0.3	<10
8	PEG Med	PAA Max	7.9	1.0	7.0	0.2	<10
		PAA Min	7.0	0.9	3.6	0.1	<10
5		PAA Max	4.2	0.6	6.5	0.2	<10
6		PAA Med	4.2	0.6	8.6	0.2	10.1
7		PAA Min	5.2	0.7	0.7	0.0	23.7
1	PEG Min	PAA Min	2.6	0.3	1.6	0.1	<10
2		PAA Min	3.4	0.5	1.4	0.0	10
3		PAA Max	2.8	0.4	6.1	0.2	<10
4		PAA Med	3.0	0.4	5.9	0.2	<10

Table 4.2: Mixed PAA/PEG samples' water contact angles, most of them are less than 10°, which is the limit of the Kruss Drop Shape Analysis. Each sample measured 5 times. And the error range is considered as 2°. h_{PEG} and h_{PAA} denotes the PEG and PAA brush heights measured by the ellipsometer. σ_{PEG} and σ_{PAA} are PEG, PAA brush grafting densities which are calculated from the thicknesses.

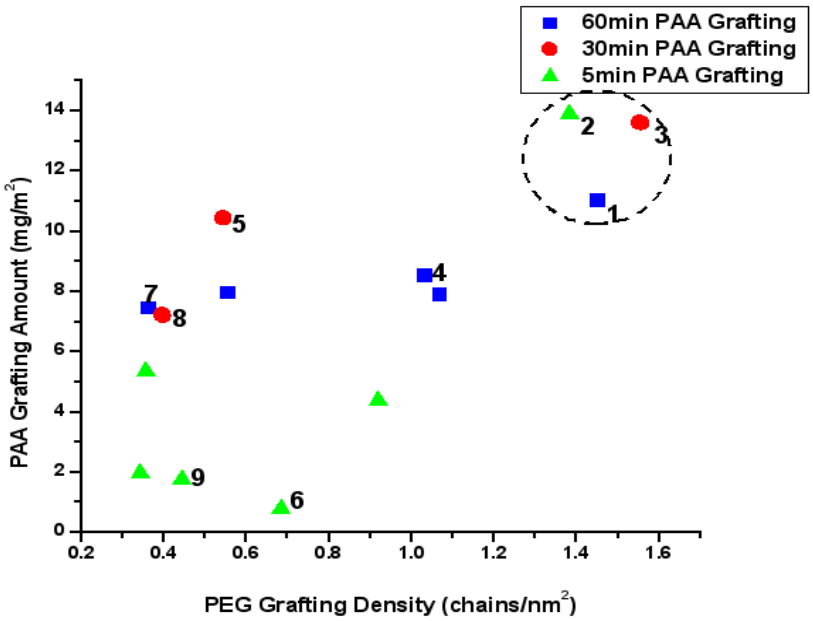

Figure 4.13: PAA grafting amounts versus PEG grafting densities under different PAA grafting times. The AFM images of the samples with the number on the right are shown in Figure 4.15 and Figure 4.16.

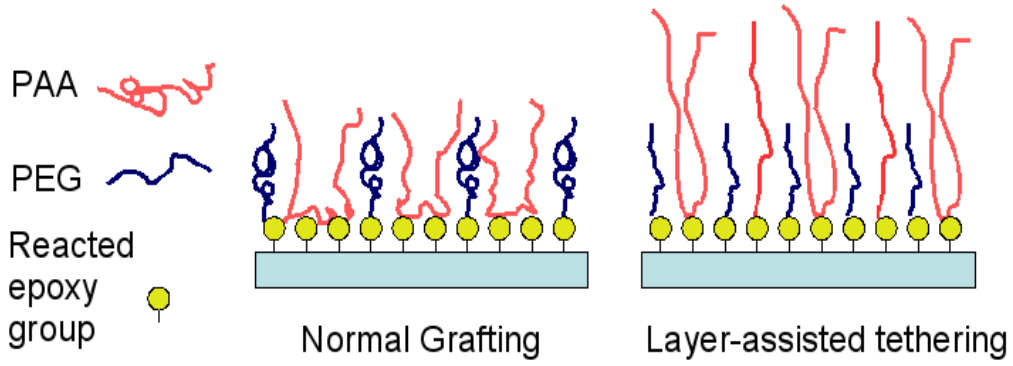

Figure 4.14: Schematics of PAA "normal grafting" and "layer-assisted tethering" grafting.

The surface morphology of the mixed brushes were obtained by tapping mode AFM. The AFM images are shown in Figure 4.15 (low resolution) and Figure 4.16 (high resolution). When compared to the PEG brush surfaces (Figure 4.5, (1a), (2a) and (3a)), no crystals structures were observed from AFM images of the mixed brushes. Because of the hydrogen bonding between the carboxyl group of PAA chains and the oxygen atom in the PEG repeating units, PEG forms an intermolecular complex with PAA. This destroys

the interactions required for crystal formation. Most images in Figure 4.16 show a similar "meteor crater" structure as the single-component PAA brushes. By taking into account the previous observations for PAA surfaces, it is apparent that the surface is covered with PAA.

The values of RMS roughness for the AFM images before and after grafting of PAA are calculated by the AFM data analysis software via Equation (3.3). The RMS values of PEG samples before grafting, after grafting PAA for different time (5mins, 30mins and 60mins) are plotted in Figure 4.17. The roughness decreases after grafting PAA chains to the surface, which also indicates changes in the surface properties.

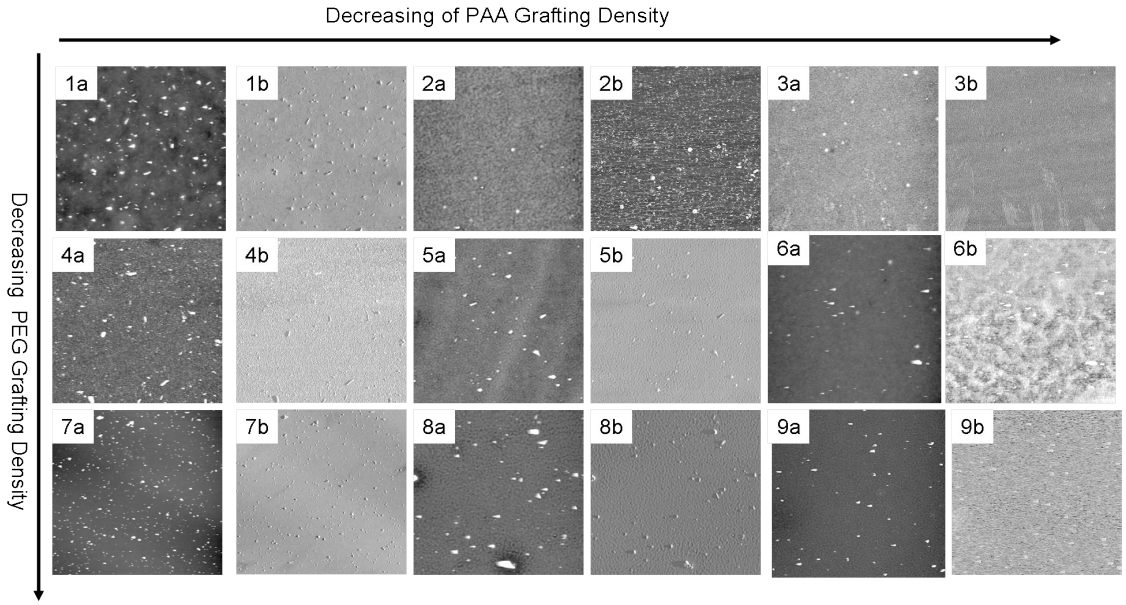

Figure 4.15: AFM images of PAA grafted to PEG whose grafting density are ~1.38chains/nm^2 (1,2,3), ~0.68chains/nm^2 (4,5,6) and ~0.44chains/nm^2 (7,8,9). Numbers in the top left of each image correspond to the Figure 4.13. Label a) and b) are height and phase images, respectively. Scan size is 10μm×10μm, vertical scale is 30nm in height and 30° in phase images.

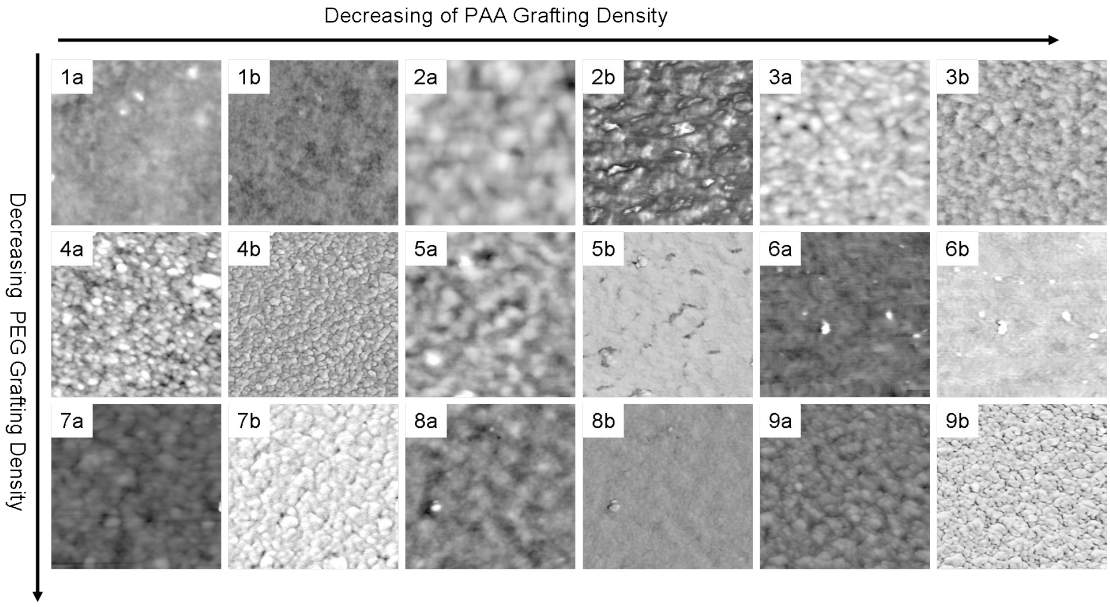

Figure 4.16: AFM images of PAA grafted to PEG whose grafting density are ~1.38chains/nm^2 (1,2,3), ~0.68chains/nm^2 (4,5,6) and ~0.44chains/nm^2 (7,8,9). Numbers in the top left of each image correspond to the Figure 4.13. Label a) and b) are height and phase images, respectively. Scan size is 1μm×1μm, vertical scale is 10nm in height and 15° in phase images.

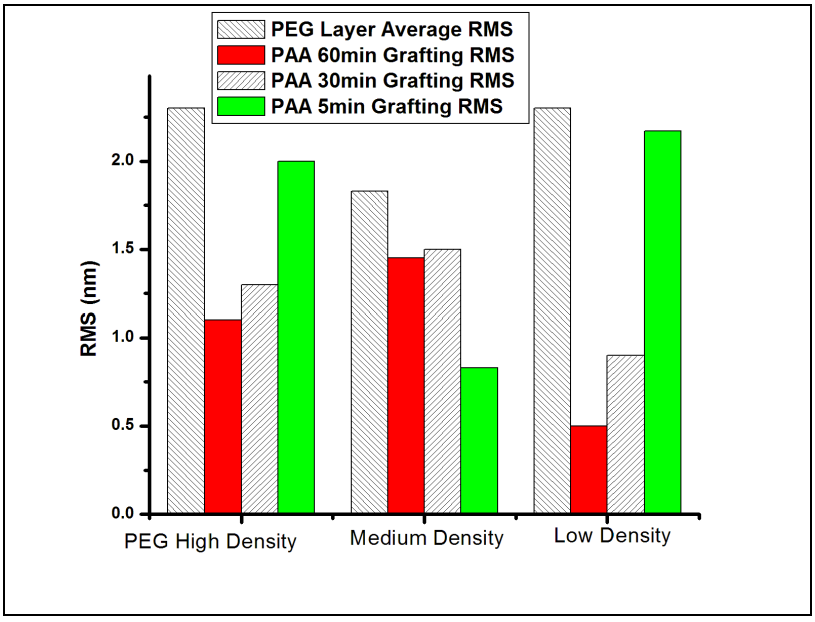

Figure 4.17: The roughnesses of PEG brush surface and PAA/PEG mixed brush surface.

Contact angle measurements on the mixed PAA/PEG brushes were conducted to quantitatively characterize their water wettability. Five HPLC water drops were placed on each sample surface to obtain the drop shapes which were further analyzed by the Kruss software to obtain the values of contact angles. The averaged contact angles are shown in Table 4.2. Most of the samples had contact angles less than 10°, indicating a very hydrophilic surface. Considering the water contact angles for PEG (approximately 22°), PGMA (approximately 60°) and PAA surfaces (~0°, nearly complete wetting), grafting of PAA onto PEG brush increases the wettability of the brush surfaces. In general, by combining data obtained from the water contact angle, AFM height/phase images and change in RMS roughness values, it is reasonable to consider that the PAA/PEG mixed brush surfaces are dominated by the highly hydrophilic PAA chains.

The mixed brush height transition in aqueous solutions was also investigated. Similar to the method described in Section 4.3, the sample with a PAA/PEG grafting density of 0.1/0.8 chains/nm^2 was scratched with a AFM tip and then scanned under light deflection contact mode AFM in ambient air, water, phosphate buffer and salted phosphate buffer containing 1mol/L NaCl. Figure 4.18 contains the AFM height images for this sample. The brush height was obtained by subtracting the substrate height from the total height which is column-averaged from the AFM images. The brush height results are shown in Figure 4.19. Qualitatively, the mixed brush had the same transition trend as the single-component PAA brush (Figure 4.12). The brush extension was observed when the sample was immersed in buffer. Increasing the solution ionic strength greatly reduced the brush height extension. However, the mixed brush height extension (20%, from ~15nm to ~18nm) was smaller than that for a single-component PAA brush

(125%, from ~20nm to ~45nm). Possible reason for the smaller extension of the mixed brush is the presence of the PEG chains, capable to interact with PAA chains.

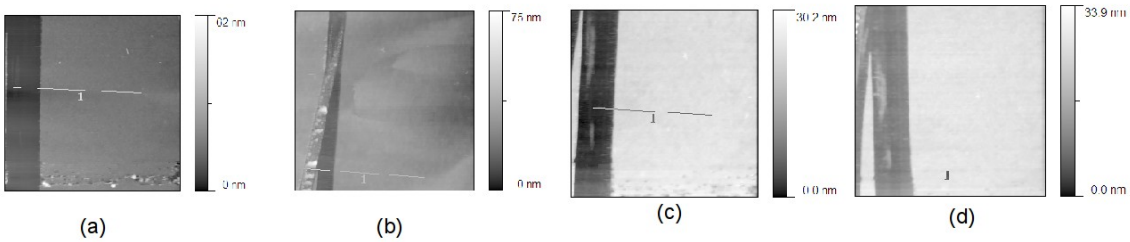

Figure 4.18: AFM height image of the scratched mixed brush by light deflection contact mode: (a)dry state, (b)in HPLC water, (c)in phosphate buffer and (d)in salted phosphate buffer with 1mol/L NaCl. Averaging directions are perpendicular to the lines.

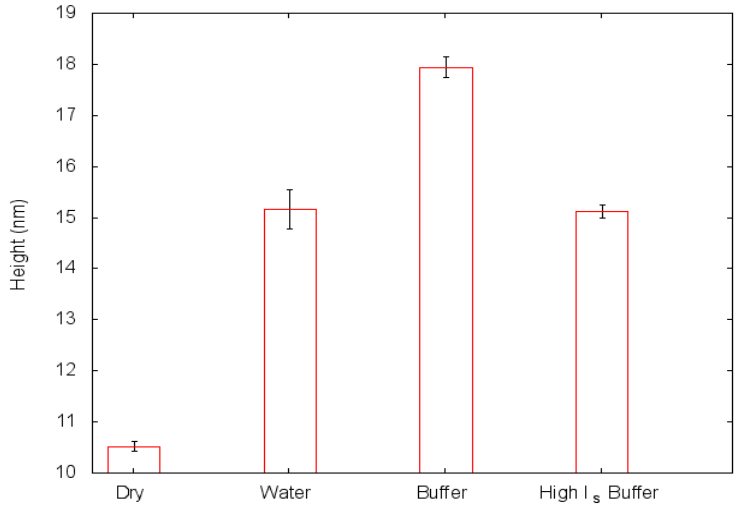

Figure 4.19: The mixed brush height measured by AFM tip scratching under different solution conditions.

4.5 Conclusions

PGMA is an effective primary layer for PEG and PAA grafting. For single PEG brushes, when grafting density is high, PEG crystals can be observed clearly on the surface while isolated crystal domains are formed when PEG grafting density is lower. PAA can be grafted to primary PGMA surfaces as well, due to its carboxylic acid groups which allow multiple connections (loop-train-tail) to form between the PAA molecules and the PGMA primary layer.

The PAA brush extends when immersed in the phosphate buffer. Brush height reduction was also observed when 1mol/L NaCl was added to the solution, because the additional ions screen out the electrostatic interactions between chains. When grafting PAA to PEG-occupied PGMA surface was conducted, PAA anchoring was provided by a "layer-assisted tethering" effect, especially when PEG grafting density exceeds approximately 1.3 chains/nm^2. AFM morphology studies and water contact angle measurements indicate that PAA chains dominated the mixed PEG/PAA brush surface after grafting.

The *in situ* mixed brush height transition under different ionic strength solutions was also investigated. It showed that the mixed brush had the similar response to different aqueous solutions as the single-component PAA brush. However, the changes in the mixed brush height were much smaller than those of single component PAA brushes.

Finally, fourteen samples with different PEG/PAA composition ratios were obtained (Table 4.2), which provided a PAA/PEG mixed brush "library".

References

(1) Motornov, M.; Sheparovych, R.; Tokarev, I.; Roiter, Y.; Minko, S. *Langmuir* **2007***, 23*, 13.

(2) Ionov, L.; Sidorenko, A.; Eichhorn, K.; Stamm, M.; Minko, S.; Hinrichs, K. *Langmuir* **2005***, 21*, 8711.

(3) Draper, J.; Luzinov, I.; Minko, S.; Tokarev, I.; Stamm, M. *Langmuir* **2004***, 20*, 4064.

(4) Houbenov, N.; Minko, S.; Stamm, M. *Macromolecules* **2003***, 36*, 5897.

(5) Motornov, M.; Sheparovych, R.; Tokarev, I.; Roiter, Y.; Minko, S. *Langmuir* **2007***, 23*, 13.

(6) Retsos, H.; Gorodyska, G.; Kiriy, A.; Stamm, M.; Creton, C. *Langmuir* **2005***, 21*, 7722.

(7) Norde, W.; Gage, D. *Langmuir* **2004***, 20*, 4162.

(8) Szleifer, I. *Current Opinion in Solid State and Materials Science,* **1997***, 2*, 337.

(9) Dong, R.; Krishnan, S.; Baird, B. A.; Lindau, M.; Ober, C. K. *Biomacromolecules* **2007***, 8*, 3082.

(10) Hollmann, O.; Gutberlet, T.; Czeslik, C. *Langmuir* **2007***, 23*, 1347.

(11) Uhlmann, P.; Houbenov, N.; Brenner, N.; Grundke, K.; Burkert, S.; Stamm, M. *Langmuir* **2007***, 23*, 57.

(12) Dai, J.; Bao, Z.; Sun, L.; Hong, S. U.; Baker, G. L.; Bruening, M. L. *Langmuir* **2006***, 22*, 4274.

(13) Czeslik, C.; Jackler, G.; Steitz, R.; von Grunberg, H. *Journal of Physical Chemistry B* **2004***, 108*, 13395.

(14) Wittemann, A.; Haupt, B.; Ballauff, B. *Physical Chemistry Chemical Physics* **2003***, 5*, 1671.

(15) Matthias Ballauff, O. B. *Current Opinion in Colloid & Interface Science* **2006***, 11*, 316.

(16) Wu, T.; Gong, P.; Szleifer, I.; Vlcek, P.; Subr, V.; Genzer, J. *Macromolecules* **2007***, 40*, 8756.

(17) Wittemann, A.; Drechsler, M.; Talmon, Y.; Ballauff, M. *Journal of American Chemical Society* **2005***, 127*, 9688.

(18) Rühe, J.; Ballauff, M.; Biesalski, M.; Dziezok, P.; Gröhn, F.; Johannsmann, D.; Houbenov, N.; Hugenberg, N.; Konradi, R.; Minko, S.; Motornov, M.; Netz, R. R.; Schmidt, M.; Seidel, C.; Stamm, M.; Stephan, T.; Usov, D.; Zhang, H. In *Polyelectrolyte Brushes;* Advances in Polymer Science; Springer: 2004; Vol. 165, 79.

(19) Currie, E. P. K.; Sieval, A. B.; Fleer, G. J.; Stuart, M. A. C. *Langmuir* **2000***, 16*, 8324.

(20) Iyer, K. S.; Luzinov, I. *Macromolecules* **2004***, 37*, 9538.

(21) Wu, S.; Soucek, M. D. *Polymer,* **1998***, 39*, 5747.

(22) Jones, R. A. L.; Richards, R. W. In *Polymers at surfaces and interfaces;* Cambridge University Press: Cambridge ; New York, 1999; 377.

(23) Zdyrko, B.; Klep, V.; Luzinov, I. *Langmuir* **2003***, 19*, 10179.

(24) Zdyrko, B.; Varshney, S. K.; Luzinov, I. *Langmuir* **2004***, 20*, 6727.

(25) Bogdan, Z. PhD Thesis, *Thin Polymer Films for Biomedical Applications: Synthesis and Characterization*, School of Materials Science & Engineering, Clemson University, Clemson, SC, 29634, 2005.

(26) "Veeco Co." In *Dimension(TM) 3100 Manual;* 2000; Vol. 4.43B, 485.

(27) Paul, D. R.; Sperling, L. H.; American Chemical Society. Meeting; American Chemical Society. Division of Polymeric Materials: Science and Engineering In *Multicomponent polymer materials;* Advances in chemistry series; The American Chemical Society: Washington, D.C., 1986; Vol. 211, 354.

(28) Gupta, B.; Plummer, C.; Bisson, I.; Frey, P.; Hilborn, J. *Biomaterials* **2002***, 23*, 863.

(29) Penn, L. S.; Huang, H.; Sindkhedkar, M. D.; Rankin, S. E.; Chittenden, K.; Quirk, R. P.; Mathers, R. T.; Lee, Y. *Macromolecules* **2002***, 35*, 7054.

(30) Khutoryanskiy, V. V.; Dubolazov, A. V.; Nurkeeva, Z. S.; Mun, G. A. *Langmuir* **2004***, 20*, 3785.

(31) Sofia, S. J.; Premnath, V.; Merrill E. W. *Macromolecules* **1998***, 31*, 5059.

CHAPTER FIVE

PROTEIN-POLYMER INTERACTIONS AT INTERFACE

5.1 Introduction

Proteins are a large macromolecules made of amino acids connected by peptide bonds between the amino group and adjacent carboxyl groups. Proteins are known to readily adsorb to various substrates[1-7]. There are at least two different strong interactions between proteins and surfaces: electrostatic forces brought about by ionic end groups and substituted groups, also due to the nature of substitute. Thus, protein can interact with charged and/or hydrophobic surfaces, either reversibly or irreversibly. These interactions are highly dependent on the size, charge and structural stability of the protein as well as the properties of the adsorbing surface[8], such as the morphology, composition, heterogeneity and the electric potential.

After adsorption onto a surface, a protein tends to undergo conformational changes and unfolds to occupy more available sites on the surface. As shown in Figure 5.1, when a protein attaches to the surface, it changes its conformation in order to have more binding sites with the surface, increasing the binding energy. When protein net charge and surface net charge are both of the same sign, such as polyelectrolyte brush, binding to the charged surface is still possible by inducing the rearrangement of charge distribution on the surface of the protein and releasing the trapped counter-ions between the protein surface and the polymer brush surface (known as *counter-ion evaporation*[9-14]) to increase the entropy of the system to favor binding. Thus, this mechanism may account for protein adsorption onto a surface which has the same type of charge as the protein[9], such as bovine serum albumin onto PAA brushes[13].

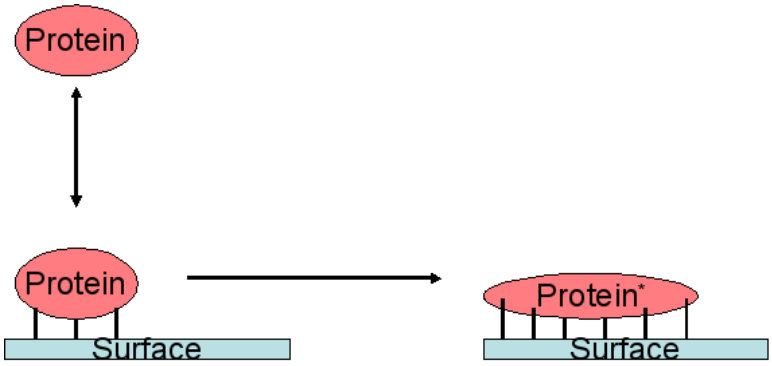

Figure 5.1: Protein adsorbed on surface, undergoing a surface rearrangement to have more binding enthalpy and protein conformational entropy.

Protein-polymer interactions have been widely studied both from experimental[1, 3, 5, 6, 15-18] and theoretical[19-21] perspectives, since this is a crucial factor for the design of novel biocompatible materials and drug delivery systems[9]. The most widely used polymers for protein adsorption are polyacrylic acid (PAA) and poly(2-vinyl pyridine) (P2VP) because their long-range electrical interactions with protein are much stronger than van der Waals or hydrophobic interactions. Both PAA and P2VP brush heights can be adjusted by changing the ionic strength, according to the general properties of polyelectrolytes discussed earlier in Chapter Two and Chapter Four.

PAA was used in this work as an adjustable protein adsorption component. At the same time, to create a protein repelling layer, poly(ethylene glycol) (PEG) was used because of its well known protein-repulsion properties[2, 20, 22]. PEG is also a neutral polymer that does not change much under different ionic strength conditions. It is hypothesized that at high ionic strength, as represented in the left image of Figure 5.2, the PAA brush is hidden below a PEG layer and a protein interacts with the PEG brush surface. Thus, the protein should be repelled from the surface. By changing the aqueous condition to a low ionic strength, the PAA chains extend out from the surface of the PEG layer, and provide binding sites (attraction) on the brush surface for the protein to interact

with, as represented in the right image of Figure 5.2. This "switchibility" can be performed multiple times because ionic tuning is the only physical change that is being carried out, and the chemical composition or structure of the brush system is not being altered. Therefore, mixed PAA and PEG brushes could be used in the construction of mixed brush systems whose protein affinity could be tuned by altering the ionic strength.

A series of experiments were set up to evaluate the protein adsorbed amount on polymer brush surface and the tuning capacity.

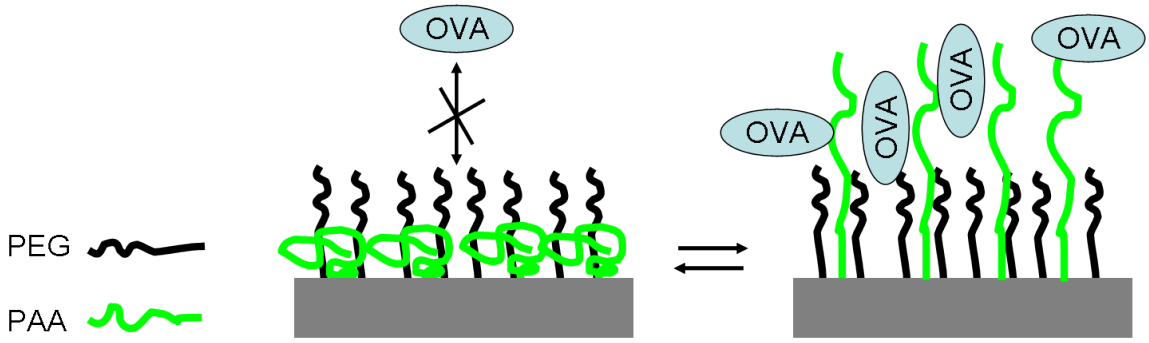

Figure 5.2: The responses of the mixed brush under different conditions, OVA denotes to the ovalbumin. Left image shows the protein adsorption "off" status and the right shows the protein adsorption "on" status.

5.2 The Analysis for TIRF results

The adsorption of the rhodamine B labeled ovalbumin onto PEG/PAA mixed brushes has been studied using TIRF (Total Internal Reflection Fluorescence). TIRF was first used by Watkins and Robertson[23] in order to study γ-globulin adsorption kinetics and thermodynamics on silicon rubber. It was further developed by Lok *et al.*[24, 25] for investigating bovine serum albumin adsorption on spin-coated poly(dimethylsiloxane) surfaces. The basic principles of the method and experimental procedures were discussed earlier in Chapter Two. In this section, additional calibration, background analysis and de-noising technologies are presented.

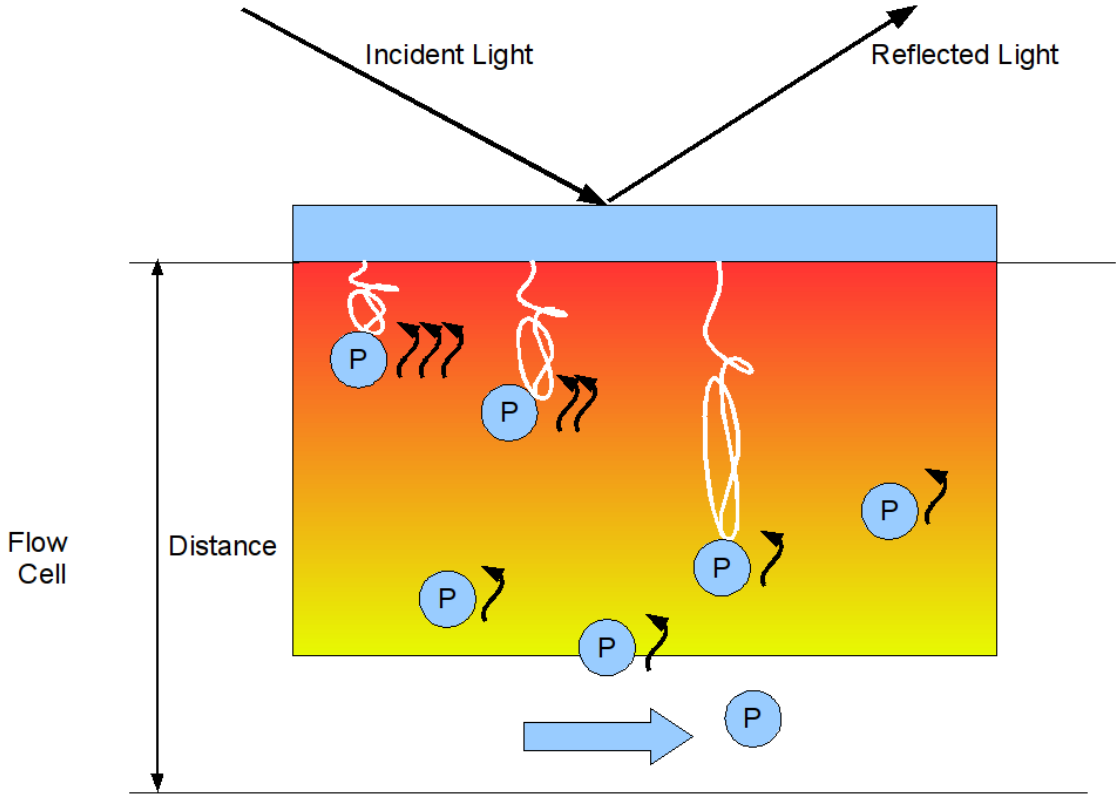

Figure 5.3: Proteins adsorbed on the polymer brush and be excited to emit fluorescence signal. Gradient color indicates the decay of the evanescent wave intensity. P denotes one protein molecule. Big arrow denotes the flowing direction of protein solution. Small arrow indicates the fluorescence emitted by the protein molecules. The fluorescence intensities generated by the same protein molecule but at different distances are different.

5.2.1 Calibration and Background Analysis

The excitation in TIRF is an evanescent wave generated at the interface between a high-refractive-index and a low-refractive-index medium. Typically, the penetration depth of this wave is on the order of 100nm. The intensity of the evanescent wave has the exponential decay relationship as follows[24, 25]:

$$I(z) = I(0)e^{-z/d} \tag{5.1}$$

where I is the intensity of a evanescent wave, $I(0)$ is the intensity at the surface, z is the distance from the substrate and d is penetrating depth depending on the incident angle and wavelength[26], which can be represented as:

$$d = \frac{\lambda_0}{4\pi}\left(n_2^2 \sin^2(\theta) - n_1^2\right)^{-1/2} \tag{5.2}$$

Name	Value
Incident Wavelength (λ_0)	532nm
Incident Angle (θ)	72.7°
Glass Refractive Index (n_2)	1.52
Solution Refractive Index (n_1)	1.33

Table 5.1: Wavelength, incident angle and the refractive indexes in the experiment system.

By inserting the data listed in Table 5.1 into Equation (5.2), the d was calculated to be 73nm. Normally, the polymer brush thickness in this study was ~20nm. Thus, as shown in Figure 5.3, the depth for the evanescent wave is larger than the thickness of the polymer brush. Therefore, not only protein adsorbed on the polymer brush, but also the free proteins in the solution can be excited. Thus, additional fluorescence background need to be considered[24].

First, in order to study the background signal contribution originating from the free protein in solution, the unmodified glass slide was placed in the flowing cell with injecting a labeled protein solution. The protein adsorption breakthrough curve was obtained by TIRF and is shown in Figure 5.4. Upon injection of protein at 2450s, the signal increased sharply in 50s. When the protein solution was replaced with pure phosphate buffer, the signal quickly decreased. This sharp increase and decrease could be assigned to the protein solution front entering the fluorescence detection regions; namely,

this sharp peak was caused by the signal of the free protein molecules excited by evanescent waves in the solution as well as the signal caused by scattering of the laser light. It should be noted that the maximum signal intensity was only 0.02 signal counts, which is only significant in the situation when adsorption is very low (for example, highly grafted PEG).

Lok *et al.*[24] found that, during TIRF measurements, the contribution of low concentration protein solutions to the signal could be ignored. Thus, to avoid introduction of obvious background caused by free protein in solution and to keep the adsorption times necessarily short, a protein concentration of ~40ppm ($\Delta = 0.01$ signal counts, measured by TIRF) was chosen for the protein adsorption study.

Evanescent waves have an exponential decay across the depth of penetration[24,25]. As shown in Figure 5.3, the gradient color indicates the decay of the intensity when the evanescent wave penetrates. The same amount of protein at a different distance from the surface could generate different fluorescence signal intensities because of the different intensities of the exciting evanescent waves. Thus, normalization of the raw intensity to the brush thickness must also need to be considered. The decaying fluorescent intensity versus the distance from the surface was calculated based on Equation (5.1) and Equation (5.2) and is shown in Figure 5.5. In Chapter Four, it was shown that the swelling of the mixed polymer brushes, measured by AFM scratching, was approximately 1.95 times the thickness of the brush in the dry state. This value was used to estimate the dilated height of each mixed brush sample. The PGMA monolayer (z = 3 nm) was selected as the reference layer. The intensities directly obtained from TIRF ($I(z)$) were all normalized to the intensity they would emit at the same distance from the reference surface ($I'(3)$) by applying Equation (5.1). Therefore, the variation of the normalized

intensities can be used to indicate the change in the protein adsorption on the mixed brush surface.

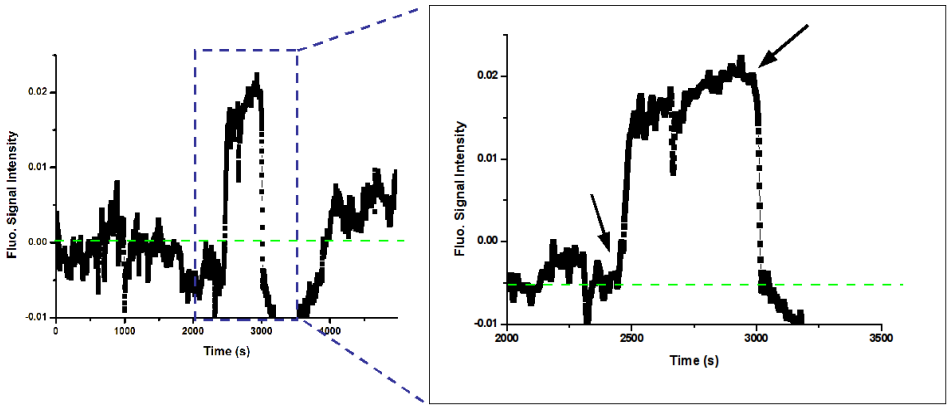

Figure 5.4: Protein adsorption breakthrough curve onto the pure glass. Protein used is ovalbumin (123.2ppm, labeling density 0.5). Protein and buffer were injected at 2450s and 2950s, as indicated by the arrows.

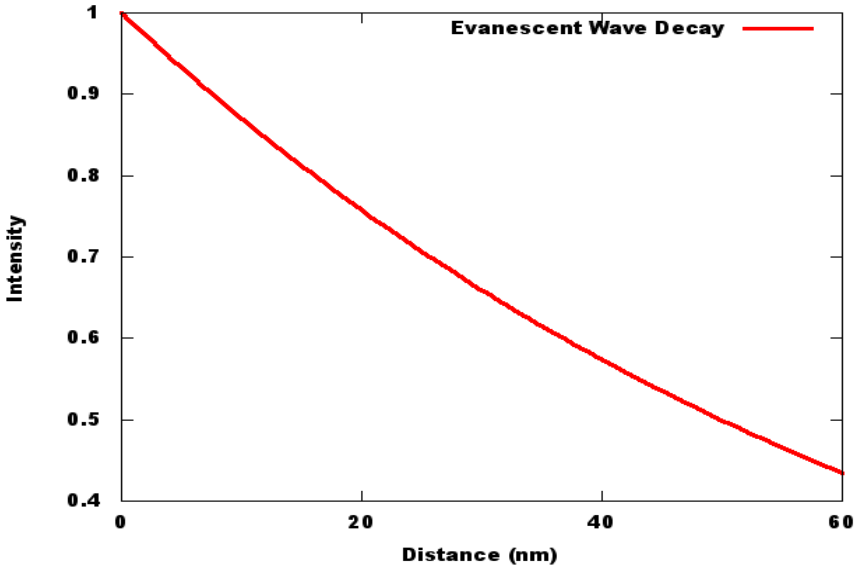

Figure 5.5: The calculated decaying intensity of the evanescent wave (calculated by Equation (5.1) and (5.2)).

5.2.2 Conversion of TIRF Signal Intensities into Amounts Protein Adsorbed

One of the benefits of TIRF is that it is an *in situ* measuring method which can acquire adsorption data in real time. Lok *et al.*[24] demonstrated that the fluorescence signal generated by an evanescent wave was not only stable but also linearly dependent on the

surface concentration of the adsorbed substance. To quantify the linear coefficient (k) to convert the fluorescence signal into the amount protein adsorbed, transport-limited theory was applied[25]. When the shear rate inside the flow cell is low, lamellar flow is established and adsorption rate near the polymer surface can be seen as:

$$\frac{k\times\Delta Fluo.Signal}{\Delta t}=\frac{d\Psi}{dt}=\frac{1}{\Gamma\left(\frac{4}{3}\right)\times 9^{1/3}}\times\left(\frac{\gamma}{DL}\right)^{1/3}DC_0 \tag{5.3}$$

where Ψ denotes the surface concentration of adsorbed protein, γ is shear rate, D is the diffusivity of the protein, L is the distance from the edge to the middle of the flow cell and C_0 is bulk protein concentration. The right part of Equation (5.3) is also called the Lévêque equation, first derived by Leveque in 1928[27]. $d\Psi/dt$ is called Lévêque rate. It should be noted that the accumulation rate of protein on the surface has a linear dependence on the bulk concentration under a constant shear rate. Equation (5.3) was used in this thesis as the basic equation used to convert the laser signal intensity into the amount of protein adsorbed.

Four ovalbumin solutions with different concentrations were injected into the TIRF cell and the protein adsorption onto the glass slides covered with PGMA was monitored. PGMA is a polymer which has high affinity for ovalbumin and thus, may guarantee transport-limited adsorption.

The breakthrough curves of the ovalbumin adsorption on PGMA surface are shown in the Appendix A4. The first 100s data was ignored because of the time needed for the establishment of the pseudo steady-state conditions. Another 100s data was

collected and a linear fit was applied to acquire the slope. The slopes and calculated Leveque rates ($d\Psi/dt$) from the slope are listed in Table 5.1.

The slopes acquired from TIRF data are plotted against the bulk concentrations of the ovalbumin in Figure 5.6. The curve obtained is similar to the Lok *et al.*'s[24] result. According to them, the slopes generated by higher concentration protein solution deviate from the linear relationship obeyed by the lower concentrations, thus should be abandoned. The slopes for lower bulk concentration (less than 25ppm) give a very good linear fit against the bulk concentration (correlation factor $r = 0.998$), which agrees well with the curve demonstrated by Lok *et al.*[24], indicating the establishment of the transport-limited adsorption in this concentration range. The largest bulk concentration's slope shows deviation from the linearity, similar to the phenomenon observed in Lok's experiments. This may due to the the saturation of the surface at higher concentrations.

By inserting the values of the diffusivity of ovalbumin which is (7.68 ± 0.17) × 10^{-7} cm^2/s (from Ref28), the shear rate (2 s^{-1}), the distance L (2.5cm) and the related protein concentrations, the Lévêque rates $d\Psi/dt$ were calculated from Equation (5.3) and are listed in Table 5.1. At the same time, $k \times \Delta(Fluo.Signal)/\Delta t = d\Psi/dt$ can be obtained from the left part of Equation (5.3). Comparing the slope and the calculated $d\Psi/dt$, the factor k can be calculated by simply dividing $d\Psi/dt$ by the slope, as listed in Table 5.1. In this thesis, k=1.8 was used to convert the fluorescence signal intensity into the protein adsorbed amount on the surface.

Protein Concentration (ppm)	Slope (10^{-4} counts/ s)	Leveque Rate (10^{-3} mg/m^2·s)	Factor k (mg/ m^2·counts)
6.6	6.36	2.79	1.7
12.4	27.4	5.20	1.9
20.4	51.3	8.57	1.8
41.0	54.8	17.2	3.1

Table 5.2: Slope data and Leveque rates calculated via Equation (5.3).

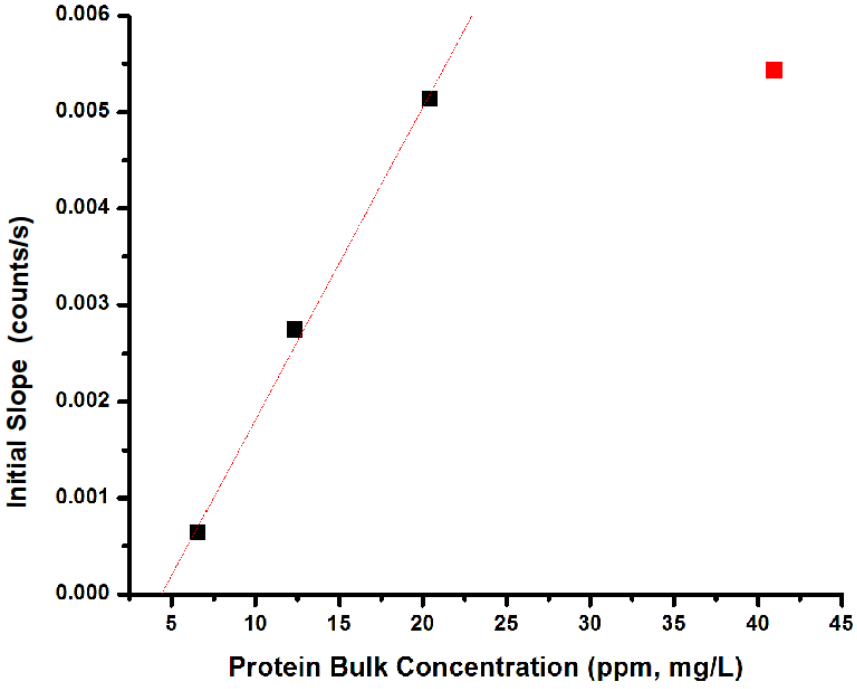

Figure 5.6: Initial slopes obtained from the protein adsorption breakthrough curves (200s-300s) versus the protein bulk concentration.

5.2.3 Further Data De-noising and Baseline Corrections

Because of the scattering of the evanescent wave, the signal obtained was noisy. This effect worsened if the total signal was weak and the signal/noise ratio was not high. Discrete Wavelet Transformation was therefore applied here, based on its successful application recently in electrochemistry to smooth data and remove drifting baselines[29-31].

The principle for WT (Wavelet Transformation) is to decompose the signal into a series of basic wavelet functions. The wavelets are considered to be the combination of translation and dilation of these basis functions:

$$\Psi_{a,b}=\frac{1}{|\sqrt{a}|}\Psi\left(\frac{t-b}{a}\right) \tag{5.4}$$

where a is a dilation variable and b is a translational variable. The signal $f(t)$ will be transformed into the series of wavelet coefficients as[32]:

$$\Psi'_{a,b}=\int_{-\infty}^{\infty} f(t)\Psi_{a,b}(t)dt \tag{5.5}$$

MatLab® was used to apply fast discrete wavelet transformation (DWT) which was first introduced by Mallat[33]. The signal is passed through two filters (high-pass and low-pass filter) simultaneously to get the approximation coefficient (cA1) and detailed coefficient (cD1). This process is conducted many times, and one series of detailed coefficients (cDx) and another of approximation coefficients (cAx) is obtained. This process could also be reversed to reconstruct the original signal as well (Figure 5.7).

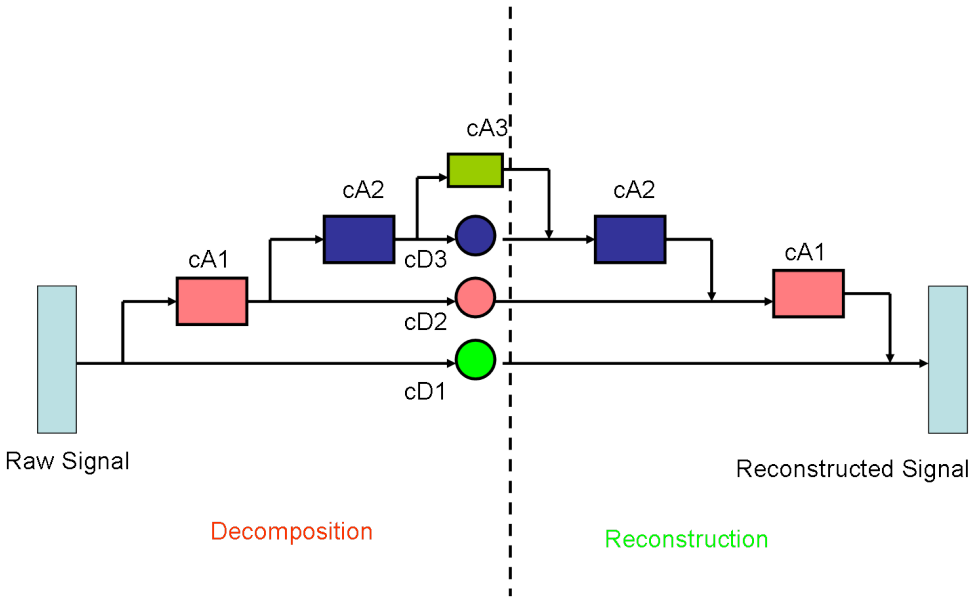

Figure 5.7: Scheme of the decomposition and reconstruction of the raw signal by the fast Discrete Wavelet Transform.

In this thesis, the TIRF breakthrough curves were decomposed, and a series of cDx and cAx coefficients was obtained. The highest order approximation coefficient cA10 was set to be zero to remove the large scale drifting. After that, the series of cAx and cDx is passed by a de-noising function to reduce the noise part[29]. (Detailed program source code is presented in the Appendix.)

One example of the adsorption breakthrough curve on the PEG brush is shown in Figure 5.8. The middle image shows the baseline corrected result, and the bottom one demonstrates the smoothed results. It can be noted that both the peak value and the peak shape are conserved during this process. Compared to other widely used smoothing methods, such as FFT filtering and Savitzky-Golay smoothing, Perrin *et al.*[30] showed that DWT smoothing could give a better removal of noise, preservation of sharp peaks and removal of baseline drift.

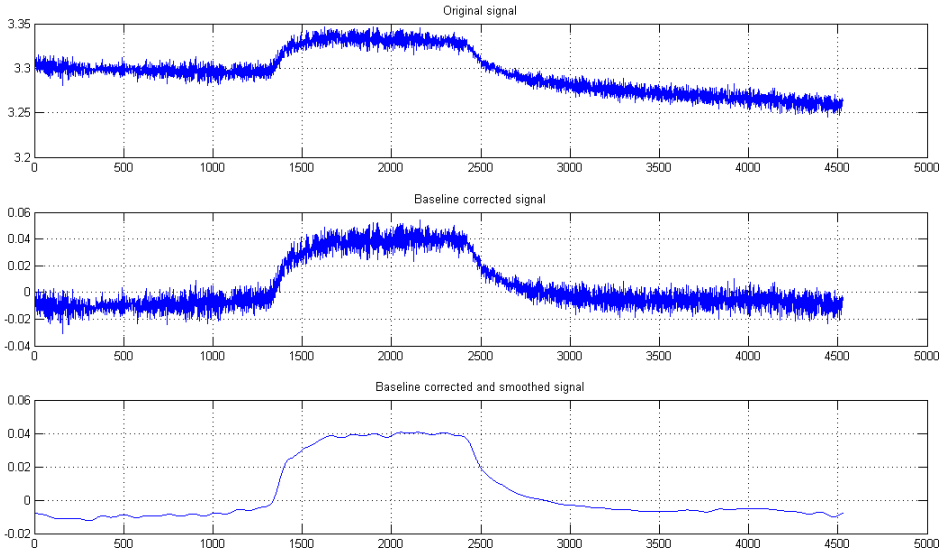

Figure 5.8: Original, DWT baseline corrected and DWT denoised breakthrough curve of ovalbumin on the PEG brush by TIRF(baseline correction: wavelets: 'db3', threshold level: 10; denoising wavelets: 'db6', threshold level: 3.).

5.3 Protein Adsorption on the Single-Component Brushes

Single-component PEG and PAA brushes were prepared following the procedures described in Chapter Four. TIRF was used to quantify the protein adsorption at equilibrium onto these brushes. The adsorption results are shown and discussed in this section.

First, single-component PEG brushes were placed in the flowing cell. Ovalbumin phosphate buffer was injected into the flowing cell. The breakthrough curves are listed in the Appendix A3. The maximum amount protein adsorbed versus PEG grafting densities are shown in Figure 5.9. The adsorption of the protein onto PEG brushes is highly dependent on the grafting density. When the grafting density was low, a significant protein adsorption was observed. With increase in the PEG grafting density, the

equilibrium adsorption of protein decreased. At high grafting density (greater than 1.3 chains/nm^2), no measurable protein adsorption was observed. It is concluded that only densely grafted PEG can repel proteins from adsorbing. This result agrees well with results obtained by other researchers[6, 34].

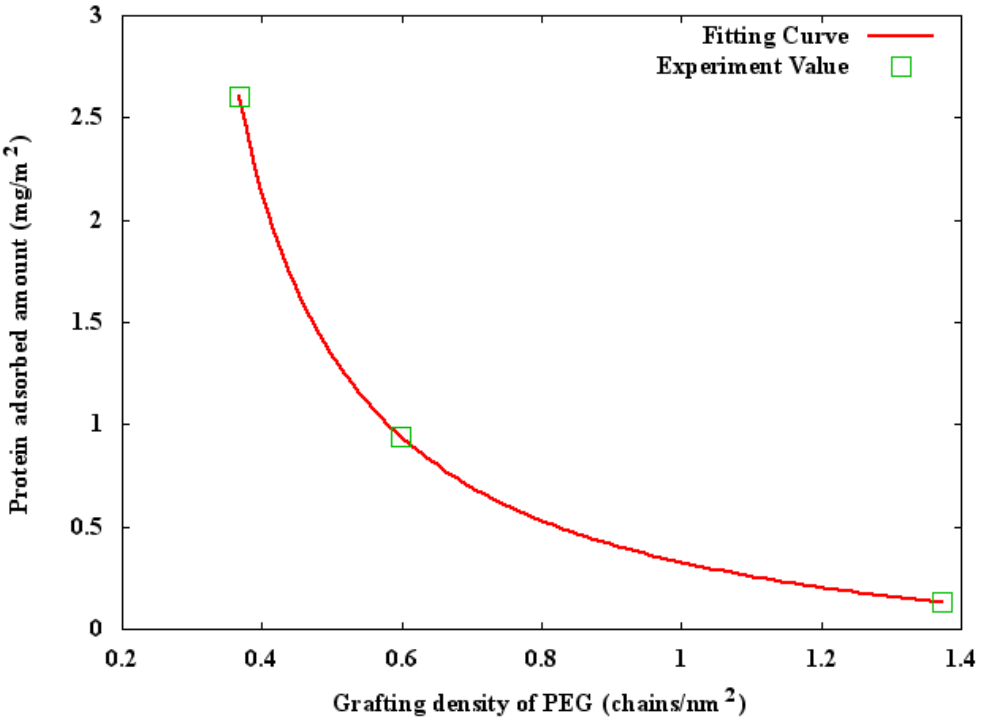

Figure 5.9: Ovalbumin adsorbed amounts onto PEG brushes at equilibrium with different grafting densities: 0.37chains/nm^2, 0.60chains/nm^2 and 1.37chains/nm^2. Line indicates the fitting curve of Equation (5.7).

To fit the data to establish the model of protein adsorption onto the PEG brush, various equations were tested and Equation (5.6) was found to fit best and used to interpolate the protein adsorption onto a single-component PEG brush under different grafting densities.

$$A_{PEG}=\frac{a}{\sigma_{PEG}+b}+c \tag{5.6}$$

A_{PEG} denotes the amount adsorbed on PEG brushes, σ_{PEG} is the PEG brush grafting density. By using the nonlinear least-squares (NLLS) Marquardt-Levenberg algorithm implemented in Gnuplot[37], coefficients a, b, c were obtained. Equation (5.6) becomes:

$$A_{PEG}=\frac{0.5}{\sigma_{PEG}-0.2}-0.3 \tag{5.7}$$

Ovalbumin adsorption onto single-component PAA brushes was also investigated. Three brushes samples, one PGMA monolayer and two PAA layers at different grafting densities were selected. An unlabeled protein solution at the same concentration was injected to detect if any protein "exchange" would occur. Pure buffer was injected to detect if adsorbed proteins could be desorbed. The ovalbumin adsorption breakthrough curves onto these samples are shown in Figure 5.10.

For PAA samples with low grafting density (0.09chains/nm^2, calculated from the PAA layer thickness: 3.3nm), a significant protein adsorption was observed.. No protein exchange was observed. Pure phosphate buffer was injected to determine if the protein could be desorbed. It shows that after injecting pure buffer solution, the desorption was small, indicating the irreversibility. Compared with the protein adsorption breakthrough curve onto a PGMA monolayer, a similar amount of protein and the irreversibility were observed. However, No measurable protein adsorption was observed on the thick PAA layer. Parallel experiments were conducted, and the results were reproducible.

This observation was contrary to most previous results[1, 5, 7, 13, 34]. The possible reason is the different grafting structures obtained in this work. In most previous papers, the

PAA brush system was composed of self-assembled PS-*b*-PAA copolymers[2, 5, 7], where PS is a substrate that has no interactions with PAA chains, as represented in the scheme (a) in Figure 5.11. Thus, the conventional brush structures were obtained. In this system, because of the multiple carboxyl acid groups, PAA forms a multi-connection "loop-train-tail" structure, as represented in the scheme (b) and (c) of Figure 5.11.

When PAA is sparsely grafted (scheme (b), Figure 5.11), the steric repulsion of the protein to prevent penetration inside the PAA grafted layer is small. The ovalbumin either could squeeze out the thin PAA layer when approaching the brush surface, or it could be adsorbed inside the brushes[1] close to the PGMA layer, with which it can still effectively interact. In addition, the charge density of a thinner PAA layer is less than that of the dense one, giving a relatively smaller electrostatic repulsion of the protein. These all may be reasons why the sparsely grafted PAA layer adsorbs a large amount of protein irreversibly as the PGMA monolayer does.

When PAA chains are densely grafted (scheme (c), Figure 5.11), both a dense PAA net structure and a large charge density have been established on the surface, which give a very high energy barrier for the protein to be adsorbed, leading to no measurable adsorption. It should be noticed that the grafting density of this protein repelling PAA sample was only 0.2 chains/nm^2, which is much smaller than the grafting density of the protein repelling PEG sample (1.37 chains/nm^2), showing the better ability to repel proteins.

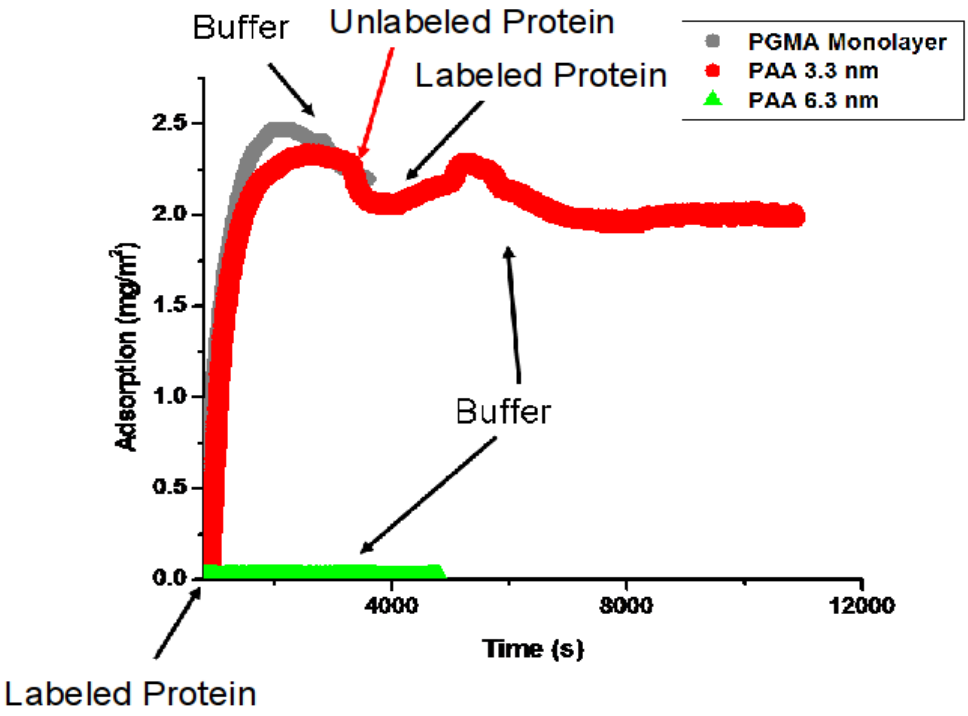

Figure 5.10: Ovalbumin adsorption breakthrough curves on three samples: two PAA brushes (Thicknesses are 3.3nm and 6.3nm) and a PGMA monolayer. Arrows indicate the time to inject related solutions.

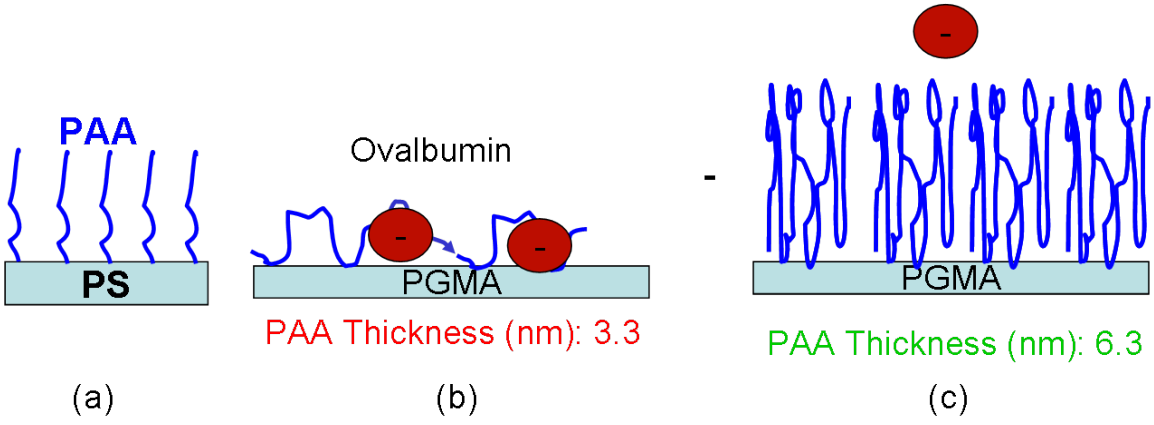

Figure 5.10: Different PAA brush structures. (a) PS-b-PAA self-assembled brush; (b) sparsely grafted PAA chains with ovalbumin adsorbed; (c) densely grafted PAA chains with ovalbumin repelling from adsorbing onto the surface.

5.4 Ovalbumin Adsorption onto PAA/PEG Mixed Brushes

Previous experiments demonstrated that both densely grafted single-component PEG and PAA brushes repel protein. What would the effect be of a combination of PAA and PEG in a mixed brush? Could these mixed brushes demonstrate some tunability in response to environmental changes? This section investigates these questions and discusses them in detail.

The most significant difference between PAA chains situated in a single-component PAA brush and the mixed brush is the chain conformations. In the single-component brush, because of the abundant free epoxy groups of the PGMA on the surface, PAA can form a significant number of train segments. On a PEG-occupied surface, fewer epoxy groups are available, and PAA becomes more extended because of "layer-assisted-tethering". Thus, PAA has less monomeric units in the train segments, which may influence the protein adsorption.

The protein adsorption breakthrough curves on mixed brushes are listed in Appendix A3. The amount of protein adsorbed at equilibrium onto these mixed brushes is listed in Table 5.2. First, it should be noted that the PEG and PAA grafting densities of samples #1 and #4 are similar. However, their protein adsorption amounts greatly different. The same situation exists between #7 and #8 as well. These results indicate that the initial hypothesis, with only PEG and PAA grafting density to be the determining factors, is questionable. Another simplified model is created in an attempt to evaluate the determining factors in this system.

Sample Number	PEG Grafting Time (hr)	PEG Grafting Density (chains/nm^2)	PAA Grafting Time (min)	PAA Grafting Density (chains/nm^2)	Protein Adsorption (mg/m^2)
1	~15	1.07	30	0.18	0.47
2	~15	1.56	15	0.31	0.30
3	~15	1.38	5	0.32	0.29
4	4	1.03	30	0.19	0.06
5	4	0.54	15	0.24	0.67
6	4	0.92	5	0.10	0.10
7	2	0.36	30	0.17	0.22
8	2	0.40	15	0.16	0.32
9	2	0.34	5	0.12	1.08

Table 5.3: PEG, PAA grafting time, PEG, PAA grafting density and their related protein adsorption amounts at equilibrium.

As a first approximation, it is supposed that the total protein adsorption onto the mixed brushes (A_{total}) include the adsorption onto PEG chains and adsorption onto PAA chains.

$$A_{total} = A_{PEG} + A_{PAA} \tag{5.8}$$

Next, the protein adsorption onto PEG chains in the mixed brushes is considered to be the same as that of a single-component PEG brush, which has the relationship shown in Equation (5.7). However, one correction must be considered for calculating protein adsorption onto PEG chains (A_{PEG}). After the mixed brushes are immersed into phosphate buffer, the PEG chains and PAA chains in the mixed brush change from a miscible to an immiscible status. As represented in Figure 5.12, the PEG and PAA brush are miscible when PAA doesn't ionize. When placed in the aqueous phosphate buffer which has the the pH approximately 7, PAA starts to ionize and the hydrogen bonding between PEG and PAA is eliminated, thus PAA and PEG phase separated. The grafting

density for PEG in mixed brushes becomes higher because the phase separation between PAA and PEG reduces the occupied surface area of PEG; namely, $S_{PEG} < S_{Total}$, where S_{PEG} is the PEG chains occupied area in mixed brush and S_{Total} is the mixed brush's surface area. It is supposed that the PEG surface occupation fraction (S_{PEG}/S_{Total}) is the same as the PEG volume fraction (f_{PEG}) in the grafted layer. The reduced grafting density of PEG in the binary brushes is $\sigma^{r}_{PEG} = \frac{\sigma_{PEG}}{S_{PEG}/S_{Total}} = \sigma_{PEG}/f_{PEG}$, where σ^{r}_{PEG} denotes the reduced PEG density and σ_{PEG} denotes the grafting density calculated from the thickness of the single-component PEG brush before PAA was anchored.

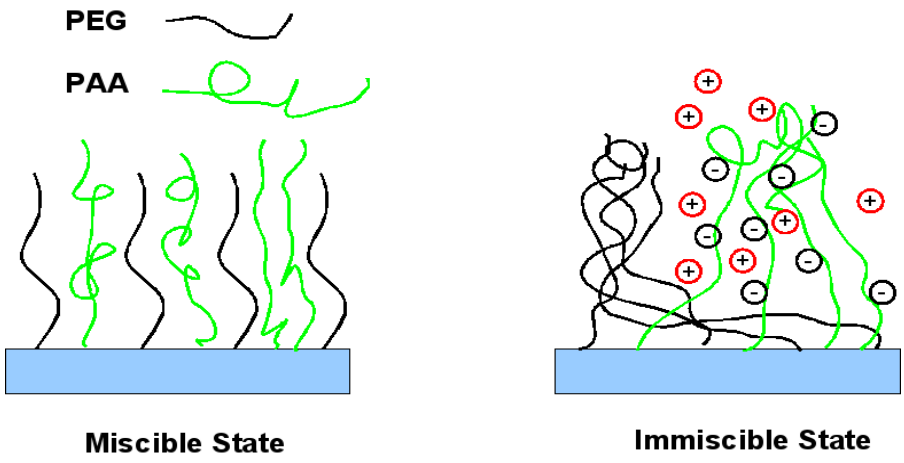

Figure 5.11: PEG and PAA are miscible when grafting, but immiscible when PAA is dissociated in phosphate buffer.

Then, the protein adsorption onto PEG chains in the mixed brush can be estimated as:

$$A_{PEG} = \frac{0.5}{\sigma^{r}_{PEG} - 0.2} - 0.3 = \frac{0.5}{\frac{\sigma_{PEG}}{f_{PEG}} - 0.2} - 0.3 \tag{5.9}$$

Because adsorption by PEG chains cannot be less than zero, if the calculated A_{PEG} is less than zero, it is considered as the indication that PEG grafting density is high enough to repel protein totally. Thus, A_{PEG} was set to be zero instead of negative value in this case.

To investigate the determining factors in protein adsorption onto PAA chains in the mixed brush A_{PAA}, it is reasonable to consider the fraction of PAA monomeric units bonded to the PGMA surface (train segment) (E) as an important parameter in considering the relevant results for the single-component PAA brush. The parameter is proportional to the PAA content in the mixed brush. That is, when the amount of PAA grafted onto the surface increases, more train segments form and the E increases.

On the other hand, because the tethering of PAA to PGMA to form a train segment is made by the reaction between carboxyl and epoxy groups on the surface, the number of available epoxy groups on the surface also determines E . The consumption of epoxy groups before PAA grafting is determined by two processes: reaction with carboxyl terminated groups in PEG and reaction with other epoxy groups on the surface causing self-crosslinking. Because of the existence of self-crosslinking, even if the PEG grafting amounts are the same, samples with different thermal history (PEG grafting time) have a different number of available epoxy groups on the substrate. Thus, different fractions of PAA monomeric units in the train segments can be obtained. Based on this analysis, E is considered to inversely correlate with the PEG grafting time. Specifically, a long PEG grafting time reduces the concentration of epoxy groups in the PGMA layer.

Thus PAA may involve fewer monomeric units in the train section than that achieved by a short PEG grafting time. At the same time, more train segments can be obtained by increasing the amount of grafted PAA. According to these discussions, E is chosen to be related to f_{PAA}/T_{PEG}. Here f_{PAA} is the volumetric fraction of PAA chains in the mixed brush, and T_{PEG} is the grafting time for PEG chains. The plot of protein adsorption onto PAA chains (A_{PAA}) against E is shown in Figure 5.13.

The adsorption of protein onto PAA chains shows a complex dependence on the parameter E and can be divided into three regimes. When E is small (i.e., smaller than 0.1 hr^{-1}), the adsorption decreases when E becomes larger. The same behavior is observed in large E (i.e., larger than 0.25 hr^{-1}) region. The adsorption approaches zero when E becomes larger. However, it is interesting to find that the adsorption increases with increasing E when it is approximately less than 0.25 hr^{-1} but greater than 0.1hr^{-1}. This indicates that different protein adsorption mechanisms may exist when altering the parameter E. However, further investigations should be conducted with more samples to reveal the complete details of these interactions.

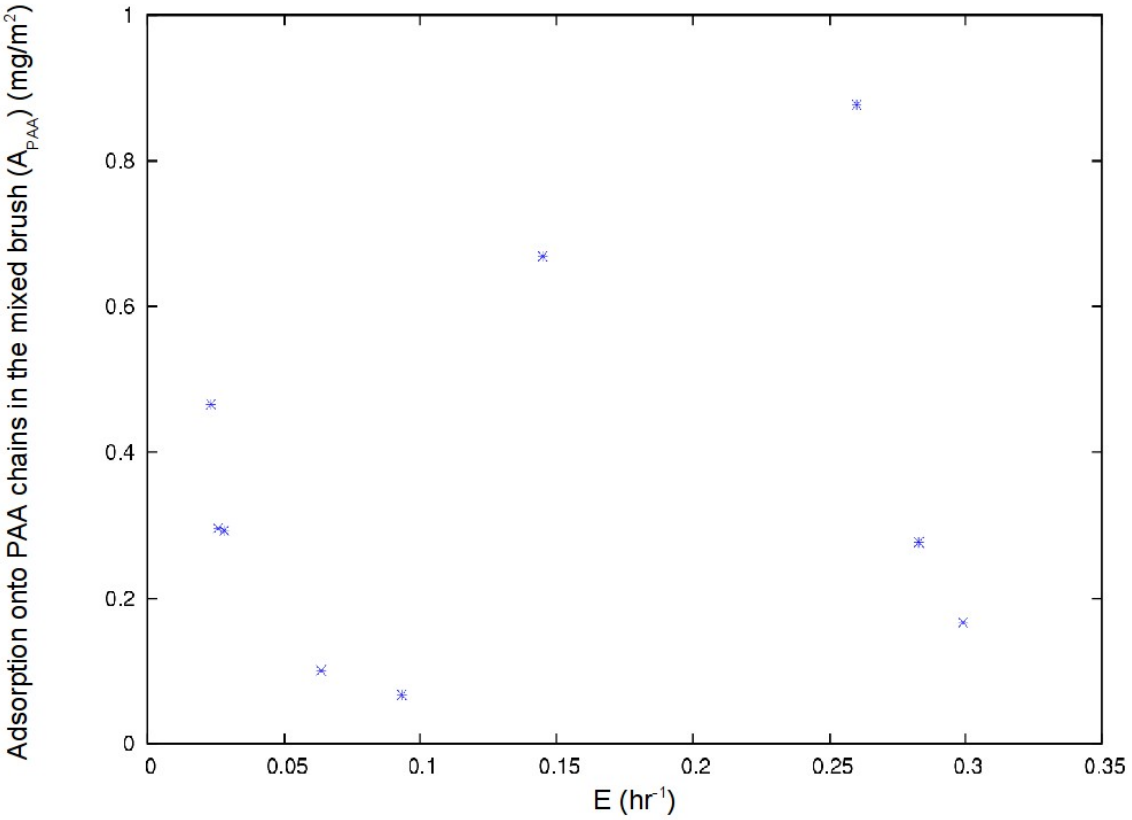

Figure 5.13: Protein adsorption to PAA components in mixed brushes (A_{PAA}) versus PAA monomeric units fractions in trains (E).

5.5 Protein Adsorption Tuning by Ionic Strength

As described in Chapters Two and Four, PAA brush height can be tuned by changing the ionic strength of the aqueous media. Thus, it may be possible to adjust the protein adsorption on PAA chains by changing the salt concentration. To keep the pH constant, 0.01mol/L phosphate buffer was used as the medium for protein adsorption. The ionic strength of this solution was approximately 10^{-2} mol/L. To study the adsorption response under different ionic strengths onto the mixed brush, different amounts of NaCl were added to this buffer, changing the total ionic strength from ~10^{-2}mol/ to ~10^{-1}mol/L and ~1 mol/L, respectively. *In situ* TIRF experiments were conducted by injecting different ionic strength protein solutions at different times onto one PEG/PAA mixed

brush. Original labeled protein solution was injected at Time O. Labeled protein solutions with ionic strength at ~10^{-1}mol/L and ~1mol/L were injected at Time A and B, respectively. Then protein solution with ionic strength at ~10^{-1}mol/L was injected again at time C to detect the reversibility. Pure phosphate buffer was injected at Time D. The protein adsorption breakthrough curve is shown in Figure 5.14.

From Figure 5.14, it can be seen that by changing the ionic strength, protein adsorption "off" status has not been observed. However, the tunability can be clearly judged from these results. At time A, increasing the ionic strength to 10 times that of the original phosphate buffer did not change the amount protein adsorbed significantly. However, a substantial increase in adsorption occurred when the ionic strength was increased to 100 times that of the original phosphate buffer (time B). This process was also reversible by changing back to the lower ionic strength solution at time C.

Figure 5.15 is repeated from Figure 4.12, which is the same sample brush height transition under different ionic strengths. It is concluded that the increased salt concentration decreased the mixed brush height but gave more ovalbumin adsorption.

Variations in protein adsorption on PAA brushes were observed in similar studies. For example, Hollmann *et al.*[1] used a neutron reflectometer to investigate the adsorption of bovine serum albumin (BSA) to PS-*b*-PAA at 20°C and 40°C. At 40°C, increasing the salt concentration decreased the PAA brush height but increased the BSA adsorption, similar to the result shown here. The same sample gave an opposite response at 20°C, which has decreased protein adsorption when the ionic strength is increasing and the brush height is decreasing. Thus, it is reasonable to conclude that the adsorption mechanism onto the polymer brush can be different with the same brush structure, but

under different conditions. However, the detailed mechanisms for protein adsorption are still unclear at present.

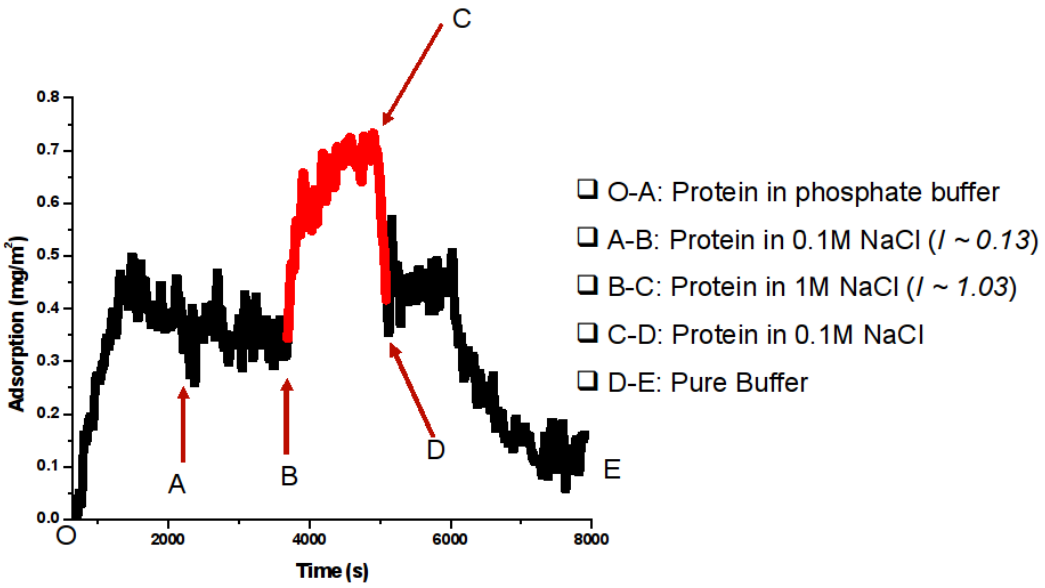

Figure 5.14: Protein adsorption on mixed PEG/PAA (thickness: 6.3/3.0 nm) brush by injecting different ionic strength buffers with same protein concentration at O, A, B, C and blank buffer at D.

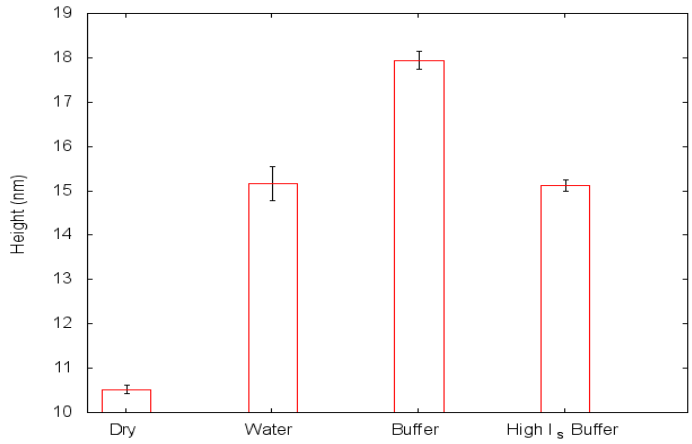

Figure 5.15: The same mixed brush height transition measured by AFM under different solution conditions. “Buffer” corresponds to the solution used at time O and “High Is Buffer” corresponds to the solution used at time B in Figure 5.14.

Protein adsorption onto a single-component PAA brush was also investigated by the same method as in the mixed brush. The protein adsorption breakthrough curve is shown in Figure 5.16. No ionic strength dependence for protein adsorption was observed,

regardless of height transition under different solutions, as shown in Figure 5.17. It is also noteable that the single PAA brush had no ovalbumin adsorption to its surface, even with a 100-fold increase in ionic strength.

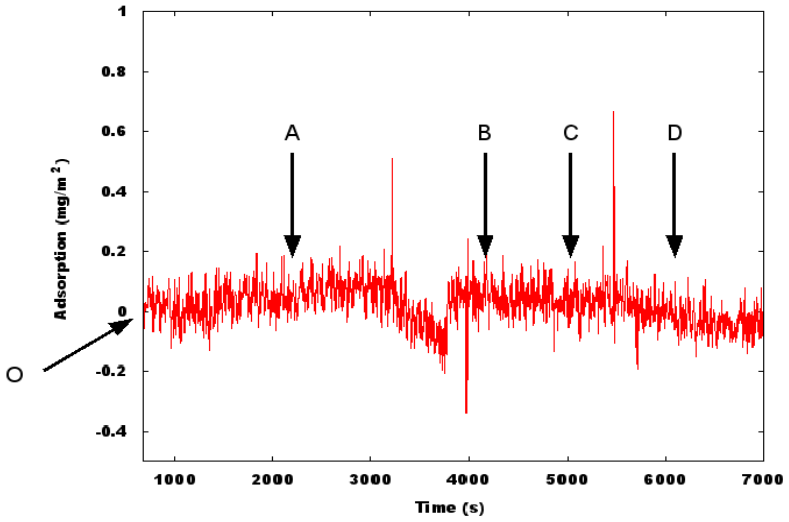

Figure 5.16: Ovalbumin adsorption breakthrough curve on a single-component PAA brush (PAA thickness is 5.8nm). O, A, B, C, D has the same meaning as in Figure 5.14.

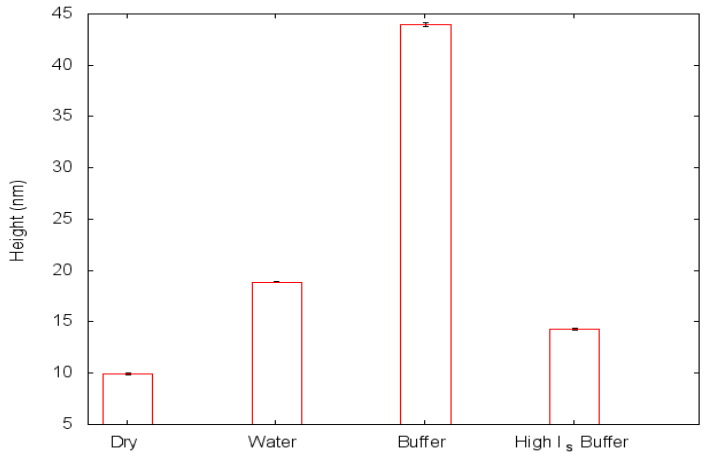

Figure 5.17: The same PAA brush height measured by AFM under different solution conditions. “Buffer” corresponds to the solution used at time O and “High Is Buffer” corresponds to the solution used at time B in Figure 5.16.

5.6 Conclusions

In this chapter, TIRF was used to measure protein adsorption onto single-component PEG, single-component PAA and the mixed PAA/PEG grafted layers. The calibration, background analysis, de-noising and baseline correction methods were discussed to provide an accurate interpretation of TIRF measurement. Then, single-component PEG brushes of different grafting densities were investigated for ovalbumin adsorption. The results indicated that protein adsorption decreased with increasing PEG grafting density. PAA brushes of different grafting densities were also studied. For low grafting density, protein adsorption was as high as that of the PGMA monolayers, which indicated that low grafting density PAA brushes might not entirely screen out PGMA monolayer interactions. For the large grafting density, PAA multi-connections structure forming on the surface that prevents ovalbumin adsorption. For the mixed brushes, the adsorption amount had a complex relationship with PEG grafting density and PAA monomeric unit fractions in train segments. Preliminary analysis showed that the relationship between adsorption onto the PAA part and the PAA monomeric unit ratio in train segments in mixed system is a non-monotonical function.

The hypothesized complete "turning off" of protein adsorption status was observed under different ionic strength solutions. However, it was found that a 100-fold increase in ionic strength increased protein adsorption in the mixed brush, which suggests that protein adsorption on mixed PEG/PAA brushes can be adjusted by varying solution conditions. The mechanism of protein adsorption behavior of mixed brushes under consideration is very complex and needs further investigation.

References

(1) Hollmann, O.; Gutberlet, T.; Czeslik, C. *Langmuir* **2007***, 23*, 1347.

(2) Dong, R.; Krishnan, S.; Baird, B. A.; Lindau, M.; Ober, C. K. *Biomacromolecules* **2007***, 8*, 3082.

(3) Uhlmann, P.; Houbenov, N.; Brenner, N.; Grundke, K.; Burkert, S.; Stamm, M. *Langmuir* **2007***, 23*, 57.

(4) Toscano, A.; Santore, M. M. *Langmuir* **2006***, 22*, 2588.

(5) Dai, J.; Bao, Z.; Sun, L.; Hong, S. U.; Baker, G. L.; Bruening, M. L. *Langmuir* **2006***, 22*, 4274.

(6) Norde, W.; Gage, D. *Langmuir* **2004***, 20*, 4162.

(7) Wittemann, A.; Haupt, B.; Ballauff, B. *Physical Chemistry Chemical Physics* **2003***, 5*, 1671.

(8) Dee, K. C.; Puleo, D. A.; Bizios, R. In *Protein-Surface Interactions;* Dee, K. C., Puleo, D. A. and Bizios, R., Eds.; An introduction to tissue-biomaterial interactions; Wiley-Liss: Hoboken, N.J., 2002; 37.

(9) Horbett, T. In *Proteins: Structure, Properties and Adsorption to Surfaces;* Ratner, B. D., Ed.; Biomaterials science : an introduction to materials in medicine; Academic Press: San Diego, 1996; 133.

(10) Fleck, C.; von Grnberg, H. H. *Physical Review E.* **2001***, 63*, 061804.

(11) Wagner, K.; Harries, D.; May, S.; Kahl, V.; Radler, J. O.; Ben-Shaul, A. *Langmuir* **2000***, 16*, 303.

(12) Manning, G. S. *Journal of Chemical Physics* **1969***, 51*, 924.

(13) Czeslik, C.; Jackler, G.; Steitz, R.; vonGrunberg, H. *Journal of Physical Chemistry B* **2004***, 108*, 13395.

(14) Gong, P.; Wu, T.; Genzer, J.; Szleifer, I. *Macromolecules* **2007***, 40*, 8765.

(15) Kato, K.; Sano, S.; Ikada, Y. *Colloids and Surfaces B: Biointerfaces,* **1995***, 4*, 221.

(16) Prime, K. L.; Whitesides, G. M. *Journal of American Chemical Society* **1993***, 115*, 10714.

(17) Robinson, S.; Williams, P. A. *Langmuir* **2002***, 18*, 8743.

(18) Sheth, S. R.; Efremova, N.; Leckband, D. E. *Journal of Physical Chemistry B* **2000**, *104*, 7652.

(19) Hlady, V.; Ho, C., H.; Britt, D., W. In *Quantitative Analysis of Protein Adsorption Kinetics;* Kallay, N., Ed.; Interfacial dynamics; M. Dekker: New York, 2000; Vol. 88, 741.

(20) Szleifer, I. *Biophysicial Journal* **1997**, *72*, 595.

(21) Szleifer, I. *Current Opinion in Solid State and Materials Science,* **1997**, *2*, 337.

(22) Andruzzi, L.; Senaratne, W; Hexemer, A.; Sheets, E. D.; Ilic, B.; Kramer, E. J. Baird, B.; Ober, C. K. *Langmuir* **2004**, *21*, 2495.

(23) Watkins, R. W.; Robertson, C. R. *Journal of Biomedical Materials Research* **1977**, *11*, 915.

(24) Lok, B.; Cheng, Y.; Robertson, C. *Journal of Colloid and Interface Science* **1983**, *91*, 87.

(25) Lok, B.; Cheng, Y.; Robertson, C. *Journal of Colloid and Interface Science* **1983**, *91*, 104.

(26) Lassen, B.; Malmsten, M. *Journal of Colloid and Interface Science,* **1996**, *179*, 470.

(27) Lévêque, M. *Ann. Mines* **1928**, *13*, 284.

(28) Kosto, K. B.; Deen, W. M. *American Institute of Chemical Engineers* **2004**, *50*, 2648.

(29) Liu, B.; Sera, Y.; Matsubara, N.; Otsuka, K.; Terabe, S. *Electrophoresis* **2003**, *24*, 3260.

(30) Perrin, C.; Walczak, B.; Massart, D. L. *Analytical Chemistry* **2001**, *73*, 4903.

(31) Rampp, S.; Prell, J.; Thielemann, H.; Posch, S.; Strauss, C.; Romstöck, J. *Journal of Clinic Monitoring and Computing* **2007**, *21*, 219.

(32) Addison, P. S. In *The illustrated wavelet transform handbook : introductory theory and applications in science, engineering, medicine and finance;* Institute of Physics Publishing: Bristol ; Philadelphia, 2002; 353.

(33) Mallat, S. *IEEE Transactions on Pattern Analysis and Machine Intelligence* **1989**, *11*, 674.

(34) Dong, R.; Krishnan, S.; Baird, B. A.; Lindau, M.; Ober, C. K. *Biomacromolecules* **2007**, *8*, 3082.

(35) Szöllősi, G. J.; Derényi, I.; Vörös, J. *Physica A: Statistical Mechanics and its Applications,* **2004***, 343*, 359.

(36) Khutoryanskiy, V. V.; Dubolazov, A. V.; Nurkeeva, Z. S.; Mun, G. A. *Langmuir* **2004***, 20*, 3785.

(37) Williams, T.; Kelley, C. *et al.* Gnuplot, http://www.gnuplot.info.

CHAPTER SIX

SUMMARY AND CONCLUSIONS

The objective of this study was to synthesize mixed polymer brushes which have adjustable protein adsorption properties. In order to implement this objective, two polymers were grafted to the surface sequentially in order to fabricate the mixed polymer brushes: poly(ethylene glycol) (PEG) which serves as a protein repelling layer and polyacrylic acid (PAA) which adsorbs protein and exhibits the brush height transition by changing the ionic strength.

To graft two polymers on the surface, PGMA was used as an anchoring layer and it demonstrated a large potential in grafting both PEG and PAA. The PEG grafting density displayed the dependency on both the grafting time and the PGMA layer thickness. In addition, the PEG grafting density influenced the PAA grafting amount during the latter grafting. The "*layer-assisted-tethering*" effect was also observed for high PEG grafting densities. Both the AFM and water contact angle measurements revealed that the mixed brush surface was occupied by PAA after the grafting. The single-component PAA and the PEG/PAA mixed brush height transitions under different ionic strength were also investigated. The result showed that the extension in the mixed brush height transition was smaller than that in the single-component PAA brush.

Single-component PEG, PAA and PEG/PAA mixed brushes with different PEG and PAA grafting densities were studied to measure the adsorption of RhB labeled ovalbumin using total internal reflection fluorescence (TIRF) to explore the determining factors in protein adsorption amount. The results showed that protein adsorption amounts on single-component PEG brushes decreased when PEG grafting density was increased.

In addition, sparsely grafted single-component PAA brush exhibited a strong affinity to the protein because of the unscreened interactions by the PGMA anchoring layer, while the densely grafted PAA brush demonstrated no measurable protein adsorption, which is better than the PEG brush with the same grafting density. However, in PEG/PAA mixed brushes, the determining factors were not as simple as the combination of PEG and PAA grafting densities hypothesized initially. A simplified model was established to separate the total adsorption into the adsorption on the PEG part and the adsorption on the PAA part. The adsorption of proteins onto PEG brushes is affected by the PEG chains grafting density. At the same time, a PAA monomeric units ratio in train segments (E) was introduced to interpret the adsorption onto PAA brushes.

Finally, the tunability of protein adsorption amount under different ionic strengths was studied too. The completely protein adsorption "off" status of the mixed PEG/PAA was not observed under these conditions. However, the result showed that the protein adsorption onto mixed brushes could be adjusted by increasing/decreasing the ionic strength of the protein solution, while in contrast the single-component PAA brush did not exhibit any variation in the protein adsorption amount at the same conditions. Further investigation is needed to clarify the interactions with protein in the mixed brushes system.

CHAPTER SEVEN

RECOMMENDATIONS FOR FUTURE WORK

Sequentially grafting PEG and PAA to PGMA surfaces via the "grafting-to" is successful in fabricating the mixed brush systems. These investigations have revealed the possibility to obtain a tunable protein adsorbing surface by constructing the mixed brush containing different protein-affinity materials. However, during the investigation, new questions emerged and could possibly guide us to further studies and a better understanding of the protein adsorption mechanism. Five recommendations for the future work are listed here, as an example.

1. "Graft-from" and then hydrolyze end-carboxyl terminated poly(*tert*-butyl acrylate) to construct PAA standard "brush" system with only one connection to the surface and investigate the protein adsorption on these brushes.
2. Synthesize additional PEG/PAA mixed brushes with different compositions and obtain the related protein adsorption amounts to establish a better model to explain the factors of protein adsorption in the mixed brush system.
3. Investigate the swelling behavior of the PEG brush under different conditions.
4. Investigate other proteins adsorptions onto the mixed brushes, such as human albumin, bovine albumin, etc.
5. Model the protein adsorption process using the kinetic adsorption models to reveal the detail kinetics during the adsorption.

APPENDICES

A.1 Wavelet Transformation Code for TIRF Data

```
function blcorrect(signal,level1 ,waveform1,level2,waveform2)
   % by Zhenqing 08/20/2007
   % blcorrect(signal,level1,waveform1,level2,waveform2)
   % This function is used for baseline correction by applying the
Discrete
    % Wavelet Transform (DWT). By disregard all the approximation
coefficient
    % then reconstructe back the curve.
    % Input your signal as signal array,the DWT level and waveform
for baseline
    % correction is level1, waveform1, while the DWT for de-noising
is level2
    % and wavenumber2.

    [C1 L1]=wavedec(signal,level1,waveform1);
    cA=appcoef(C1,L1,waveform1,level1);
    l=length(cA);
    C1(1:l)=0;
    A0=waverec(C1,L1,waveform1);
    [C2 L2]=wavedec(A0,level2,waveform2);
    % Al=wrcoef('a',C2,L2,waveform2,level2);
    [thr,sorh,keepapp]=ddencmp('den','wv',A0);
    Al=wdencmp('gbl',C2,L2,waveform2,level2,thr,sorh,keepapp);
    subplot(3,1,1);plot(signal);title('Original signal')
    subplot(3,1,2);plot(A0);title('Baseline corrected signal')
    subplot(3,1,3);plot(Al);title('Baseline corrected and smoothed
signal')
```

A.2 Average AFM Image Profile for Scratching

```
function matrixcal(filename)

%This function is to open the data file generated by Gwyddion and
then
%average the line first to let user decide which range he wants to
%choose for height measurement. Then do a calculation about the
height
%and the error range of the measurement.

data=load("-ascii",filename);

%First do a column average.

cx=zeros(256,1);
for i=1:256
  cx(i,1)=mean(data(:,i));
end
plot(cx(:,1))

startpoint=input("Please give me the starting point: ");
endpoint=input("Please give me the end point: ");

delta=zeros(256,1);

for j=1:256
  delta(j,1)=data(j,endpoint)-data(j,startpoint);
end
mdelta=mean(delta(:,1))*1e9;
errdelta=std(delta(:,1))./sqrt(256).*1e9;
disp("The mean is: "),disp(mdelta)
disp("The error is: "),disp(errdelta)
end
```

A.3 Grafting of Single-component PEG and PAA brushes

Number	Annealing time (hr)	PEG brush height (nm)	PEG brush grafting density (chains/nm^2)
1	~15	8.1	1.1
2		8.3	1.1
3		11.0	1.4
4		11.9	1.6
5		10.5	1.4
6	4	7.9	1.0
7		7.0	0.9
8		4.2	0.6
9		4.2	0.6
10		5.2	0.7
11	2	2.6	0.3
12		3.4	0.5
13		2.8	0.4
14		3.0	0.4

Table A.1: Single-component PEG brushes grafting densities obtained by different grafting time.

PAA Grafting Time (min)	PAA Brush Thickness (nm)	PAA Grafted Amount (mg/m^2)
5	3.7	4.6
30	4.9	6.1
60	6.2	7.8
900	7.5	9.4

Table A.2: Single-component PAA brush heights and grafted amount calculated obtained by annealing for different time.

A.4 Protein adsorption breakthrough curves obtained by TIRF

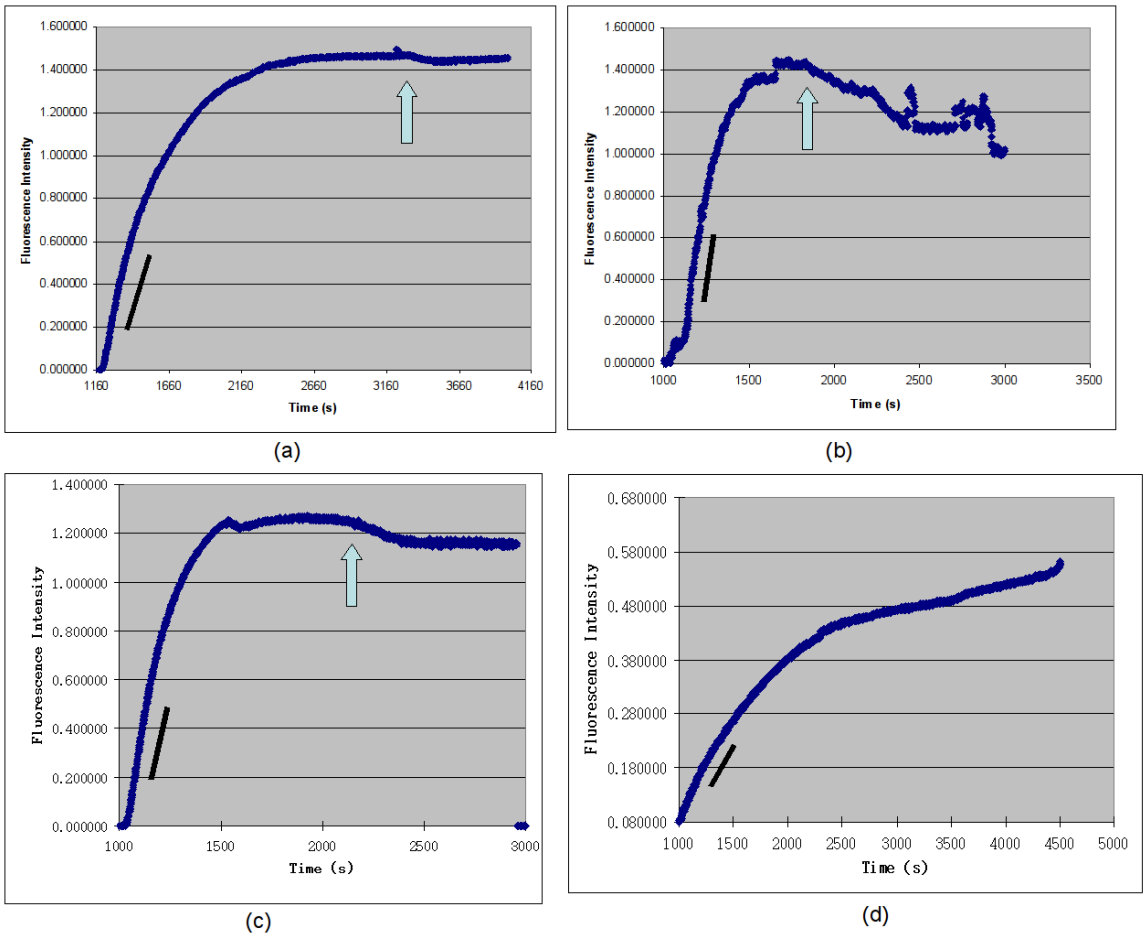

Figure A.1: The breakthrough curves of ovalbumin phosphate solutions with different concentrations onto PGMA surface obtained by TIRF. The concentrations of ovalbumin are (a) 12.4ppm, (b) 41.0ppm, (c) 20.4ppm, (d) 6.6ppm. Arrows indicates the time of injection of the pure phosphate buffer. Lines indicating the range used to linear fit to obtain the initial slopes.

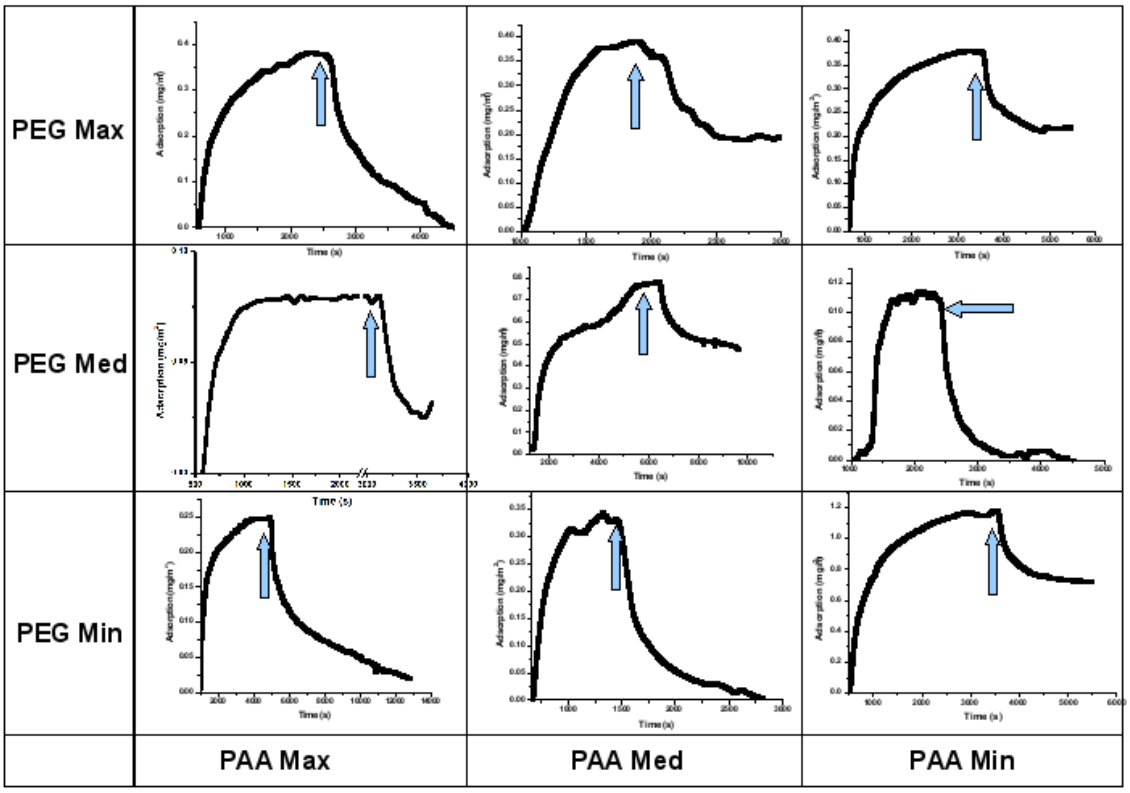

Figure A.2: Ovalbumin adsorption breakthrough curves on the mixed brushes. PEG and PAA grafting times are listed in the left and lower panels. (Detailed grafting densities are included in Table 4-2).

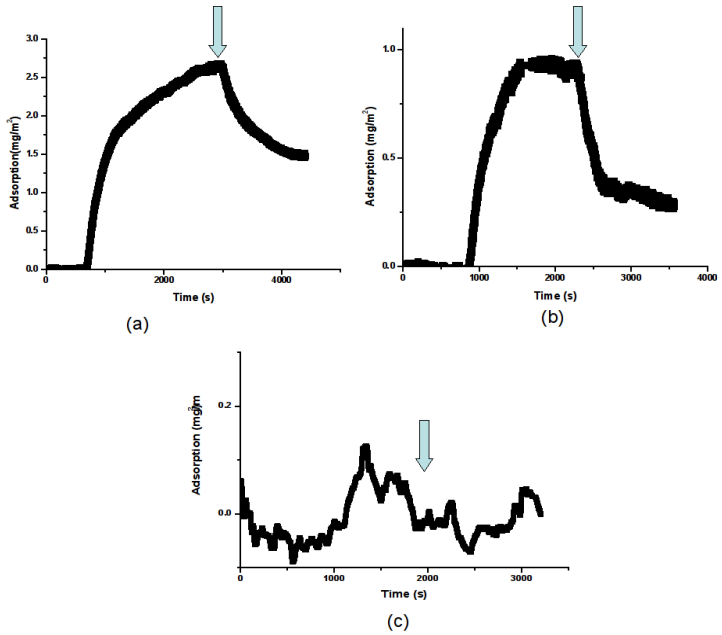

Figure A.3: Ovalbumin adsorption breakthrough curve on PEG brushes with different grafting densities: 0.37 chains/nm^2(a), 0.60 chains/nm^2(b) and 1.37 chains/nm^2(c). Arrows indicate the time when pure phosphate buffer were injected.